Materials Advances

Accepted Manuscript

This article can be cited before page numbers have been issued, to do this please use: A. Singh and T. Soundappan, *Mater. Adv.*, 2026, DOI: 10.1039/D5MA01247C.

ROYAL SOCIETY OF CHEMISTRY

rsc.li/materials-advances

View Article Online
DOI: 10.1039/D5MA01247C

Multifaceted Advances in TiO_2-Based Photocatalysts for PFAS Degradation: A Critical Review of Mechanisms, Modifications, and Challenges

Avtar Singh[a,] *, Thiagarajan Soundappan

[a]*Department of Chemistry, School of Science, Navajo Technical University, Crownpoint, NM-87313, United States of America*

Abstract

The global persistence of per- and polyfluoroalkyl substances (PFAS), often referred to as "forever chemicals", poses significant environmental and human health risks, driving regulatory action and intensified research into effective remediation strategies. Photocatalysis has emerged as a promising, sustainable approach for PFAS degradation via light-driven redox processes. Titanium dioxide (TiO_2) remains the benchmark photocatalyst due to its chemical stability, low toxicity, and strong oxidative potential; however, its practical application is limited by rapid electron-hole recombination, restricted visible-light absorption, and pH-dependent surface charge behavior, necessitating acidic conditions for optimal performance. These constraints reduce its efficacy against the robust carbon–fluorine bonds characteristic of PFAS and complicate large-scale deployment. Recent advances focus on multifunctional TiO_2-based systems, including metal and nonmetal doping, carbonaceous composites, heterojunctions, molecularly imprinted polymers, and adsorptive concentrate-and-destroy supports. Integration with advanced oxidation and reactor-level engineering approaches, such as photoelectrocatalysis (i.e., photocatalysis under applied bias), applied bias and hybrid oxidants, has further advanced photocatalytic degradation technology under broader operating conditions. This review provides a critical comparative assessment of these strategies, highlighting mechanistic insights, structure-activity relationships, and practical limitations related to pH, stability, and scalability. By consolidating recent innovations and operational considerations, this work offers guidance for the rational design of efficient, field-relevant, and sustainable photocatalytic technologies for global PFAS remediation.

Keywords: Titanium dioxide (TiO_2), Photocatalysis, Defluorination, Per- and Polyfluoroalkyl substances (PFAS), Environmental remediation

View Article Online
DOI: 10.1039/D5MA01247C

1. Introduction

Scientific and technological progress has transformed modern society, improving healthcare, sanitation, transportation, and daily life. Central to these advances, materials science has enabled breakthroughs, from polymers to semiconductors and nanomaterials, elevating global living standards [1-3]. However, history highlights the unintended environmental consequences of innovation, exemplified by chlorofluorocarbons (CFCs), asbestos, DDT, and plastics. Today, per- and polyfluoroalkyl substances (PFAS) represent a pressing concern. Often termed "forever chemicals," PFAS are characterized by strong C-F bonds, high chemical stability, bioaccumulation potential, and extreme environmental persistence [5-8]. First synthesized in the late 1930s and commercialized by the 1940s [9], PFAS have been extensively applied in Teflon™ coatings, Scotchgard™ treatments, aqueous film-forming foams (AFFFs), textiles, semiconductor manufacturing, food packaging, and aerospace industries [9,10]. Global production exceeded 85,000 metric tons annually by the early 2000s [10], resulting in widespread contamination of industrial zones, remote ecosystems, Arctic wildlife, and human blood samples worldwide [11]. Their persistence, mobility, and toxicity now pose severe environmental and public health challenges [12].

Diverse remediation strategies have been explored for PFAS contamination, including adsorption (activated carbon, ion-exchange resins, MOFs, engineered clays) [13-19]; advanced oxidation processes (AOPs) such as Fenton chemistry, persulfate activation, and electrochemical oxidation [20-22]; photocatalysis [23]; thermal methods (incineration, supercritical water oxidation) [23-25]; biological approaches with PFAS-tolerant microbial consortia [26-28]; plasma-based treatments [29-30]; membrane separation (nanofiltration, reverse osmosis) [31-32]; and hybrid strategies integrating ultrasound, photolysis, or catalysis [33-35]. Among these, photocatalysis has gained attention as a sustainable, environmentally benign approach. By harnessing sunlight or artificial UV light, photocatalysis generates reactive oxygen species (ROS) capable of cleaving robust C-F bonds [23,36-38]. While numerous new strategies and materials are being explored in this field, a few recent examples of advancements include carbazole-cored super-photoreductants for low-temperature PFAS and PTFE defluorination [39], $CdIn_2S_4$ micro-pyramids [40], Fe/g-C hybrids [41], rGO/WO_3 nanoflowers [42], and Pb-doped TiO_2/rGO composites [43], many achieving near-complete PFAS degradation through synergistic redox and radical-mediated pathways.

Within this context, titanium dioxide (TiO_2) remains at the core of photocatalysis, alone and in hybrid systems, owing to its high stability, low toxicity, cost-effectiveness, and strong oxidative potential under UV irradiation [44-48]. The d^0 electronic configuration of Ti^{4+} results in Ti 3d-O 2p hybridization, producing a ~3.0-3.2 eV bandgap suitable for UV-driven photocatalysis. Upon excitation, TiO_2 generates electron-hole (e^--h^+) pairs that drive ROS formation, particularly $^{\bullet}OH$ and $O_2^{\bullet-}$, which are central to pollutant degradation [49,50]. Photocatalytic performance is strongly influenced by crystal polymorph (anatase, rutile, brookite), lattice structure, and facet-specific reactivity. For example, anatase {001} facets (surface energy ~0.90 J m^{-2}) exhibit higher reactivity than {101} facets (~0.44 J m^{-2}) [51-53]. A representative strategy involves selective Pt

View Article Online
DOI: 10.1039/D5MA01247C

single-atom deposition on facet-engineered TiO_2, fluoride ions stabilize {001} facets, APTMS (aminopropyltrimethoxysilane) anchors guide Pt precursors to {101}, and mild UV irradiation reduces Pt to single atoms. This spatially separates oxidative and reductive sites, holes migrate to {001} for $^{\bullet}OH$ generation, while Pt atoms on {101} trap electrons for reductive defluorination, enabling simultaneous oxidative-reductive PFAS degradation. Surface chemistry further modulates TiO_2 activity, with hydroxyl groups, coordinatively unsaturated Ti sites, oxygen vacancies, and Ti^{3+} centers serving as active sites for adsorption, charge separation, and visible-light absorption [54-59]. Controlled defect introduction via hydrogenation, electrochemical reduction, ion-thermal processing, ultrasonication, $NaBH_4$ treatment, microwave irradiation, plasma, or laser ablation enhances photocatalytic efficiency by suppressing e^--h^+ recombination and extending optical response. Additional strategies include metal, nonmetal doping for bandgap tuning, heterojunction construction and plasmonic-carbonaceous composites for charge separation, co-catalyst loading to enhance e^--h^+ utilization, surface functionalization to promote pollutant adsorption, modulation of reactive species for optimized ROS balance, hierarchical nanostructures, and mixed anatase-rutile interfaces that facilitate charge migration [60-64]. Hydrophilic or fluorophilic surface tailoring has been shown to enhance interactions with polar and fluorinated substrates [65,66]. Synergistic integration of TiO_2 photocatalysis with electrochemical [67], photo-Fenton [68], or piezocatalytic [69] processes generates additional radical pathways, while immobilization in thin films and porous monoliths improves scalability. TiO_2-based photocatalytic systems, owing to their intrinsic stability, structural tunability, and broad adaptability, continue to serve as a cornerstone for ROS-mediated PFAS degradation. **Figure 1** shows key strategies for enhancing photocatalysts in environmental remediation.

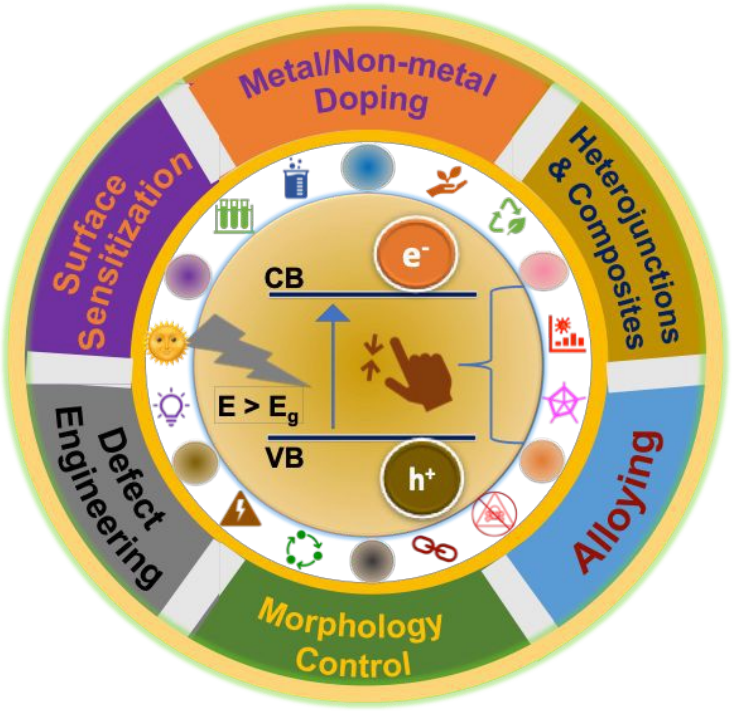

Figure 1. Key strategies for enhancing photocatalysts in environmental remediation to improve light absorption, charge separation, and pollutant degradation, enabling next-generation, effective, and field-applicable solutions.

View Article Online
DOI: 10.1039/D5MA01247C

This review presents a comprehensive evaluation of TiO_2-based photocatalysts for PFAS degradation, covering pristine and modified materials, including defect-engineered, single-atom, carbonaceous, heterojunction, and adsorptive designs. It critically examines operational parameters, mechanistic pathways, and structural modifications that govern adsorption, charge separation, reactive species generation, and oxidative–reductive defluorination. Hybrid and integrated strategies, such as photoelectrocatalysis, advanced oxidation, and reactor-level innovations, are discussed to address inherent limitations like charge recombination, UV dependence, and mass-transfer constraints. By connecting mechanistic insights with practical considerations, including stability, recyclability, matrix effects, energy efficiency, and scalability, this review provides guiding principles for designing next-generation TiO_2-based photocatalysts that are efficient, robust, and field-relevant for sustainable PFAS remediation.

2. Chemical, Environmental, and Health Context of PFAS

Per- and polyfluoroalkyl substances (PFAS) are a global environmental concern due to their chemical stability, persistence, and widespread applications. PFAS originated in 1938 when Dr. Roy J. Plunkett at DuPont accidentally synthesized polytetrafluoroethylene (PTFE) while developing chlorofluorocarbon refrigerants [70,71]. Commercialized as Teflon™ in 1948, PTFE's robust C–F bonds confer thermal and chemical stability, catalyzing thousands of PFAS compounds used in firefighting foams, surfactants, textiles, microelectronics, and other applications [72,73]. These properties also render PFAS "forever chemicals," leading to persistence and bioaccumulation in soils, water, air, and biota [74–77]. Despite phase-outs of legacy PFAS such as PFOA and PFOS, new analogs continue to be produced with similar mobility and toxicity [78]. PFAS comprise over 14,000 compounds, broadly classified as non-polymeric or polymeric (**Fig. 2**) [79,80]. Non-polymeric PFAS contain a hydrophobic perfluoroalkyl chain (-CnF2n-) linked to polar groups (carboxylate, sulfonate), enabling surfactant applications like AFFFs, metal plating, and cleaning agents [81]. Polymeric PFAS, including PTFE and FEP, are high-molecular-weight fluoropolymers used in cookware, electronics, and waterproof fabrics. Chain length and functional groups influence mobility, bioaccumulation, and degradability: short-chain PFAS are highly mobile yet hard to remove, whereas long-chain PFAS readily bioaccumulate [82,83]. Emerging variants with unknown fate challenge regulatory and analytical frameworks, prompting tools like PFAS-Atlas for chemical mapping and prioritization [84,85].

PFAS are detected in surface water, groundwater, drinking water, soils, vegetation, and biota worldwide, including remote Arctic and Antarctic regions [86–90]. HRMS and LC-MS/MS detect PFAS at parts-per-trillion levels, revealing widespread contamination and bioaccumulation [91–93]. Human exposure occurs via ingestion, inhalation, and dermal contact [94–96]. Epidemiological studies, the C8 Health Project (>69,000 individuals), link chronic PFOA exposure to testicular and kidney cancers, thyroid disorders, ulcerative colitis, and pregnancy-induced hypertension [97,98]. PFAS interact with nuclear receptors (PPARα, CAR, PXR), perturb lipid metabolism, immunity, and hormonal regulation, and cross the placental barrier [99–101]. Blood levels correlate with diet, smoking, and use of PFAS-containing products [102,103].

View Article Online
DOI: 10.1039/D5MA01247C

Ecologically, PFAS induce biochemical disturbances at environmental concentrations. Metabolomic studies reveal altered gene expression in zebrafish larvae, liver glycogen depletion, and shifts in earthworm metabolites [104–106]; rodent studies report neurological and metabolic effects at low doses [107,108]. Risk assessments indicate low-to-moderate global risk, though industrial discharges can elevate exposures [109–111]. AFFFs remain a major source, with contamination documented at military, industrial, and civilian sites [111–119]. Research now focuses on fluorine-free alternatives, supported by U.S. DoD SERDP and ESTCP programs [119,120]. International regulations are emerging: most Australian states restrict PFAS foams for non-aviation use [121,122], and in 2023, five EU member states proposed banning all PFAS in firefighting foams [123]. Temporary exemptions highlight the need to integrate material innovation, regulation, and deployment to mitigate legacy and future PFAS exposure.

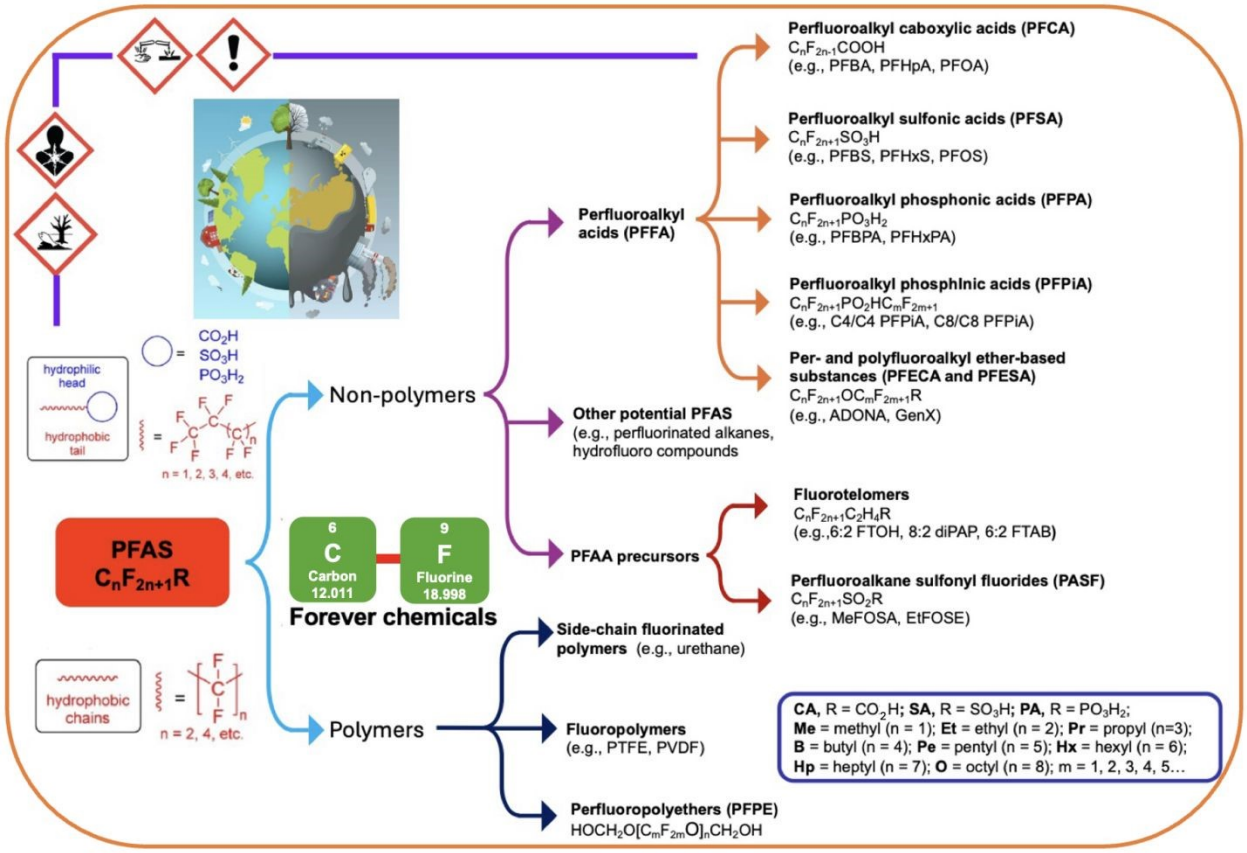

Figure 2. Classification of PFAS based on structural features, categorized into polymeric and non-polymeric groups.

3. Prospective Approaches to PFAS Elimination

PFAS contamination in aqueous and soil matrices presents distinct remediation challenges. Water treatment strategies include adsorption, membrane filtration, and advanced oxidative or reductive methods, such as photocatalysis, electrochemical oxidation, electron beam irradiation, and hydrothermal alkaline treatment [124-126]. While adsorption and membranes effectively concentrate PFAS, they often generate secondary waste requiring destructive post-treatment

View Article Online
DOI: 10.1039/D5MA01247C

[124]. Advanced oxidative and reductive processes target mineralization but typically demand high energy, specialized catalysts, or extreme conditions, limiting large-scale applicability. Hybrid treatment trains that combine selective concentration with destructive pathways improve degradation efficiency while mitigating cost and secondary pollution [124]. However, complex aqueous matrices containing competing ions or natural organic matter can inhibit reactive species, underscoring the need for site-specific optimization [127]. As summarized in **Fig. 3**, PFAS treatment technologies include both destructive methods, such as photocatalysis, electrochemical oxidation, and hydrothermal or mechanochemical degradation, and non-destructive approaches, including adsorption, membrane filtration, and phytoremediation. Hybrid systems that combine selective concentration with destructive pathways are also highlighted, illustrating strategies to enhance mineralization efficiency while minimizing secondary pollution.

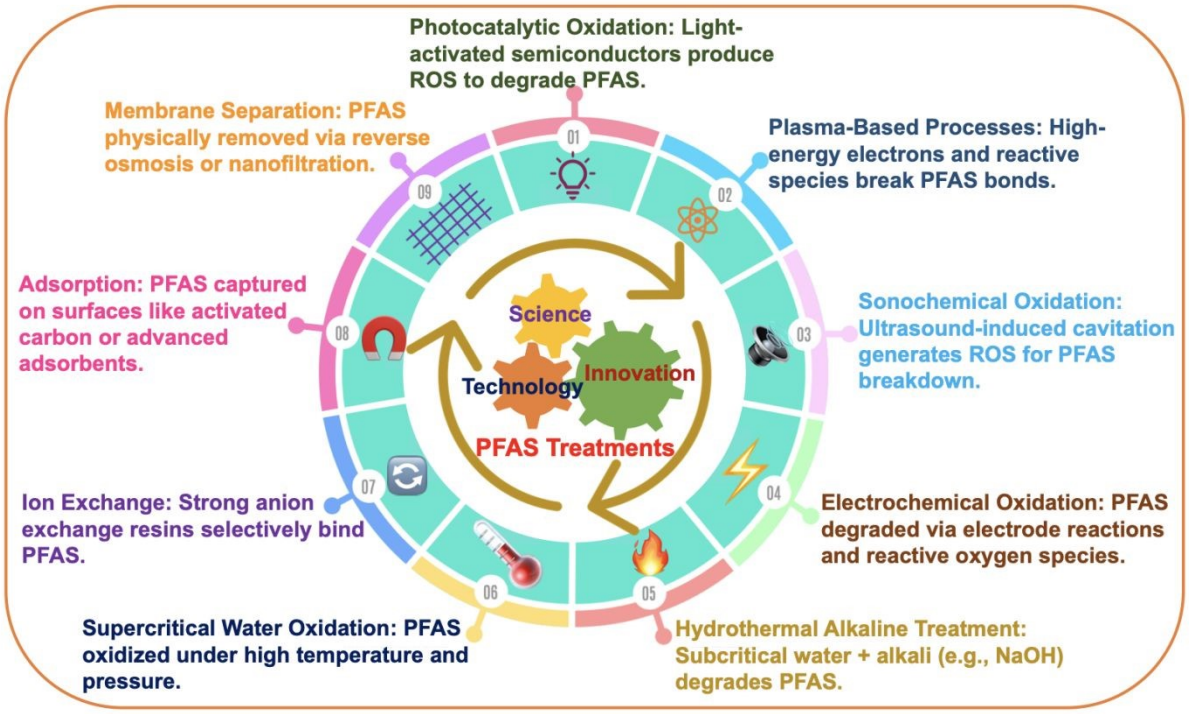

Figure 3. Overview of destructive and non-destructive technologies for PFAS treatment, highlighting conventional approaches and advanced degradation strategies. NOTE: a few parts of this figure are adapted from open sources like Freepik (https://www.freepik.com/) and Pixabay (https://pixabay.com/).

Soil remediation faces additional hurdles due to heterogeneity and strong C-F bonds promoting PFAS retention [128]. Physical approaches, such as soil washing or amendment-induced immobilization, usually provide only temporary containment [129,130]. Thermal strategies, including incineration and smoldering combustion (>500-900 °C), effectively destroy PFAS but require careful control of toxic fluorinated emissions [128,131-134]. Energy-efficient smoldering of PFAS-laden granular activated carbon (GAC) and soils has achieved complete destruction for ~44% of PFAS on GAC and ~16% in soils, with emissions efficiently scrubbed by GAC [135]. Hydrothermal and supercritical water oxidation under alkaline conditions can remove >95% of

View Article Online
DOI: 10.1039/D5MA01247C

PFAS, though effluent management remains critical [136]. Mechanochemical degradation using high-energy ball milling with additives (KOH, persulfate) provides non-thermal, onsite alternatives [137,138]. Advanced oxidative and reductive methods, including electron beam irradiation and persulfate-based systems, generate radicals capable of cleaving C-F bonds but face high energy demands and matrix interference [124,137]. Electrochemical remediation shows promise, particularly for short-chain PFAS, while phytoremediation offers a low-cost, sustainable option by sequestering PFAS in biomass for subsequent treatment [139-146].

Artificial intelligence (AI) and machine learning (ML) offer transformative potential for catalyst design and process optimization. By analyzing large PFAS datasets and reaction pathways, ML can predict outcomes and guide selection of optimal materials and operational conditions [147-150]. Hybrid systems combining photocatalysis with electrochemical or mechanochemical processes exploit synergistic effects, enhancing mineralization efficiency and reducing by-product formation. Circular economy strategies, such as mechanochemical defluorination recovering fluorine as reusable salts, further enable sustainable PFAS waste management [151]. Among destructive methods, photocatalysis is particularly attractive, as it harnesses solar energy under ambient conditions to generate reactive oxygen species capable of mineralizing PFAS into environmentally benign products. Catalyst design approaches, including size-exclusion, charge heterogeneity, amphiphilic surface modification, and molecular imprinting, enhance PFAS adsorption and orientation, improving degradation even in complex matrices [152-154]. TiO_2)-based photocatalysts are especially prominent due to their intrinsic tunability and versatility, allowing strategies such as facet engineering, doping, and heterojunction construction to create structurally and functionally diverse photocatalysts. This multifaceted platform underpins the focus of this review on strategies to enhance photocatalytic efficiency and selectivity for PFAS degradation.

4. Mechanistic Foundations and Limitations of TiO_2

Titanium dioxide (TiO_2) is widely recognized as a benchmark photocatalyst due to its strong oxidation potential, chemical stability, and cost-effectiveness [155]. Upon absorption of photons with energy equal to or greater than its band gap (~3.2 eV for anatase), electrons are excited from the valence band to the conduction band, generating e^-–h^+ pairs. Valence-band holes (h^+) serve as potent oxidants, while conduction-band e^- participate in interfacial reduction reactions, including oxygen reduction, leading to secondary reactive species under aerobic conditions [3,156-158] (**Fig. 4a**). The overall photocatalytic efficiency is governed by the quantity of photo-generated charge carriers, their oxidation–reduction potentials, and charge-carrier recombination dynamics.

Per- and polyfluoroalkyl substances (PFAS), particularly perfluorocarboxylates (PFCAs) and perfluorosulfonates (PFSAs), exhibit exceptionally strong carbon–fluorine (C–F) bonds [159], which underpin their environmental persistence and resistance to conventional radical-mediated oxidation [124]. For representative compounds such as PFOA and PFOS, the fully fluorinated alkyl chains lack abstractable hydrogen atoms, rendering hydroxyl radical (•OH) attack largely ineffective for initiating degradation [160]. As a result, indirect oxidation pathways involving •OH

View Article Online
DOI: 10.1039/D5MA01247C

contribute minimally to PFAS transformation, and reaction initiation is increasingly attributed to direct interfacial electron transfer between the pollutant and the photoexcited semiconductor via valence-band (VB) holes [160, 161, 162]. For PFCAs, adsorption onto TiO_2 surfaces facilitates direct VB hole oxidation, triggering Kolbe-type decarboxylation of the head group (**Fig. 4b**) and generating carbon-centered radicals that undergo stepwise chain shortening to progressively shorter PFCAs (e.g., PFHpA, PFHxA, PFPeA, PFBA, PFPrA), accompanied by the formation of CO_2 and fluoride ions [124,161,162]. These transformations are surface-controlled, making adsorption affinity and interfacial charge-transfer efficiency the primary determinants of degradation kinetics. Although photoexcited electrons react readily with dissolved oxygen to form superoxide radicals ($\bullet O_2^-$), this species is widely regarded as ineffective for PFAS degradation, and its role remains controversial [161]. In oxygenated systems, electron scavenging by O_2 further suppresses reductive pathways by limiting the availability of excited electrons [163].

Complementary photoreductive pathways (**Fig. 4c**) have also been reported, particularly under anoxic conditions and in the presence of hole scavengers [158, 161]. In these systems, conduction-band electrons or hydrated electrons (e_{aq}^-) are injected into the PFAS molecule, leading to direct reductive cleavage of C–F bonds (**Fig. 4c**) or, in some cases, reductively induced decarboxylation of PFCAs [164]. However, such reductive mechanisms are strongly disfavored under environmentally relevant conditions due to efficient electron scavenging by oxygen and the generally low sorption affinity of semiconductors for PFAS [165]. While some studies report that $\bullet O_2^-$ scavengers hinder PFOA degradation, suggesting a possible role in initiating decarboxylation via nucleophilic substitution, others propose that $\bullet O_2^-$ may indirectly generate •OH under acidic conditions, thereby contributing to oxidative pathways [161]. Consequently, the role of superoxide remains unresolved. Ateia et al. [162] proposed that PFAS degradation is primarily triggered by direct electron transfer to valence-band holes, with •OH and $\bullet O_2^-$ playing a minimal role in initiating the reaction. In contrast, earlier studies by Hori et al. [166] showed that the presence of moisture does not alter the primary degradation rate of fluorotelomer alcohols on TiO_2 but does enhance the breakdown of fluorinated byproducts and the formation of CO_2. This suggests that •OH radicals may be more important for the secondary oxidation and mineralization of intermediates rather than for the initial activation of PFAS molecules.

TiO_2's intrinsic properties, including polymorphism, defect tolerance, electronic tunability, high dielectric constant, and chemical robustness, support diverse modification strategies. Its polymorphs (anatase, rutile, brookite) can accommodate dopants, enabling band-gap modulation and the introduction of defect or mid-gap states that extend light absorption and influence charge-carrier dynamics. Facet engineering, particularly exposure of high-energy anatase {001} facets (~0.90 J m^{-2}), provides selective adsorption and reaction sites that enhance surface redox processes [167]. Surface features such as coordinatively unsaturated Ti sites, oxygen vacancies, and Ti^{3+} species improve charge separation, broaden optical absorption, and facilitate PFAS adsorption and interfacial electron transfer [168-170]. Morphological flexibility, from nanoparticles to ordered mesoporous films, allows tuning of surface area, porosity, and light-harvesting efficiency, directly influencing adsorption, charge migration, and catalytic performance [171, 172]. Combined with chemical robustness under diverse aqueous conditions, TiO_2 remains durable for long-term photocatalytic applications [173].

View Article Online
DOI: 10.1039/D5MA01247C

Compared with alternative photocatalysts such as ZnO, g-C_3N_4, or CdS, which can suffer from photocorrosion, limited charge mobility, or toxicity, TiO_2 provides a balanced combination of stability, tunability, and cost-effectiveness [174,175]. This multifaceted nature underpins rational design strategies, including doping, defect engineering, composite formation, and morphological control, that enhance PFAS degradation. The following sections focus on these intrinsic and engineered advances, highlighting their relevance for efficient PFAS mineralization under environmentally realistic conditions.

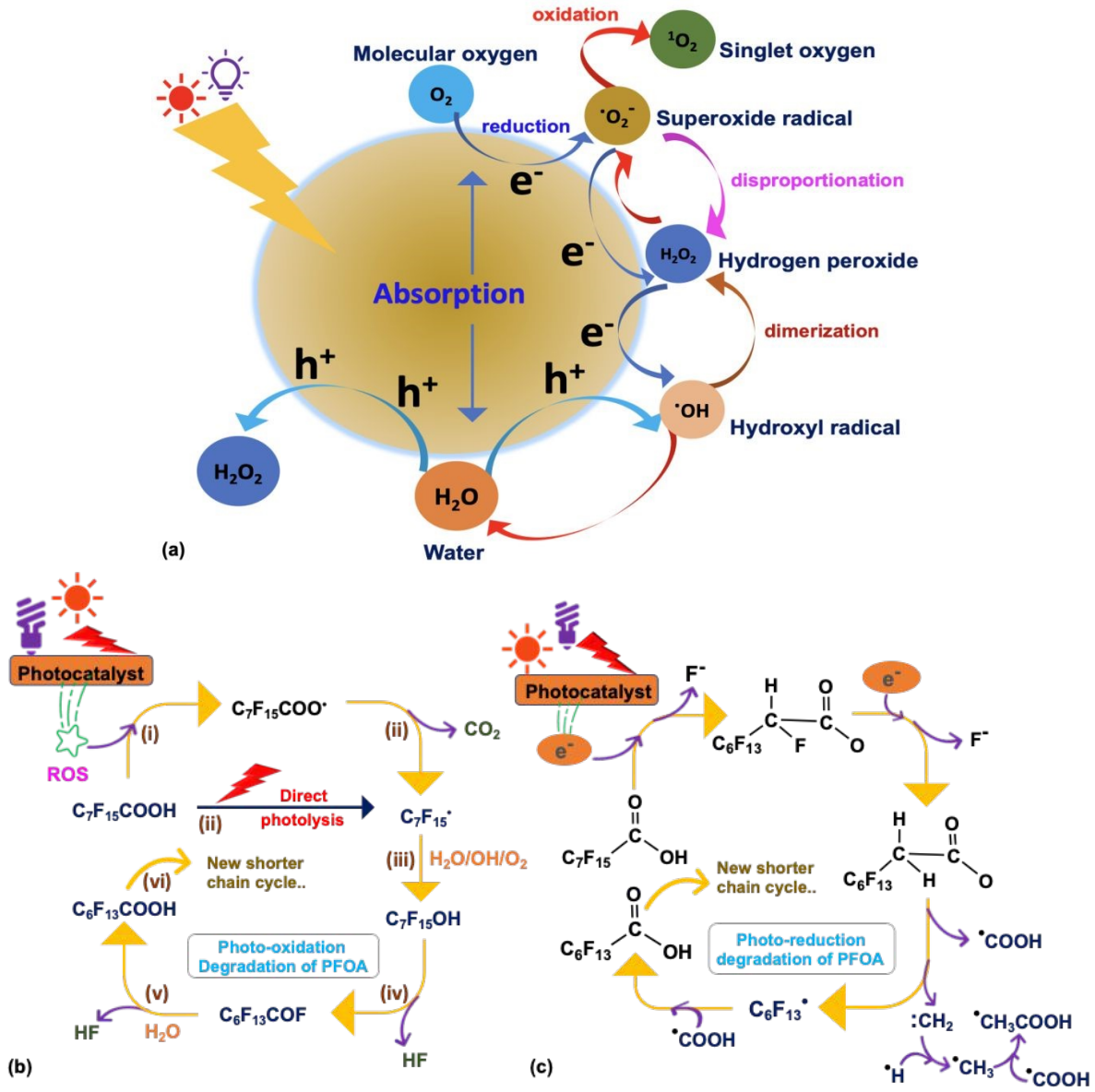

Figure 4. (a) General photocatalytic mechanism depicting electron–hole pair formation and subsequent redox reactions; (b) General pathway of photo-oxidative degradation of PFOA; (c) Typical pathway of photo-reductive degradation of PFOA.

View Article Online
DOI: 10.1039/D5MA01247C

5. Pristine TiO_2 Photocatalysis Performance and Challenges

Among TiO_2 polymorphs, anatase (Eg ≈ 3.2 eV) is the most widely employed for photocatalysis due to its more negative conduction band potential, slower e^--h+ recombination, and higher surface area compared to rutile (~3.0 eV) and brookite (~3.3 eV) [176, 177]. Rutile offers superior thermal stability, and brookite remains underexplored due to synthetic challenges, while anatase generally exhibits higher photocatalytic activity for pollutant degradation under typical conditions, partly because its formation is kinetically favored at temperatures below ~600 °C, leading to smaller crystallite sizes and a higher density of active surface sites [178,179]. TiO_2 synthesis via chemical (sol-gel, hydrothermal, precipitation), physical (thermal oxidation, vapor deposition), or green/biological routes imparts control over size, crystallinity, morphology, and surface chemistry, which govern charge dynamics, reactive oxygen species (ROS) generation, and PFAS adsorption [180-183]. Both commercial TiO_2 (e.g., P25) and laboratory-tailored variants serve as references for mechanistic studies and catalyst development.

Foundational studies show that while TiO_2 efficiently mineralizes conventional organics, PFAS resist degradation due to strong C–F bonds and thermodynamically stable perfluoroalkyl backbones [184-186]. Perfluorocarboxylic acid (PFCA) degradation typically follows a photo-Kolbe decarboxylation pathway, initiated at the terminal carboxyl group (**Fig. 5a**) [185]. Solution pH is a critical factor influencing TiO_2 photocatalytic activity, as it affects surface charge, PFAS adsorption, aggregation, and reactive species generation [186]. The point of zero charge (pH_{pzc}) of TiO_2 is approximately 6.25. PFOA exists as an anion ($C_7F_{15}COO^-$) above its pKa (2.8) [186]. When pH ranges from 2.8 to 6.25, adsorption of $C_7F_{15}COO^-$ on the positively charged TiO_2 surface (Ti–OH_2^+) is enhanced by electrostatic interactions, facilitating oxidative degradation. Above pH 6.25, the surface is negatively charged (Ti–O^-), reducing adsorption and photocatalytic efficiency. Acidic conditions thus favor PFCA adsorption and degradation, whereas perfluorosulfonic acids (PFSAs) show limited reactivity, highlighting functional group–dependent degradability [184]. Panchangama et al. reported >99% decomposition of long-chain PFCAs (PFOA, PFNA, PFDA) under acidic conditions, though overall mineralization reached only 38-54% [185]. Solution pH also influences the distribution and reactivity of key species. Acidic conditions favor heterogeneous ROS-driven oxidation, while alkaline conditions can enhance the formation of hydrated electrons (e_{aq}^-) in homogeneous systems, supporting reductive mineralization pathways. High H_3O^+ concentrations in acidic media can scavenge e_{aq}^-, reducing reductive contributions, whereas alkaline conditions stabilize e_{aq}^-, facilitating C–F bond cleavage and minimizing short-chain PFCA accumulation [160]. Optimal TiO_2 loadings (~0.66 g L^{-1}) enabled complete PFOA removal within 7 h; higher doses reduced efficiency due to light scattering and aggregation. Sonication-assisted TiO_2 photocatalysis under near-neutral conditions improved mass transfer, ROS formation, and dispersion, achieving 64% PFOA degradation over 8 h, with sol-gel TiO_2 outperforming P25 [186]. Surface charge effects were decisive: below the point of zero charge (~pH 6–7), TiO_2 is positively charged, enhancing adsorption; above it, repulsion limits efficiency (**Fig. 5b**).

View Article Online
DOI: 10.1039/D5MA01247C

Reductive TiO_2 photocatalysis complements oxidative pathways for highly resistant PFAS. Conduction-band electrons, stabilized by hole scavengers (e.g., oxalic acid), facilitate the formation of $CO_2^{\bullet-}$ radicals that promote stepwise C–F bond cleavage. Wang et al. achieved 86.7% PFOA degradation at pH 2.47 with oxalic acid (as a hole scavenger) versus 17.8% under perchloric acid (used to maintain the same pH but without providing hole-scavenging ability), with a pseudo-first-order rate constant $k = 1.16 \times 10^{-2}$ min^{-1} (**Fig. 5c**), over 11 times higher than oxidative-only conditions [187-190]. Kinetic and mechanistic studies highlight two key PFAS degradation pathways under UV/O_2, a stepwise photo-redox route generating shorter-chain PFCAs, and a direct β-scission pathway producing CO_2 and HF [191] (**Fig. 5d** and **Fig. 5e**). Fluoride accumulation on TiO_2 surfaces can passivate active sites, limiting mineralization (~32%) and fluoride release (~29%). Oxygen availability modulates pathway selectivity: varying atmospheres (air, O_2, N_2) shifts the balance between photo-redox and β-scission [192]. Biosynthesized TiO_2 nanoparticles offer sustainable alternatives. Plant extracts or microorganisms produce nanoscale TiO_2 with tunable size and morphology, enhancing PFAS adsorption and ROS generation [193-195]. Albizia lebbeck-derived TiO_2 achieved 95.6% PFOS degradation and 56.1% defluorination at pH 2 under UV-vis irradiation [195]. Smaller crystallites (8.8 nm at pH 12 vs 12.1 nm at pH 8) improved charge separation and surface activity, illustrating the dual advantage of green synthesis: environmental benignity and enhanced photocatalytic efficacy. All above studies indicated, pristine TiO_2 efficiently decomposes PFAS under optimized conditions, yet challenges including surface interactions, catalyst passivation, functional group specificity, and reaction condition control constrain complete mineralization, highlighting the need for advanced material design and hybrid strategies.

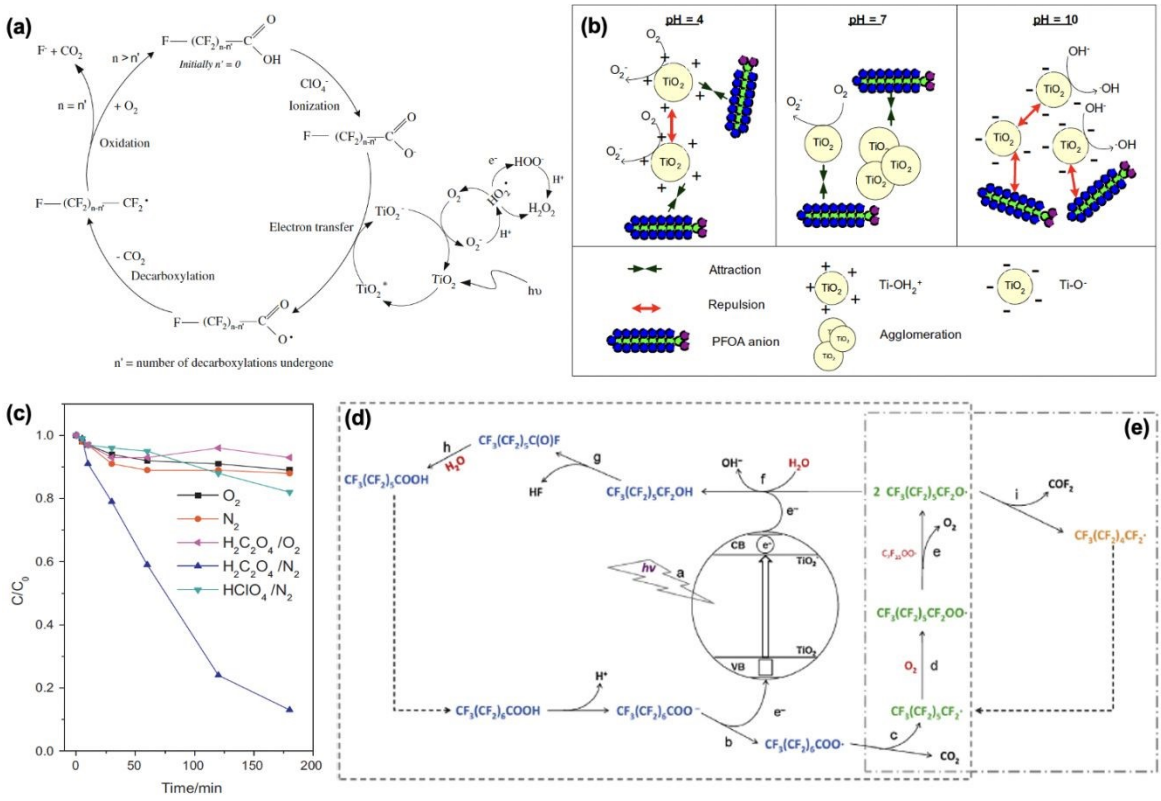

View Article Online
DOI: 10.1039/D5MA01247C

Figure 5. (a) Proposed photocatalytic decomposition cycle of PFCAs on TiO_2 under UV light, involving ionization, electron transfer, decarboxylation, and oxidation. Successive CF_2-unit losses yield shorter-chain PFCAs until complete mineralization to CO_2 and F^- ions, with O_2 serving as the terminal electron acceptor Reproduced from reference [185] with permission from Elsevier BV, copyright 2009; (b) Schematic of TiO_2 surface charge effects on PFOA degradation across pH: $Ti–OH_2^+$ dominates at acidic pH, Ti–OH at neutral (pH 6–7, zero-point charge), and $Ti–O^-$ at basic pH. Despite expected higher degradation at low pH due to electrostatic attraction, experiments showed greater PFOA removal at basic pH (10), indicating radical-driven processes outweigh surface charge effects Reproduced from reference [186] with permission from Elsevier BV, copyright 2009 [186]; (c) Photocatalytic degradation of PFOA by TiO_2 under 254 nm UV. Adsorption was <8%. After 180 min, removal reached 10.5% (O_2), 12.4% (N_2), 6.6% with oxalic acid (O_2), and 86.7% with oxalic acid (N_2). At pH 2.47 ($HClO_4$), only 17.8% removal occurred. Rate constants were 1.16×10^{-2} min^{-1} (oxalic acid) vs. 1.0×10^{-3} min^{-1} ($HClO_4$). Defluorination was 16.5% with TiO_2/oxalic acid but <1% otherwise Reproduced from reference [187] with permission from Elsevier BV, copyright 2011; Proposed reaction mechanism for PFOA degradation in the presence of a TiO_2 photocatalyst, incorporating both photo-redox (d) and β-scission (e) pathways Reproduced from reference [191] with permission from Elsevier BV, copyright 2015 [191].

Murgolo et al. [196] evaluated nanostructured TiO_2 films on stainless steel mesh and P25 TiO_2 (50–100 mg L^{-1}) for groundwater PFOS (200–400 μg L^{-1}) under UV (254 nm, 60 min, pH 7.85), observing negligible degradation and highlighting the importance of reaction optimization. Furtado et al. [197] applied Response Surface Methodology (RSM) to assess pH, catalyst dosage, and irradiation time. Acidic pH enhanced TiO_2 protonation and PFOS adsorption, while moderate catalyst loadings optimized light penetration and active site availability. A 2^2 factorial design (2.23% experimental error) yielded PFOS removal (%) = 27.31 + 2.59 × pH − 4.14 × catalyst dosage. Pareto analysis identified pH as the dominant factor (**Fig. 6a**), and response surface plots (**Fig. 6b**) indicated optimal removal at low pH and moderate-to-high TiO_2 loadings. Under optimized conditions (1.45 g L^{-1} TiO_2, pH 4.0), PFOS (100 μg L^{-1}) degradation reached 83% after 8 h, with predicted maximum oxidation of 86% and initial rate 0.64 h^{-1} (**Fig. 6c**).

Sansotera et al. studied PFOA photomineralization on commercial P25 TiO_2, monitoring TOC and fluoride release, and characterizing the photocatalyst by XPS and XRD [198]. The reaction followed pseudo-first-order kinetics (k_a = 0.033–0.057 h^{-1}) via Kolbe decarboxylation, producing C7 radicals, shorter-chain PFCAs, and HF. FT-IR spectra (**Fig. 6d**) indicated adsorption via carboxylate and C-F interactions within 2-4 h, with transient perfluorinated alcohols at 1210 cm^{-1}, followed by signal reduction after 9 h as mineralization progressed. XPS indicated early-stage surface fluorine (85–90%) with mineralization plateauing at ~32% and fluoride release ~29%. XRD revealed stable anatase (~25 nm) and partially amorphized rutile (47 → 33 nm), highlighting that surface interactions, radical dynamics, and adsorption, rather than crystal structure, control efficiency.

UV irradiation type strongly affects TiO_2 performance. Low-pressure (LPUV, 254 nm) lamps provide narrow spectra, whereas medium-pressure (MPUV, 200-400 nm) lamps deliver higher photon flux and broader irradiation [199]. Ochiai et al. [200] achieved near-complete degradation of 5 mM PFOA using 1.5 wt% P25 under MPUV (250-375 nm, ~600 mW cm^{-2} at 254 nm), with pseudo-first-order kinetics ($k = 8.6 \times 10^{-2}$ dm^3 h^{-1}),~6× faster than direct photolysis

View Article Online
DOI: 10.1039/D5MA01247C

and 5-100× faster than other catalysts (e.g., tungstic heteropoly acid 2.1×10^{-3}, β-Ga_2O_3 1.7×10^{-2} dm³ h^{-1}) [201,202]. **Figure 6e** describes the TiO_2-assisted photocatalytic pathway where MPUV light initiates C–C bond cleavage in PFOA, leading to sequential shortening of perfluoroalkyl chains and eventual mineralization into CO_2 and F^-.

PhotoTOP is a TiO_2-based platform for PFAS precursor characterization that operates under mild conditions (~60 °C) without added chemicals, enabling direct LC-MS analysis with minimal matrix interference [203]. It uses anatase TiO_2 (~390 nm, pH_{pzc} 3.6) to generate steady-state hydroxyl radicals (•OH, 1.1–1.5 $\times 10^{-12}$ M), allowing controlled oxidation that preserves the original perfluoroalkyl chain lengths. This contrasts with the higher-temperature TOP assay (85 °C) and persulfate-based methods, which often produce ultrashort PFCAs such as trifluoroacetic acid due to harsher conditions and stronger chain-shortening potential [203-205]. PhotoTOP quantitatively converted eight PFAA precursors into PFCAs with mass balances of 82–115% after 4 h (**Fig. 6f**), performing reliably across complex matrices including soil extracts (15 mg L^{-1} DOC), PFAS-coated papers, and technical mixtures. Unlike traditional methods, it also allows direct oxidation of solids, capturing non-extractable precursors, although this proceeds approximately 10× slower than extract oxidation. Compared to literature-reported TOP assays and chemical oxidation approaches, PhotoTOP offered milder, more selective oxidation, higher tolerance to matrix effects, and mechanistic insight into precursor–PFCA transformations (R^2 = 0.88). Its main limitation is the need for a controlled UV setup, but this enables reproducible •OH generation and predictable oxidation kinetics. PhotoTOP provided a practical and mechanistically informative approach that bridges analytical characterization and photocatalytic treatment of PFAS precursors, complementing existing methods in the literature.

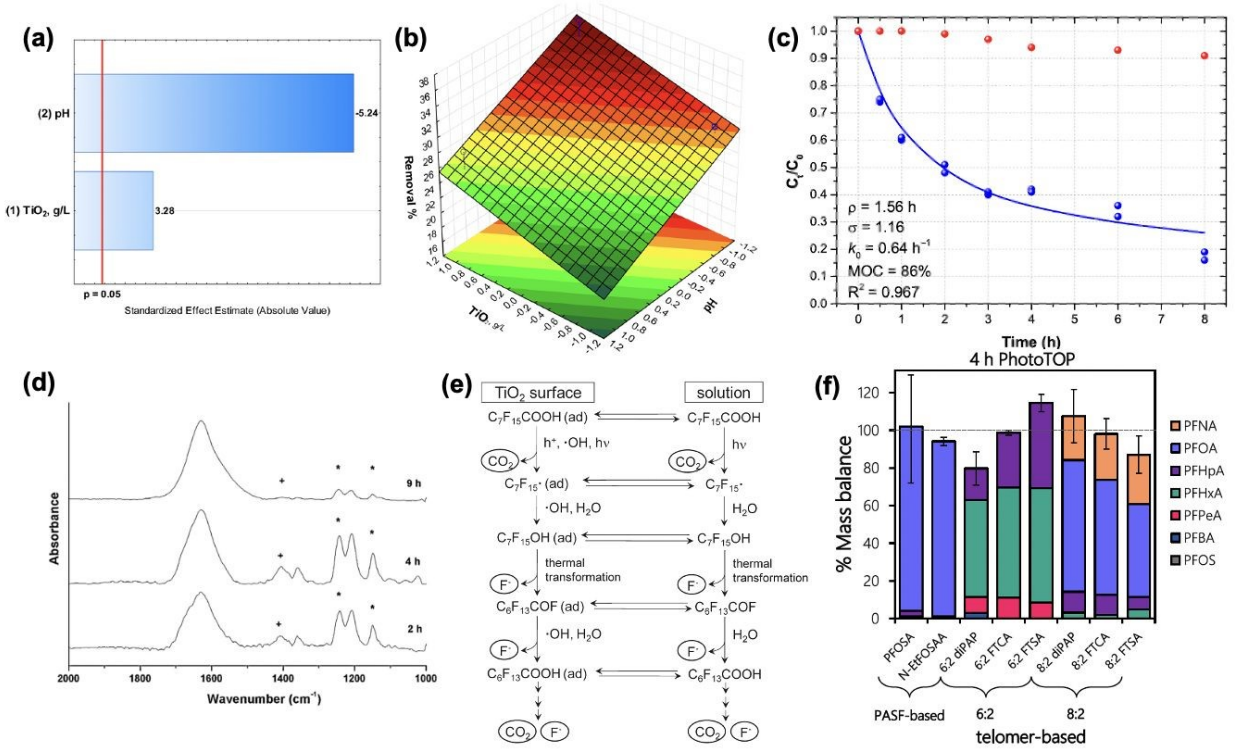

View Article Online
DOI: 10.1039/D5MA01247C

Figure 6. Optimization of PFOS removal using TiO_2/UV photocatalysis via response surface methodology (RSM): (a) Pareto chart showing the relative effects of suspension pH and TiO_2 dosage on PFOS removal; bars crossing the significance line (p = 0.05) indicate statistically significant factors, highlighting pH as the dominant parameter, (b) Response surface plot highlighting maximum removal at low pH with moderate catalyst loading, (c) Time-dependent PFOS degradation measured by HPLC-MS/MS: (blue dots) TiO_2/UV photocatalysis, (red dots) direct photolysis Reproduced from reference [197] with permission from Elsevier BV, copyright 2021; (d) FT-IR spectra of TiO_2 during PFOA photodegradation: Early spectra (2–4 h) show adsorption of PFOA and intermediates via C–F and carboxylate vibrations, while signals decrease after 9 h, reflecting progressive mineralization Reproduced from reference [198] with permission from Elsevier BV, copyright 2014; (e) Stepwise decomposition of PFOA under UV-visible light, showing direct photolysis and TiO_2-assisted photocatalysis. PFOA undergoes sequential C–C cleavage, F^- elimination, and hydrolysis to form shorter-chain perfluorocarboxylic acids, ultimately mineralizing to CO_2 and F^- Reproduced from reference [200] with permission from American Chemical Society, copyright 2011; (f) Mass balance of representative PFAA precursors after 4 h of TiO_2/UV treatment, showing chain-length–dependent PFCA distributions Reproduced from reference [203] with permission from Elsevier BV, copyright 2022 [203].

6. TiO_2 Modification and Hybrid Strategies

Pristine TiO_2 generates reactive species capable of degrading PFAS, however, low visible-light absorption, rapid e^--h^+ recombination, and the high stability of C-F bonds limit its performance. To address these challenges, TiO_2 modifications and hybrid strategies aim to enhance light harvesting, charge separation, and surface reactivity. Approaches include metal and non-metal doping, single-atom incorporation, semiconductor coupling, immobilization on supports, and hybrid system design, all intended to maximize photocatalytic potential for persistent contaminants.

6.1. Modified TiO_2 Systems

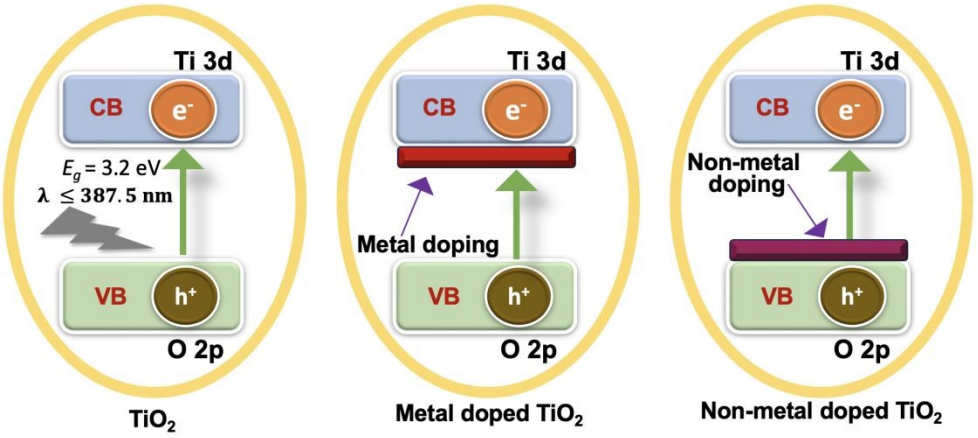

Figure 7. Schematic illustrating the effects of metal and non-metal dopants on the properties and activity of TiO_2-based photocatalysts.

View Article Online
DOI: 10.1039/D5MA01247C

Metal and non-metal doping of TiO_2 is a widely employed strategy to enhance photocatalytic activity under visible light, addressing the intrinsic wide bandgap of anatase TiO_2 (~3.2 eV) that limits UV-only activation [206-209] (**Fig. 7**). Metal doping introduces mid-gap states, improves visible-light absorption, promotes charge separation, and generates oxygen vacancies that facilitate PFAS adsorption and reactive oxygen species formation [210. 204]. Transition metals (Fe, Co, Cu) create Ti^{3+} centers and oxygen defects; noble metals (Ag, Au, Pt) enhance interfacial charge transfer and suppress e^-–h^+ recombination; rare-earth metals (La^{3+}, Ce^{3+}, Gd^{3+}, Nd^{3+}) serve as electron traps and increase surface area [210-214]. Dopants are incorporated via sol-gel, hydrothermal, electrospinning, or surface impregnation methods [215,216]. Non-metal doping (N, S) extends visible-light activity without metal toxicity by introducing states above the valence band and narrowing the bandgap. Substitutional N (~0.14 eV above VB) and interstitial N (~0.73 eV) reduce the bandgap to ~2.6 eV, while S lowers it from 3.203 eV to 2.753–2.545 eV depending on concentration [217-220]. Excessive doping can create recombination centers, necessitating careful optimization [221]. Although extensively studied in general photocatalysis, their application for PFAS degradation on TiO_2 remains emerging. Early reports suggest that such modifications enhance visible-light absorption, promote charge separation, and increase ROS generation, thereby potentially improving degradation kinetics and defluorination efficiency.

Estrillan et al. [222] demonstrated visible-light photocatalytic degradation of PFOA using Fe and Nb co-doped TiO_2 (Fe:Nb-TiO_2) via sol-gel synthesis. XRD confirmed retention of the anatase phase with reduced crystallite size (~15 nm), suppressing anatase-to-rutile transformation. Under UV-vis irradiation (200-600 nm) with 0.1 mM PFOA, pH 4.3, and catalyst loading of 0.5 g L^{-1}, Fe:Nb-TiO_2 achieved nearly double the degradation efficiency of SG-TiO_2, whereas AO-TiO_2 P25 showed minimal activity. Enhanced performance was attributed to larger surface area (>120 m^2/g vs ~100 m^2/g for SG-TiO_2), Fe^{3+}-induced bandgap narrowing (~3.2 → 2.8 eV), and Nb^{5+} sites that trap photogenerated electrons, suppressing recombination and extending visible-light absorption. Maximum PFOA removal occurred at pH 4 due to electrostatic attraction between negatively charged perfluorooctanoate anions and positively charged TiO_2, facilitating valence band hole-driven oxidation. At neutral or higher pH, surface speciation shifts to Ti-OH or Ti-O^-, weakening adsorption, while the Fe-TiO_2 point of zero charge (pzc 7.2) and PFOA's low pKa (2.8) limit adsorption and photocatalytic activity under alkaline conditions [185-186].

UV-activated TiO_2 modified with transition metals such as Fe and Cu was studied for PFOA degradation (**Fig. 8a-Fig. 8c**) [223]. XRD characterization revealed mixed anatase-rutile phases, with Fe-TiO_2 containing zero-valent Fe and Cu-TiO_2 showing Cu^0 and Cu_2O. Under UV irradiation (0.5 g L^{-1} catalyst, pH 5, 298 K, 12 h), Cu-TiO_2 achieved 91% PFOA decomposition with 19% defluorination, outperforming UV/TiO_2 (14% decomposition) and UV/Fe-TiO_2 (69% decomposition, 9% defluorination). Enhanced activity of Cu-TiO_2 arises from stronger electron trapping via Cu^0/Cu^+ species, suppressing e^-/h^+ recombination more effectively than Fe^{2+}/Fe^0 (standard reduction potentials: +0.34 V vs −0.44 V), increasing valence band hole availability [224]. Cu deposition also introduces localized energy levels in the TiO_2 bandgap, enhancing UV absorption, while redox cycling of Cu facilitates electron transfer and perfluoroalkyl radical formation. Studied by Li et al. [225], noble-metal-doped TiO_2 (Pt, Pd, Ag) was investigated for PFOA degradation. Unlike transition metals, noble metals with high work functions efficiently

View Article Online
DOI: 10.1039/D5MA01247C

capture electrons, suppress e^-/h^+ recombination, and enhance valence band hole-driven oxidation, with localized surface plasmon resonance (LSPR) extending absorption into the visible range [226,227]. Li et al. [225] reported Pt-, Pd-, and Ag-modified TiO_2 (5 nm metal nanoparticles on 20-40 nm TiO_2 aggregates) for PFOA degradation. At pH 3, 60 mg L^{-1} PFOA, and 0.5 g L^{-1} catalyst, Pt-TiO_2 achieved 100% decomposition and 34.8% defluorination after 7 h UV irradiation, with a pseudo-first-order rate constant 12.5× higher than pure TiO_2. Pd-TiO_2 and Ag-TiO_2 achieved 94.2% and 57.7% decomposition with defluorination of 25.9% and 8.1%, respectively. Larger work functions of Pt (5.65 eV), Pd (5.55 eV), and Ag (4.26 eV) form Schottky barriers, efficiently trapping conduction-band electrons. Degradation proceeds via h_{VB}^+-driven stepwise CF_2 cleavage, producing shorter-chain PFCAs and fluoride ions (**Fig. 8d** and **Fig. 8e**). Rate constants increase with higher initial PFOA concentrations, demonstrating sustained photoactivity under elevated pollutant loads.

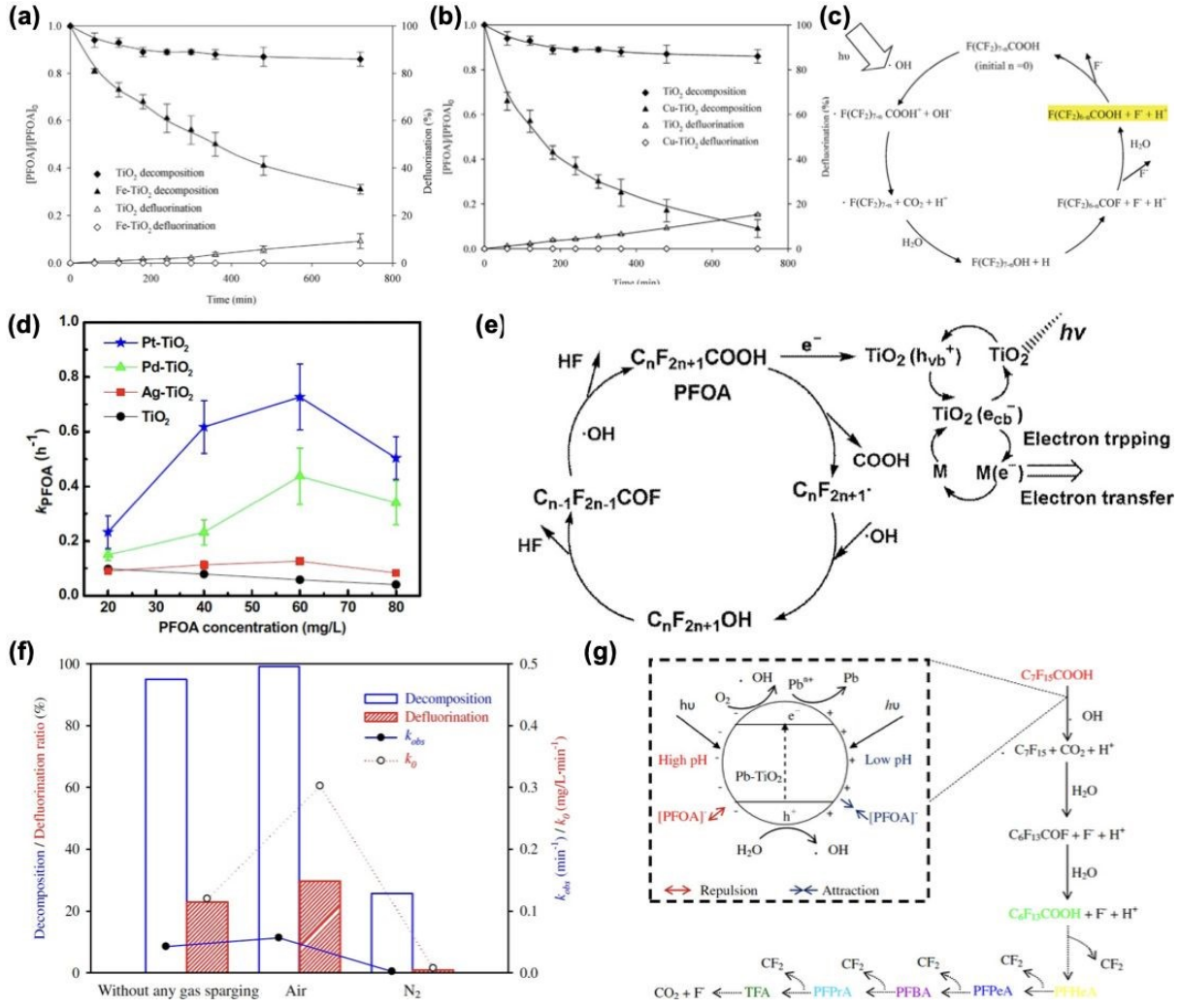

Figure 8. Photocatalytic degradation of PFOA using TiO_2-based materials: (a) Comparison of degradation and defluorination efficiency: bare TiO_2 (~14% degradation in 12 h), Fe–TiO_2 (~69% degradation, 9% defluorination), (b) Cu–TiO_2 (~91% degradation, 19% defluorination), (c) Schematic of PFOA

View Article Online
DOI: 10.1039/D5MA01247C

decomposition under UV/TiO_2: •OH-mediated C–C bond cleavage and stepwise defluorination to shorter-chain PFCAs and F^-, with Fe or Cu doping enhancing •OH generation and electron–hole separation Reproduced from reference [223] with permission from Elsevier BV, copyright 2015; (d) Rate constants for PFOA degradation using pure TiO_2 and noble-metal-doped TiO_2, Pt and Pd show superior electron-trapping effects, (e) Mechanism of PFOA degradation on TiO_2 and M–TiO_2: UPLC–MS showed stepwise CF_2 loss, mainly forming PFHpA (up to 19.1 mg/L). Pt–TiO_2 and Pd–TiO_2 accelerated PFHpA generation (16–19 mg/L in 3–5 h) vs Ag–TiO_2 (9.7 mg/L in 7 h). About 80% F^- remained in solution, with ~20% lost to adsorption/gas. Decomposition followed Kolbe decarboxylation and HF elimination, yielding shorter PFCAs, CO_2, and F^- Reproduced from reference [225] with permission from Elsevier BV, copyright 2016; Photocatalytic decomposition of PFOA by Pb–TiO_2: (f) PFOA decomposition and defluorination under different pH and atmospheres: highest at pH 3 (~99%/30%) with air; low under N_2 (~26%/1%), (g) Mechanistic pathway: UV-excited Pb–TiO_2 generates perfluoroalkyl radicals that undergo stepwise HF elimination and hydrolysis, forming shorter-chain PFCAs and finally CO_2 and F^-. Pb improves efficiency by trapping electrons and reducing electron–hole recombination Reproduced from reference [228] with permission from Elsevier BV, copyright 2016.

Pb-modified TiO_2 has emerged as an effective non-noble alternative. Pb introduced via photodeposition maintains the anatase-rutile framework, with XRD confirming Pb^0, PbO, and PbO_2 incorporation without lattice disruption [228]. Pb species act as electron traps, enhancing charge separation. Under UV irradiation, Pb-TiO_2 exhibited a pseudo-first-order rate constant of 0.5136 h^{-1}, 32.5× higher than UV/TiO_2 (0.0158 h^{-1}), achieving nearly complete PFOA decomposition (99.9%) in 12 h, with a half-life of 1.3 h compared to 43.9 h for pristine TiO_2. Acidic conditions (pH 3) and O_2-rich environments further promoted decomposition via •OH formation, while N_2 sparging drastically reduced activity (**Fig. 8f**). Mechanistic analysis (**Fig. 8g**) indicates sequential C-C cleavage, •OH attack, and chain shortening to CO_2 and F^-, with Pb acting as an efficient electron trap. Optimal Pb:TiO_2 ratio (2:100) and catalyst loading (0.5-1.0 g L^{-1}) maximized degradation efficiency. Compared to noble-metal TiO_2, Pb-TiO_2 leverages acidic, oxygenated conditions to achieve faster kinetics and more complete degradation, highlighting the potential of strategic heavy-metal doping for PFAS remediation. Noble-metal doped TiO_2 catalysts (Pt, Pd, Ag) achieve faster and more complete PFOA degradation with higher defluorination than transition-metal doped TiO_2, highlighting the effect of dopant type on both reaction kinetics and partial mineralization. Pb–TiO_2 also shows high activity, reaching 99.9% degradation and 22.4% defluorination in 7 h [228], comparable to Pt–TiO_2 but slightly lower in defluorination. Among transition metals, Cu–TiO_2 shows moderate performance, while Fe–TiO_2 is less effective, and Fe:Nb-TiO_2 mainly promotes stepwise chain-shortening [222,227].

6.2. Single-Atom Catalysis (SACs) on TiO_2

Single-atom catalysts (SACs) have gained considerable attention in photocatalysis due to maximal metal atom utilization, uniform active sites, and unique reaction pathways compared to conventional nanoparticles [229-231]. TiO_2-based SACs are particularly attractive for PFAS remediation, as isolated metal atoms can modulate charge separation, electronic structure, and interfacial interactions, enhancing pollutant degradation [232,233].

View Article Online
DOI: 10.1039/D5MA01247C

Weon et al. (2021) demonstrated the integration of facet-engineered TiO_2 with single-atom Pt (Pt_1) cocatalysts [51]. Anatase TiO_2 crystals with {001} and {101} facets were synthesized, with fluoride ions stabilizing {001} (~80% surface area) and APTMS anchors selectively immobilizing $PtCl_6^{2-}$ on {101}, followed by photoreduction to atomically dispersed Pt_1 (~0.2 nm, confirmed by HAADF-STEM). This design exploited intrinsic band-driven charge separation, electrons migrate to {101} and holes to {001}, ensuring site-specific Pt_1 placement and maximizing electron utilization. Pt_1/facet-engineered TiO_2 produced ~5× more $^{\bullet}OH$ than PtNP/TiO_2 and ~2× more than bare P25 TiO_2, achieving ~15× higher PFOA degradation ($k = 0.15\ min^{-1}$ vs $0.01\text{-}0.02\ min^{-1}$ for controls; **Fig. 9a**). Quenching and EPR studies revealed selective $^{\bullet}OH$ generation, enabling a reductive hydro defluorination pathway (**Fig. 9b**). The single-atom design facilitated (i) efficient electron transfer from the TiO_2 conduction band to Pt_1, (ii) selective proton reduction forming Pt-$H^{\delta-}$ species, and (iii) hydrogen spillover onto TiO_2 to generate reactive Ti-$H^{\delta+}$ species that cleave C-F bonds, forming Ti-F. XPS confirmed Ti-F formation, and fluorine mass balance indicated ~58% retention in Ti-F bonds, with minimal free F^- or HF. This accumulation of Ti–F bonds represented a key catalyst deactivation pathway, as surface fluorination progressively blocks active Ti–OH sites and suppresses interfacial redox reactions. Importantly, Weon et al. demonstrated that this fluoride-induced deactivation is fully reversible. A mild NaOH washing step converted inactive Ti–F back to catalytically active Ti–OH ($>Ti–F + OH^- \leftrightarrow >Ti–OH + F^-$), restoring photocatalytic activity without Pt loss or aggregation. This regeneration strategy directly addresses long-term durability concerns by decoupling high defluorination efficiency from permanent catalyst poisoning. Moreover, the atomically dispersed Pt_1 remained stable during reaction and regeneration cycles, indicating strong metal–support interactions and resistance to sintering or leaching, two common degradation routes in Pt nanoparticle-based systems. This work highlights the synergistic effect of facet engineering and single-atom cocatalysts for dual-pathway PFAS degradation with minimal noble-metal usage.

View Article Online
DOI: 10.1039/D5MA01247C

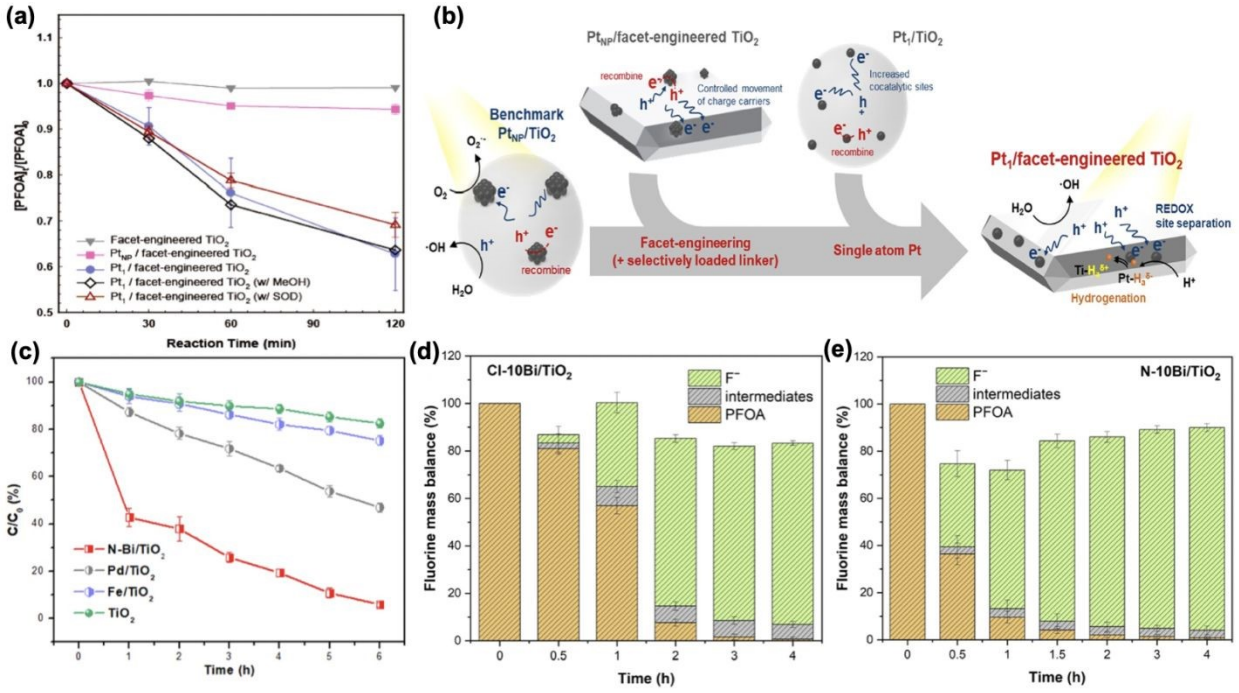

Figure 9. Photocatalytic hydrodefluorination of PFOA using Pt-loaded TiO_2: (a) Facet-engineered TiO_2 shows negligible PFOA degradation, Pt nanoparticle/TiO_2 improves performance moderately, and single-atom Pt_1/facet-engineered TiO_2 achieves the highest degradation, with a pseudo-first-order rate constant ~15× higher than PtNP/TiO_2, demonstrating efficient C–F bond hydrodefluorination. (b) Single-atom Pt_1/TiO_2 and Pt_1/facet-engineered TiO_2 show higher PFOA degradation than Pt nanoparticles due to efficient hydrogen spillover. Ti–F bonds form (58% of fluorine), with negligible free fluoride. Performance decline from Ti–F accumulation is reversible via NaOH. Facet engineering with Pt_1 shifts the pathway from $O_2^{\bullet-}$ to surface hydrogen species, enabling effective hydrodefluorination; Photocatalytic defluorination of PFOA by Bi single-atom-loaded TiO_2 Reproduced from reference [51] with permission from American Chemical Society, copyright 2021; (c) Pure TiO_2 shows low PFOA degradation (~15%) and defluorination (~2%). Fe or Pd doping slightly improves activity, while Bi single atoms (Bi SAs) significantly enhance defluorination (up to 70%), (d) Under xenon lamp, N-10Bi/TiO_2 achieves complete PFOA removal within 2 h and high defluorination (~85%) after 4 h, outperforming Cl-10Bi/TiO_2, (e) Short-chain PFCAs (PFHpA, PFHxA, PFPeA) are detected as intermediates. N-10Bi/TiO_2 shows rapid defluorination and maintains >65% activity over four cycles, demonstrating stability and practical potential Reproduced from reference [234] with permission from American Chemical Society, copyright 2023.

As an alternative to noble-metal modification strategies, non-precious single-atom catalysts (SACs) have gained increasing attention. In this context, Bi single-atom catalysts (Bi-SACs) on TiO_2, synthesized via green, UV-assisted methods, exhibit uniform metal dispersion and strong photocatalytic performance [234]. N-Bi/TiO_2 (from $Bi(NO_3)_3$) and Cl-Bi/TiO_2 (from $BiCl_3$ forming BiOCl nanoclusters) were investigated for PFOA degradation. N-10Bi/TiO_2 achieved ~85% defluorination under xenon lamp irradiation in 4 h, while Cl-10Bi/TiO_2 reached ~76% (**Fig. 9c-9e**). Pristine TiO_2 and Fe- or Pd-modified TiO_2 showed negligible activity. Enhanced performance of Bi-TiO_2 arises from improved charge separation (photocurrent, EIS), side-on PFOA adsorption, and Bi···F interactions that polarize C-F bonds, as supported by DRIFTS, DFT, and FDTD simulations

View Article Online
DOI: 10.1039/D5MA01247C

[235]. Unlike Pt_1/TiO_2 systems that proceed via reductive hydrodefluorination, Bi-TiO_2 operates through oxidative-defluorination, enabling rapid breakdown of PFOA and shorter-chain PFCAs. N-10Bi/TiO_2 also demonstrated excellent recyclability, maintaining >90% PFOA removal over four cycles with only slight decreases in defluorination (~65%). These results establish Bi-TiO_2 as an efficient, stable, and sustainable non-noble-metal SAC for PFAS remediation.

6.3. Hybrid Photocatalysts

Hybrid photocatalysts have been widely investigated for PFAS remediation, wherein TiO_2 is integrated with complementary materials to tailor its physicochemical and photochemical characteristics and broaden its functional scope. This section discusses key hybridization strategies **studied for PFAS degradation**, including coupling TiO_2 with other semiconductors or oxides to form heterojunctions or Z-scheme architectures, carbon-modified TiO_2 to facilitate electron transport and pollutant adsorption, and the integration of advanced material hybrids.

6.3.1. TiO_2 Coupled with Other Semiconductors or Oxides

TiO_2-based heterojunctions have been explored as a means to modify charge-transfer pathways and light-response characteristics for PFAS degradation [236,237]. Coupling TiO_2 with semiconductors such as Sb_2O_3, BiOBr, BN, or ReS_2 enables the formation of type-II, p–n, and S-scheme heterojunctions, promoting spatial separation of charge carriers and expanded utilization of visible light. These hybrid systems provide additional electron- and hole-driven pathways that help degrade persistent PFAS.

Yao et al. developed mesoporous Sb_2O_3/TiO_2 heterojunctions for PFOA degradation [238]. SEM and TEM revealed bowl-like anatase TiO_2 particles (~10 nm) uniformly embedded with Sb_2O_3 nanocrystals, producing red-shifted light absorption and a narrowed bandgap (3.30 → 2.91 eV). At 10 ppm PFOA and 0.25 g L^{-1} catalyst, 3%-Sb_2O_3/TiO_2 achieved 81.7-81.8% removal in 120 min, with a pseudo-first-order rate constant 4.2× faster than P25 (12.6×10^{-3} min^{-1} vs 6.3×10^{-3} min^{-1}, **Fig. 10a**). ESR, PL, and TR-PL analyses identified $O_2^{\bullet -}$ and h^+ as dominant reactive species, while $^{\bullet}OH$ was negligible, indicating a shift from conventional hydroxyl-mediated pathways (**Fig. 10b**).

BiOBr-modified P25 (P25/BiOBr) forms a p-n heterojunction, facilitating efficient charge separation [239]. Under simulated solar irradiation, P25/BiOBr achieved 99.7% PFOA degradation within 100 min, outperforming P25 (<1%), BiOBr alone (13.4%), and commercial In_2O_3 (16.8%, **Fig. 10c**) [240]. ATR-FTIR and adsorption studies indicated unidentate binding of PFOA to Bi^{3+}, enhancing surface adsorption (q_m = 21.94 mg g^{-1}) and direct hole-mediated oxidation. Mechanistically, photogenerated holes dominated, with negligible contribution from $^{\bullet}OH$, electrons, or superoxide anions, consistent with BiOBr's VB energy (1.99 V vs NHE) being insufficient for water oxidation (**Fig. 10d**) [241242]. In real water from Tangxun Lake (pH 3.5), degradation was efficient but slowed at natural pH 6.8 due to reduced adsorption and competing ions (Cl^-, SO_4^{2-}, NO_3^-) and NOM, low NO_3^- or humic acid (~10 mg L^{-1}) enhanced removal, while higher concentrations (>100 mg L^{-1}) inhibited it [243].

View Article Online
DOI: 10.1039/D5MA01247C

The development of BN/TiO_2 composites advanced PFAS photocatalysis degradation [36]. Combining commercial TiO_2 (P25, 80 wt% anatase/20 wt% rutile, 21 nm) with hexagonal BN (~1 µm) via simple calcination forms a type-II n-n heterojunction that promotes efficient interfacial charge separation [244,245]. UPS and diffuse reflectance UV-vis spectroscopy revealed valence band positions of -7.0 eV (TiO_2) and -6.9 eV (BN), with band gaps of 3.1 eV and 5.4 eV, respectively. This configuration allows TiO_2 photoexcitation under UV-C (254 nm) and UV-A (365 nm), while BN primarily facilitates e^--h^+ separation. Transient photocurrent measurements showed ~47× and ~70× higher steady-state current for BN/TiO_2 relative to BN and TiO_2, indicating enhanced charge separation and reduced recombination. Under UV-A, BN/TiO_2 degraded 120 µM PFOA to <2.4 µM within 120 min (t½ = 55 min), compared to 77 µM remaining with TiO_2 alone (t½ ≈ 350 min), achieving 37% versus 19% defluorination. Under UV-C, BN/TiO_2 further accelerated mineralization (t½ = 13 min) and reached >50% defluorination after 60 min, outperforming BN (t½ = 10 min, 29% defluorination) and TiO_2 (t½ = 80 min, 7% defluorination, **Fig. 10e**). BN/TiO_2 also showed practical advantages, requiring fluence doses of ~4-8 J cm^{-2} and EE/O_{output} values of 102 and 253 kWh m^{-3} $order^{-1}$ under UV-C and UV-A, representing >10× improved energy efficiency compared to TiO_2.

Chen et al. constructed an S-scheme ReS_2-TiO_2 heterostructure via electrostatic self-assembly, combining oppositely charged semiconductors to enhance interfacial electron transfer and suppress recombination [246]. TEM and elemental mapping confirmed uniform Re, S, Ti, and O distribution, while XPS and Raman analyses revealed increased oxygen vacancies (21 to 26%) and surface -OH groups (13 to 17%), boosting radical generation. Photocatalytic tests demonstrated that 2% ReS_2-TiO_2 achieved 98% PFOA removal with ~75% defluorination in 120 min under UV, surpassing TiO_2 (62%) and ReS_2 alone. Radical trapping and ESR studies identified $^{\bullet}O_2^-$ and $^{\bullet}OH$ as dominant species, with ReS_2 coupling significantly enhancing their formation. In-situ XPS and DFT calculations elucidated the S-scheme mechanism: an internal electric field drives electron transfer from TiO_2 to ReS_2 in the dark, while upon illumination, TiO_2 CB electrons migrate to ReS_2 VB, promoting charge separation, extending carrier lifetime, accelerating electron transfer, and increasing active site availability (**Fig. 10f-h**) [247,248]. For TiO_2 heterojunctions, 3% Sb_2O_3/TiO_2 achieved 81.8% PFOA degradation in 2 h [238], BiOCl/TiO_2 reached 96% degradation with 82% defluorination in 8 h, BiOBr/TiO_2 showed 100% degradation and 65% defluorination in 8 h, BiOI/TiO_2 gave 88% degradation with ~20% defluorination in 8 h [239], BN/TiO_2 degraded 120 µM PFOA to <2.4 µM in 120 min with 37% defluorination under UV-A and >50% under UV-C in 60 min [36], and ReS_2-TiO_2 (2 wt%) removed 98% PFOA with ~75% defluorination in 120 min [246].

View Article Online
DOI: 10.1039/D5MA01247C

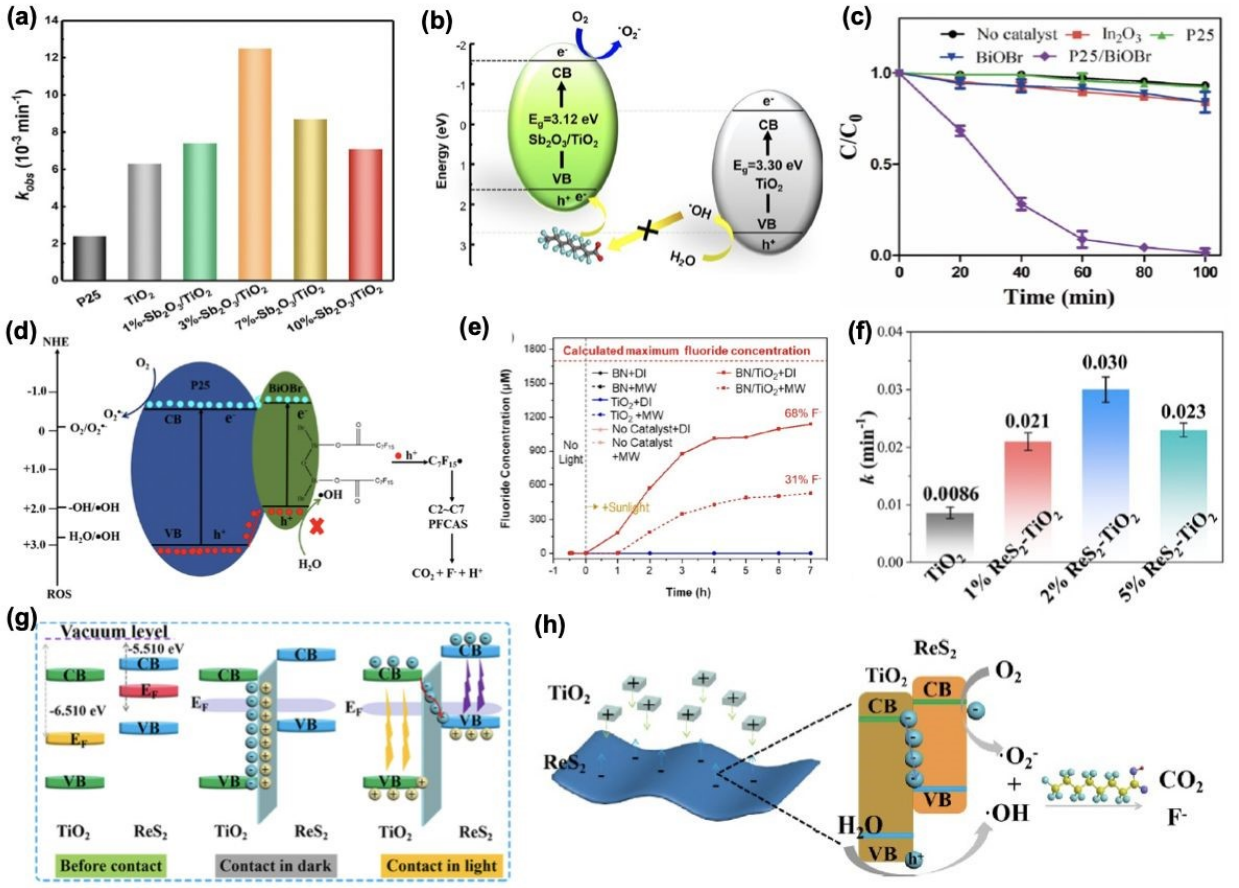

Figure 10. Photocatalytic degradation of PFOA: (a) Comparison of calculated degradation rate constants for P25, TiO_2, and TiO_2 modified with 1%, 3%, 7%, and 10% Sb_2O_3, (b) Schematic showing how the 3%-Sb_2O_3/TiO_2 heterojunction enhances photocatalytic PFOA degradation Reproduced from reference [238] under the Creative Commons Attribution (CC BY); (c) PFOA degradation under simulated solar light, where P25/BiOBr achieved 99.7% removal in 100 min, significantly higher than BiOBr (13.4%), commercial In_2O_3 (16.8%), P25, or blank, attributed to its high adsorption capacity ($q_{\square}$ = 21.94 mg g^{-1}), (d) Proposed photodegradation pathway over P25/BiOBr: holes generated on P25 migrate to BiOBr, oxidizing adsorbed PFOA, followed by stepwise decarboxylation and hydrolysis, producing short-chain PFCAs and ultimately CO_2 and F^- Reproduced from reference [239] with permission from Elsevier BV, copyright 2022; (e) Fluoride ion release profiles during PFOA degradation under natural sunlight irradiation using BN/TiO_2, compared with controls Reproduced from reference [36] with permission from Elsevier BV, copyright 2022; (f) Degradation rate constants for different x% ReS_2-TiO_2 samples, (g) Proposed electron transfer mechanism in the ReS_2–TiO_2 S-scheme heterostructure, illustrating band bending and internal electric field formation driven by Fermi level differences, (h) Proposed photocatalytic mechanism of the ReS_2–TiO_2 system under UV irradiation, showing charge transfer, oxygen vacancy trapping, radical generation ($\cdot O_2^-$, $\cdot OH$), and subsequent PFOA degradation Reproduced from reference [246] with permission from Elsevier BV, copyright 2025.

View Article Online
DOI: 10.1039/D5MA01247C

6.3.2. Carbon-Based Hybrid Photocatalysts

Carbon materials enhance TiO_2 photocatalysis by improving charge transfer, suppressing electron–hole recombination, and increasing pollutant adsorption [249-253]. π-Conjugated structures act as electron reservoirs, enabling rapid electron migration, while the high surface areas of carbon nanotubes, graphene, and activated carbon concentrate pollutants near catalytic sites. This synergy boosts reactive oxygen species generation and extends TiO_2's light response into the visible range.

Fe/TNTs@AC demonstrated a "concentrate-and-destroy" mechanism, achieving 91.3% PFOA removal in 4 h UV irradiation, outperforming TNTs@AC (23.8%), non-calcined Fe/TNTs@AC (68.7%), and calcined TNTs@AC (83.3%) (**Fig. 11a**) [254]. Fe modification and calcination enhanced defluorination (~62% of PFOA-bound F^-), 1.5-4× higher than other materials. Optimal calcination (550 °C) and 1 wt% Fe loading maximized performance. Fe/TNTs@AC adsorbed ~99% of PFOA over pH 4-11 within 2 h, with α-Fe_2O_3/TNTs interacting electrostatically with the carboxylate head and AC providing hydrophobic and anion-π interactions with the tail [255]. Adsorption orientation shifted from side-on (acidic/neutral) to tail-on (alkaline), slightly reducing defluorination at pH ≥ 9. Reusability tests confirmed stable adsorption (>99%) and ~60% defluorination over six cycles, with minimal Fe (<1.7 mg L^{-1}) and no Ti leaching. Mechanistic studies revealed h^+-driven oxidation as dominant, with $^{\bullet}OH$ mediating stepwise defluorination of perfluoroalkyl radicals, $^{\bullet}O_2^-$ was negligible (**Fig. 11b**). Fukui index and ESP analyses identified the carboxylate head as the primary reactive site, supporting the proposed degradation pathway [256].

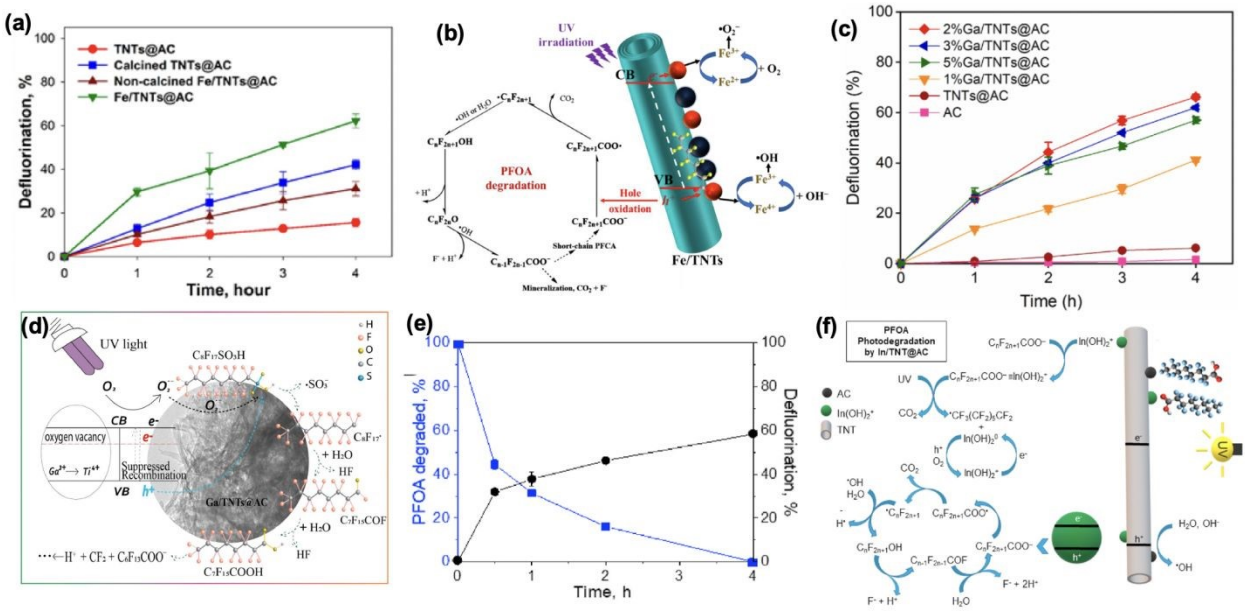

Figure 11. (a) Photocatalytic defluorination of PFOA, showing ~62% conversion of organic fluorine to F^- by Fe/TNTs@AC under UV irradiation, significantly higher than TNTs@AC and other controls, (b) Proposed photocatalytic degradation mechanism of PFOA on iron (hydr)oxide-impregnated nanoparticles under UV irradiation, showing adsorption, hole/electron generation, radical formation, and stepwise defluorination

View Article Online
DOI: 10.1039/D5MA01247C

via photo-Kolbe-like decarboxylation Reproduced from reference [254] with permission from Elsevier BV, copyright 2020; (c) Kinetics of PFOS defluorination for neat AC, TNTs@AC, and Ga/TNTs@AC with varying Ga content under UV irradiation, (d) Proposed mechanism for enhanced solid-phase photocatalytic degradation and defluorination of PFOS by Ga/TNTs@AC, highlighting multi-point adsorption, Ga-induced oxygen vacancies, charge separation, and generation of reactive species (h^+ and $O_2^{\bullet-}$) Reproduced from reference [257] with permission from Elsevier BV, copyright 2021 [257]; (e) Photodegradation and defluorination of PFOA pre-adsorbed on In/TNTs@AC under UV irradiation, showing rapid degradation (>50% in 30 min) and ~60% defluorination after 4 h, (f) Proposed stepwise photocatalytic degradation and defluorination pathway of PFOA on In/TNTs@AC, highlighting dual adsorption, In-facilitated redox cycling, and formation of perfluoroalkyl intermediates during UV irradiation Reproduced from reference [260] with permission from Elsevier BV, copyright 2022.

Titanate nanotubes (TNTs) have been further modified to enhance photocatalytic PFAS degradation through metal doping and carbon integration [257-260]. Gallium-doped TNT-activated carbon composites (Ga/TNTs@AC) demonstrated synergistic adsorption-photocatalysis for PFOS removal. Both TNTs@AC and 2%Ga/TNTs@AC achieved near-complete PFOS adsorption within 10 min, far exceeding bare AC (equilibrium in 120 min) despite its higher surface area [257] Langmuir analysis indicated a maximum surface-area-normalized adsorption capacity of 0.225 mg/m² for 2%Ga/TNTs@AC, ~2.1× higher than AC, highlighting the combined effects of Ga doping and AC in creating electrostatic, hydrophobic, and π-anion binding sites [258,259]. Under UV irradiation, 2%Ga/TNTs@AC achieved 75.0% PFOS degradation and 66.2% defluorination within 4 h, significantly outperforming TNTs@AC (13.1%/6.2%) and AC alone (**Fig. 11c**), with the underlying mechanism illustrated in **Fig. 11d**. The system exhibited broad pH tolerance (3.5-10.5), with alkaline conditions favoring $O_2^{\bullet-}$ generation and defluorination. XPS and EPR confirmed Ga^{3+} induced oxygen vacancies that acted as electron traps, improving charge separation and ROS formation, supported by reduced PL emission.

Indium-doped TNT-AC composites (In/TNTs@AC) were developed for PFOA remediation [260]. Characterization showed an interwoven TNT-AC framework, with In present mainly as In_2O_3 and minor In^0 phases [261,262]. XRD confirmed anatase retention with reduced interlayer spacing, while FTIR and N_2 adsorption indicated partial surface-group removal and slightly reduced pore volume, favoring PFOA adsorption. Batch tests achieved >99% PFOA removal within 30 min via hydrophobic and electrostatic/Lewis acid-base interactions at In_2O_3 sites [263]. Under UV irradiation, In/TNTs@AC achieved nearly complete PFOA degradation within 4 h with ~60% defluorination, outperforming AC, TNTs@AC, and In_2O_3@AC due to synergistic adsorption and enhanced charge separation via heterojunction formation (**Fig. 11e** and **Fig. 11f**). TNT-based composites exhibit clear dopant-dependent behavior in PFAS degradation [254,257,260]. Fe modification promotes redox-driven pathways and enhances defluorination, Ga doping improves oxygen-vacancy-mediated charge separation favoring sulfonated PFAS removal, and In doping enables combined hydrophobic and Lewis acid–base adsorption with In_2O_3 heterojunction-assisted photocatalysis, favoring carboxylated PFAS. Overall, dopant selection governs charge transport, vacancy chemistry, and PFAS-specific interactions, providing a mechanistic basis for rational design of TNT-based photocatalysts.

View Article Online
DOI: 10.1039/D5MA01247C

Multi-walled carbon nanotubes (MWCNTs) serve as supports to improve adsorption and charge separation [264]. TiO_2-MWCNT composites synthesized via sol-gel with varying TiO_2:MWCNT ratios were tested under 365 nm UV (8 h) with 30 mg L^{-1} PFOA. Adsorption equilibrium on MWCNTs occurred within 30 min (~18% PFOA). A 5:1 TiO_2-MWCNT composite achieved 89% PFOA degradation, surpassing P25 (37%) and physical mixtures (60%) (**Fig. 12a**). Optimized 10:1 loading yielded 94% degradation, whereas 20:1 caused aggregation and reduced efficiency.

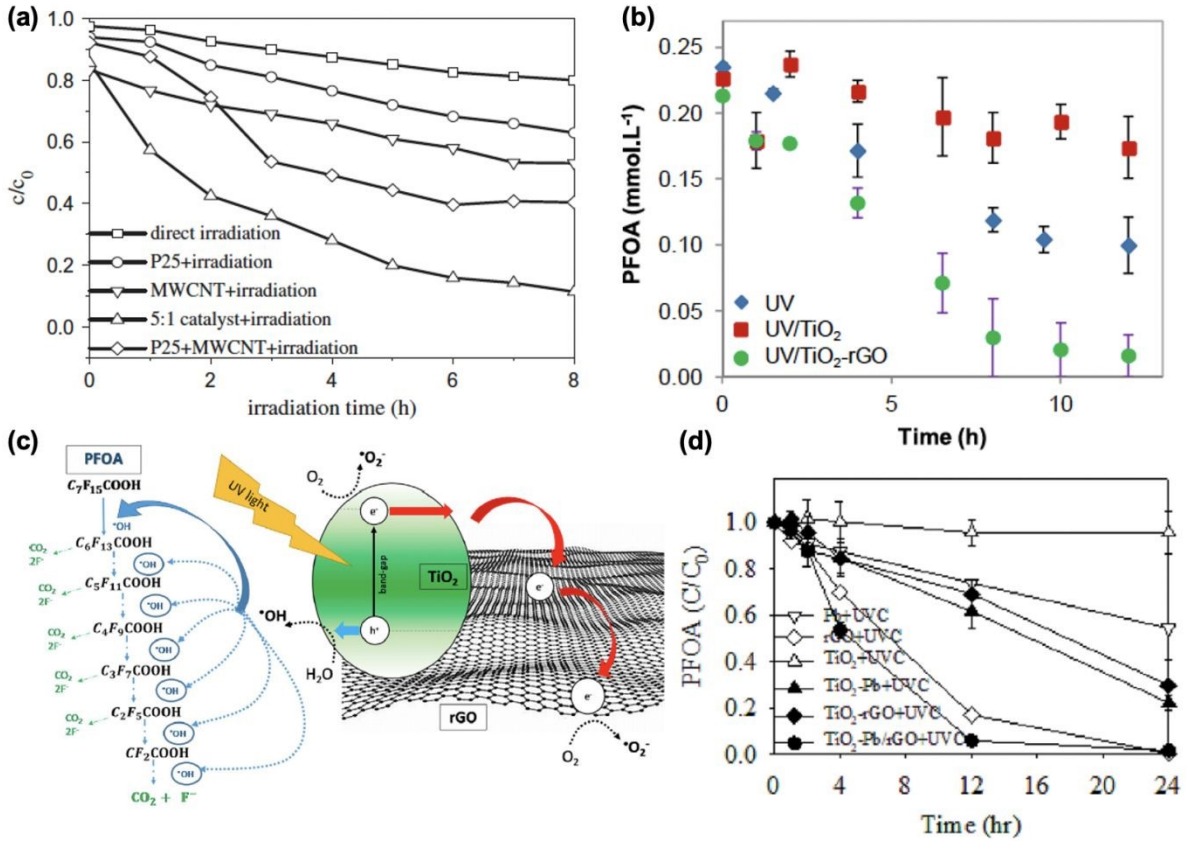

Figure 12. Photocatalytic degradation of PFOA and PFOS over various TiO_2-based and modified photocatalysts: (a) Comparison with a physical mixture of P25 and MWCNTs (5:1) Reproduced from reference [264] with permission from Elsevier BV, copyright 2012 [264]; (b) Comparison of PFOA degradation after 12 h under UV irradiation using TiO_2, TiO_2–rGO composite, and GO control, showing enhanced removal with TiO_2–rGO due to improved light penetration and reduced electron–hole recombination, (c) Proposed photocatalytic degradation pathway of PFOA over TiO_2–rGO, highlighting the role of rGO in enhancing charge separation, radical generation ($^{\bullet}OH$ and $O_2^{\bullet-}$), stepwise perfluoroalkyl cleavage, and eventual formation of CO_2 and F^- Reproduced from reference [265] with permission from Elsevier BV, copyright 2018; (d) PFOA removal under UVC irradiation using TiO_2, Pb, rGO, TiO_2–Pb, TiO_2/rGO, and TiO_2–Pb/rGO, showing enhanced degradation with composite materials due to synergistic effects of rGO and Pb doping Reproduced from reference [267] with permission from Wiley, copyright 2023.

TiO_2 photocatalysis is significantly boosted through integration with reduced graphene oxide (rGO), which has been studied for the degradation of various pollutants [265-268]. Ruiz et al. investigated TiO_2-rGO composites for PFOA degradation under UV irradiation [265]. While bare

View Article Online
DOI: 10.1039/D5MA01247C

TiO_2 removed only 24 ± 11% of PFOA after 12 h, TiO_2-rGO achieved 93 ± 7% removal under identical conditions (**Fig. 12b**), representing a ~4-fold improvement. The enhanced activity is attributed to: (i) one-atom-thick rGO sheets that reduce light screening, (ii) efficient electron transfer from TiO_2 to rGO, and (iii) prolonged charge-carrier lifetimes, which enhance $^{\bullet}OH$ and $O_2^{\bullet-}$ generation (**Fig. 12c**). Total organic carbon decreased by 62%, and 20% of fluorine was removed through combined adsorption (6.8%) and partial volatilization of short-chain products. Kinetic analysis revealed a chain-length-dependent degradation: k_{PFPeA} = 2.14 h^{-1} > k_{PFHxA} = 0.54 h^{-1} > k_{PFHpA} = 0.27 h^{-1} > k_{PFOA} = 0.163 h^{-1}, indicating faster degradation of shorter-chain PFCAs. In subsequent studies, TiO_2-rGO degraded both DCA and PFOA, but complete mineralization occurred only for DCA, highlighting the strong recalcitrance of fluorinated compounds [266]. Chowdhury et al. developed a synergistic Pb-doped TiO_2/rGO system (TiO_2-Pb/rGO) for PFOA remediation under UVC irradiation [267] (**Fig. 12d**). The composite achieved 98% PFOA removal and 32% defluorination, surpassing TiO_2-Pb, TiO_2/rGO, and TiO_2-Fe/rGO. Pb outperformed Fe for defluorination (34% vs 15%) due to its more favorable standard reduction potential. The TiO_2-Pb/rGO system was effective under UVA, UVB, and UVC, with UVC slightly more efficient, achieving a low electrical energy per order (E_{EO}) of 4.05 kWh/m³ for 98% PFOA removal.

Ultra-small TiO_2 quantum dots (QDs) have been developed and uniformly distributed on supports to enhance photocatalytic efficiency by maximizing the active surface area [268–270]. Sodium dodecyl sulfate (SDS) was used to regulate Ti^{3+} ion distribution, minimizing TiO_2 particle size. The resulting QDs (~2.55 nm) were assembled into three-dimensional sulfonated graphene (SG) aerogels, forming 3D SG-TiO_2 QD aerogels [269]. Compared to conventional TiO_2 nanoparticles (15-40 nm) [271], these QDs exhibit enhanced photon absorption and reduced e-h+ recombination. Photocatalytic PFOA degradation followed first-order kinetics, with QDa (SG–TiO_2 QDs synthesized at higher SDS concentration) achieving the highest rate constant (k_{app} = 1.898 × 10^{-4} s^{-1}), outperforming QDb (SG–TiO_2 QDs synthesized at lower SDS concentration) (1.530 × 10^{-4} s^{-1}), aggregated TiO_2 NPs (9.283 × 10^{-5} s^{-1}), and previously reported TiO_2- or graphene-based systems (**Fig. 13a**).The synergistic combination of SG aerogels and TiO_2 QDs enhanced adsorption, promoted uniform QD dispersion, reduced band gap, and improved photogenerated charge utilization, enabling persistent and high-efficiency PFAS degradation even in flow-through setups (**Fig. 13b**).

Carbon quantum dots (CQDs) have emerged as effective modifiers of TiO_2 photocatalysts, enhancing visible-light absorption and promoting efficient charge separation [272,273]. High-purity CQDs synthesized via hydrothermal treatment of mussel shell biomass (MCQD) and electrochemical exfoliation of graphite rods (Exfol.CQD) [274] were coupled with TiO_2 to form composite photocatalysts. Photocatalytic experiments under UVC and visible light demonstrated substantially improved degradation of perfluorooctanoic acid (PFOA) and short-chain PFCAs (C3–C6). Stepwise decomposition of longer-chain PFCAs (e.g., PFHxA-C6, PFPeA-C5) to shorter intermediates (PFBA-C4, PFPrA-C3) was observed, with higher intermediate concentrations under UVC irradiation (PFHxA 11.5 μg L^{-1}, PFPeA 11.9 μg L^{-1}) than under visible light (PFHxA 9.8 μg L^{-1}, PFPeA 8.2 μg L^{-1}), reflecting more rapid generation of reactive species at higher photon energies. Corresponding defluorination efficiencies reached 32% (visible) and 34.5% (UVC) for Exfol. CQD/TiO_2, compared to 11.6% and 21.8% for bare TiO_2. Photocurrent and IMVS/IMPS

View Article Online
DOI: 10.1039/D5MA01247C

analyses confirmed faster electron transfer (τ = 0.317 ms) and longer hole lifetimes (T_R = 35.9 ms), highlighting the role of CQDs in charge separation. **Figure 13c** shows improved PFOA photodegradation by CQD/TiO_2 under UVC due to enhanced charge separation, while **Fig. 13d** illustrates a mechanism involving direct hole oxidation and ROS-driven stepwise defluorination.

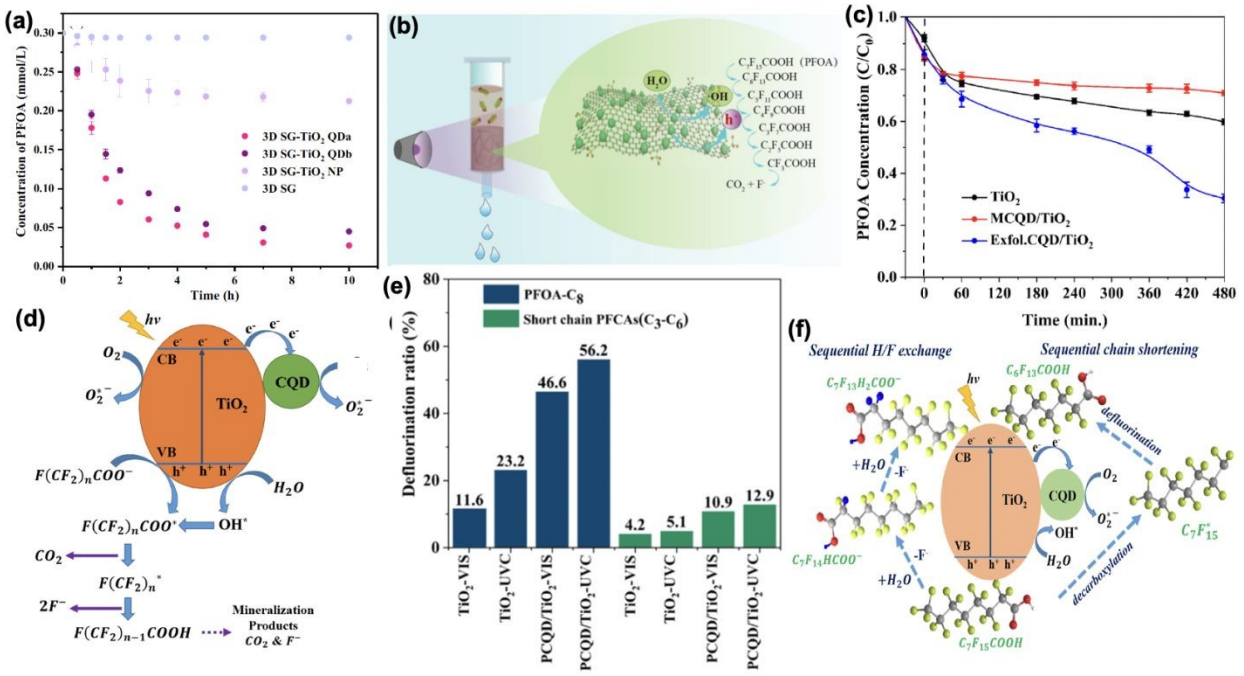

Figure 13. (a) PFOA degradation profiles and simulated concentrations over time for 3D SG-TiO_2 QDa, 3D SG-TiO_2 QDb, 3D SG-TiO_2 NP, and 3D SG, showing faster kinetics for smaller TiO_2 QDs and supporting stepwise formation of shorter-chain PFCAs, (b) Proposed mechanism for PFOA removal by 3D SG-TiO_2 QDa, showing combined adsorption on the hydrophobic aerogel surface and photocatalytic degradation via h^+-induced and •OH-mediated pathways, leading to stepwise formation of shorter-chain PFCAs and fluoride release Reproduced from reference [271] with permission from Elsevier BV, copyright 2020; (c) Photodegradation of PFOA over TiO_2, Exfol.CQD/TiO_2, and MCQD/TiO_2 under UVC (200–280 nm). Exfoliated CQDs enhance electron transfer, reduce electron–hole recombination, and improve photocatalytic efficiency compared to bare TiO_2, (d) Proposed mechanism for PFOA decomposition using TiO_2 and CQD/TiO_2 photocatalysts. Upon light irradiation, electron–hole pairs are generated; holes in the valence band directly oxidize PFOA, while electrons in the conduction band participate in reactive oxygen species formation, enabling stepwise defluorination and formation of shorter-chain PFCAs Reproduced from reference [274] with permission from Elsevier BV, copyright 2025; (e) Defluorination efficiency of PFOA and short-chain PFCAs (C3–C6) under UVC and visible light using TiO_2 and PCQD/TiO_2 photocatalysts. The PCQD/TiO_2 composite showed significantly higher defluorination percentages (46.6–56.2% for PFOA, 10.9–12.9% for short-chain PFCAs) compared to pristine TiO_2, (f) PFCA degradation over PCQD/TiO_2 proceeds via two main pathways: chain shortening, where reactive holes and radicals break C–C bonds to form shorter-chain PFCAs, and H/F exchange, where α-C–F bonds are sequentially replaced by hydrogen, releasing fluoride ions. Reactive oxygen species (·OH, O_2·$^-$) generated by the photocatalyst drive these processes Reproduced from reference [275] with permission from Elsevier BV, copyright 2025.

View Article Online
DOI: 10.1039/D5MA01247C

Similarly, peanut-shell biomass-derived CQDs (PCQD/TiO_2) extended TiO_2's photoresponse from UV to visible light and reduced the band gap from 3.04 to 2.92 eV, acting as electron reservoirs and further enhancing e^-/h^+ separation [275]. PFOA and other long-chain PFCAs degraded into shorter intermediates, with defluorination efficiencies significantly improved (PFOA: 56.2% UVC, 46.6% visible vs 23.2% and 11.6% for bare TiO_2) (**Fig. 13e**). Both Exfol. CQD and PCQD composites exhibited stepwise PFCA degradation driven by superoxide ($^{\bullet}O_2^-$), hydroxyl radicals ($^{\bullet}OH$), and photogenerated holes, maintaining stable performance over multiple cycles. **Figure 13f** illustrates the mechanism: extended light absorption, improved e^--h^+ separation, and reactive radical generation drive chain shortening, decarboxylation, and H/F exchange, achieving efficient mineralization. Among the three CQDs, PCQD/TiO_2 demonstrates the highest overall efficiency, achieving 67.2% degradation of long-chain PFOA under UVC and 48.5% under visible light, while also effectively degrading short-chain PFCAs such as PFHxA (41.3%) and PFPeA (52.1%). Exfol.CQD/TiO_2 performs comparably for long-chain PFOA (69% UVC, 50% visible) but is less effective for short-chain PFCAs (PFHxA 40%, PFPeA 35%, PFBA 31.6%, PFPrA 21.6%). In contrast, MCQD/TiO_2 consistently exhibits the lowest activity (PFOA 29% UVC, 20% visible) with limited short-chain PFCA data. This quantitative comparison underscores that both the CQD precursor and synthesis method critically influence TiO_2 photocatalytic performance, with biomass-derived PCQDs offering a sustainable and broadly effective approach for PFAS remediation under both UVC and visible light.

6.3.3. Emerging Hybrid Systems

Supporting materials have been explored to enhance TiO_2 photocatalysis by improving catalyst stability, dispersion, and charge transport, leading to more effective utilization of photogenerated charge carriers [276–280]. Among these, MXenes and zeolites exemplify distinct strategies for augmenting TiO_2 performance in PFAS degradation. MXenes, two-dimensional transition metal carbides and nitrides, combine high conductivity, tunable surface chemistry, and layered architecture, enabling rapid electron transfer and heterojunction formation with TiO_2 [276]. Hydrophilic surfaces and interlayer expansion enhance nanoparticle interaction, light utilization, and accessibility of active sites.

In one approach, hydrothermally synthesized MXene/TiO_2 composites demonstrated a layered structure with TiO_2 nanoparticles anchored on MXene sheets, as confirmed by SEM, XRD, and XPS [281]. These composites coupled rapid adsorption with photocatalysis: PFOA adsorption reached equilibrium within 30 min ($q_m \approx 16.06$ mg/g), following pseudo-second-order kinetics and Langmuir isotherms, with efficiency strongly influenced by pH. Under UV irradiation, MXene/TiO_2 achieved 94.6 % degradation and 58.4 % defluorination within 9 h, surpassing UV alone, UV/MXene, or UV/TiO_2 systems (**Fig. 14a**). The Schottky barrier at the MXene–TiO_2 interface facilitated hole transfer, improving e^--h^+ separation and extending catalyst durability. Comparative analysis with advanced photocatalytic systems including MXene nanosheets, Ti4O7/MXene, COFs/MOFs and ZIF-67/ Au-PCN reveals that MXene/TiO2 system competitive advantage in persistent pollutant remediation (M5, M6. M7). In a separate study, an intercalation strategy using deep eutectic solvents (DESs) was developed to overcome the limited interlayer spacing of Ti_3C_2 MXene, which typically hinders in-situ TiO_2 crystal growth [282]. The resulting

View Article Online
DOI: 10.1039/D5MA01247C

Ti_3C_2-DES exhibited expanded c-lattice parameters compared to HF-etched MXene, allowing greater water intercalation and more effective Ti atom oxidation. This promoted in-situ TiO_2 crystal growth with exposed (001) and (101) facets, forming heterojunctions for enhanced charge separation. Combined with the high conductivity of the Ti_3C_2 substrate, this system enabled efficient carrier transport, achieving nearly 100 % PFOA removal and 49 % defluorination in 16 h. In contrast, Ti_3C_2-HF/TiO_2 and commercial P25 TiO_2 exhibited only modest efficiencies (22 % removal, 12 % defluorination, and 30 % removal, 9 % defluorination, respectively) (**Fig. 14b–14c**), consistent with the morphological and mechanistic insights highlighted in **Fig. 14d-14e**. Quantitatively, these results illustrate that faster C–F bond cleavage does not always correspond to higher overall PFOA removal. Together, these studies [281, 282] demonstrate that MXene/TiO_2 hybrids can be engineered through hydrothermal or DES-driven strategies to maximize synergistic adsorption–photocatalysis, enhance charge separation, and significantly boost PFAS degradation, highlighting the versatility of MXenes as co-catalysts and structural supports for next-generation water treatment photocatalysts.

TiO_2/zeolite nanocomposite materials were studied for photocatalytic PFPA degradation, leveraging the complementary properties of both components [283]. TiO_2 provides photocatalytic activity, while zeolites offer thermally and chemically stable scaffolds with high surface area and porous, hydrophobic structures that pre-concentrate pollutants, prevent nanoparticle aggregation, and, when modified (e.g., alum-coated), enhance fluoride adsorption. Waste-derived Na-Y zeolite (68.7 % purity) supported TiO_2 via sol-gel or hydrothermal methods, resulting in higher surface area (273 m^2/g vs 46.3 m^2/g for P25), reduced bandgap (2.75 eV vs 3.28 eV), and preserved structural integrity (EDX Ti:Si:Al = 42.4:34.9:22.7). Systematic evaluation using ANOVA and response surface (RS) methodology identified pH (alkaline, pH 13) as the most influential factor, followed by dosage and TiO_2/zeolite ratio, with reaction temperature contributing moderately. The RS 3D plots (**Fig. 14f-14h**) visually depict the interplay between these factors, highlighting the optimal ranges of dosage, zeolite ratio, temperature, and pH for maximum defluorination. Under these optimal conditions (0.5 g/L catalyst, 10 % TiO_2/zeolite, 85 °C, pH 13), PFPA defluorination reached 58.7–60.2 %, with elevated surface area, pore structure, and charge properties promoting $^{\bullet}OH$-mediated degradation. These results highlight the synergy of TiO_2 and zeolite scaffolds and demonstrate a statistically validated approach for optimizing photocatalytic PFAS remediation.

Further advancement is represented by F-TiO_2@MIL-125, integrating tailored adsorption and photocatalytic functionalities [65]. While MIL-125 displayed smooth plate-like morphology (1 nm), TiO_2@MIL-125 retained disc-like structure with smoother surfaces, and F-TiO_2@MIL-125 preserved structural integrity with superficial nano-debris despite fluorine functionalization. BET analysis showed a surface area decrease from 1201.71 m^2/g (MIL-125) to 85.25 m^2/g (F-TiO_2@MIL-125), accompanied by an increase in pore diameter (2.13 → 12513.48 nm), favoring PFOA diffusion. F-TiO_2@MIL-125 exhibited rapid adsorption (within 200 s) and superior monolayer capacities (185.151 µmol/g), outperforming MIL-125, F-MIL-125, and TiO_2@MIL-125. Photocatalytic tests (**Fig. 14i**) under simulated sunlight demonstrated that only TiO_2@MIL-125 and F-TiO_2@MIL-125 sustained PFOA degradation beyond 2 h, with F-TiO_2@MIL-125 achieving the highest rate constant (K_{app} = 1.221 × 10^{-4} s^{-1}), surpassing TiO_2–rGO (0.453 × 10^{-4} s^{-1}) and

View Article Online
DOI: 10.1039/D5MA01247C

fluorinated TiO_2 (0.360×10^{-4} s^{-1}). This enhanced performance was attributed to a narrowed bandgap (3.12 eV), redshifted absorption (460 nm), increased VB electron density, and improved electron–hole separation, as confirmed by UV–vis, Mott–Schottky, photocurrent, and EIS analyses. Mechanistically, PFOA removal involved F···F interactions for enrichment, followed by h^+ and •OH-mediated oxidation through stepwise defluorination. These studies highlight that MXenes, zeolites, and MIL-125-derived supports enhance TiO_2 photocatalysis via complementary mechanisms: adsorption, heterojunction-facilitated charge separation, structural stability, and tailored surface chemistry, achieving superior PFAS removal and defluorination compared to conventional TiO_2 catalysts.

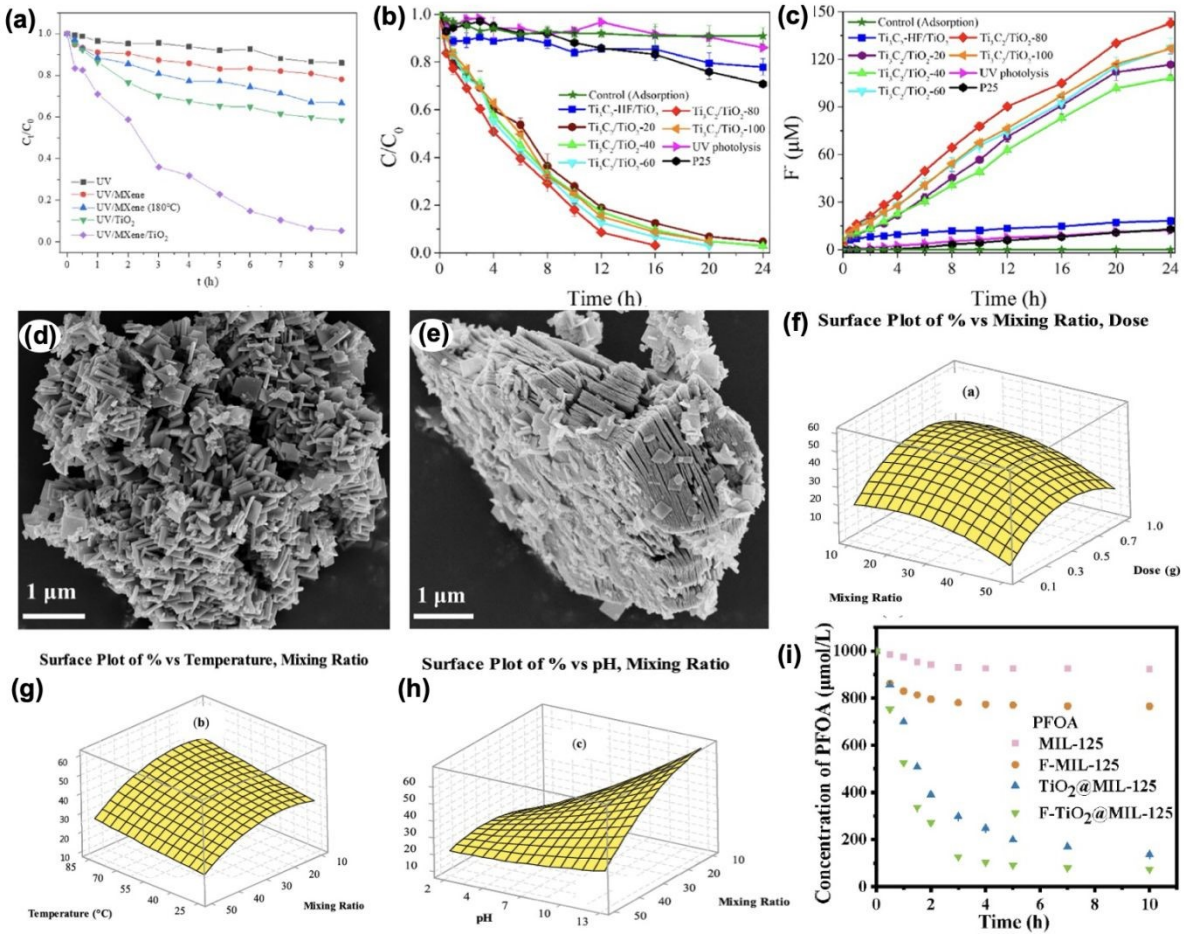

Figure 14. (a) Photocatalytic degradation of PFOA under different systems: UV alone, MXene, hydrothermally treated MXene (180 °C), TiO_2, and MXene/TiO_2 composite. The MXene/TiO_2 composite achieved the highest degradation (94.6%) due to enhanced light absorption and improved electron–hole separation, while UV alone showed minimal PFOA removal (13.96%) Reproduced from reference [281] with permission from Elsevier BV, copyright 2025; Photocatalytic degradation of PFOA using Ti_3C_2/TiO_2-based catalysts: (b) PFOA removal under adsorption, UV photolysis, Ti_3C_2-HF/TiO_2, P25, and Ti_3C_2/TiO_2–80, (c) fluoride ion (F^-) generation and defluorination efficiency for the same systems, (d) TiO_2 distribution within Ti_3C_2-DES showing intercalation into interlayers, (e) TiO_2 growth on Ti_3C_2-HF surface for comparison. The intercalation strategy (Ti_3C_2/TiO_2–80) significantly enhances both PFOA degradation

View Article Online
DOI: 10.1039/D5MA01247C

(>99.9%) and defluorination (49%) compared to conventional TiO_2 systems Reproduced from reference [282] with permission from Elsevier BV, copyright 2020; Three-dimensional RS (Response Surface) diagrams illustrating the optimal operating conditions for maximum treatment efficiency: (f) effect of catalyst dosage (0.5–0.7 g) and zeolite mixing ratio (~10%) on efficiency; (g) influence of zeolite ratio (~10%) and reaction temperature (up to 85 °C); (h) effect of zeolite ratio (~10%) and pH (up to 13). The diagrams indicate that treatment efficiency improves with decreasing zeolite ratio, increasing temperature, and higher pH under the specified conditions Reproduced from reference [283] with permission from Elsevier BV, copyright 2024; (i) PFOA degradation by MIL-125, F-MIL-125, TiO_2@MIL-125, and F-TiO_2@MIL-125 showed fastest kinetics for F-TiO_2@MIL-125 with K_a□□ = 1.221×10^{-4} s^{-1}, higher than other TiO_2-based catalysts, while only TiO_2@MIL-125 and F-TiO_2@MIL-125 continued significant degradation after 2 h Reproduced from reference [65] with permission from Elsevier BV, copyright 2022 [65].

6.4. Advanced Photocatalysis-Centric Approaches

Recent developments in TiO_2-based photocatalysis have focused on integrated strategies that improve overall performance by combining structural and functional modifications. Among these, photoelectrocatalysis (PEC) combines photocatalysis with an applied bias to accelerate interfacial reactions, while advanced oxidation processes (AOPs) exploit synergistic reactive oxygen species (ROS) pathways to mineralize persistent contaminants efficiently [284-287]. Molecularly imprinted photocatalysts (MIPs) offer selective adsorption and degradation by creating tailored recognition sites for specific pollutants [288-290]. This section highlights the mechanistic advantages and potential of these advanced strategies for PFAS degradation.

6.4.1. Photoelectrocatalysis

View Article Online
DOI: 10.1039/D5MA01247C

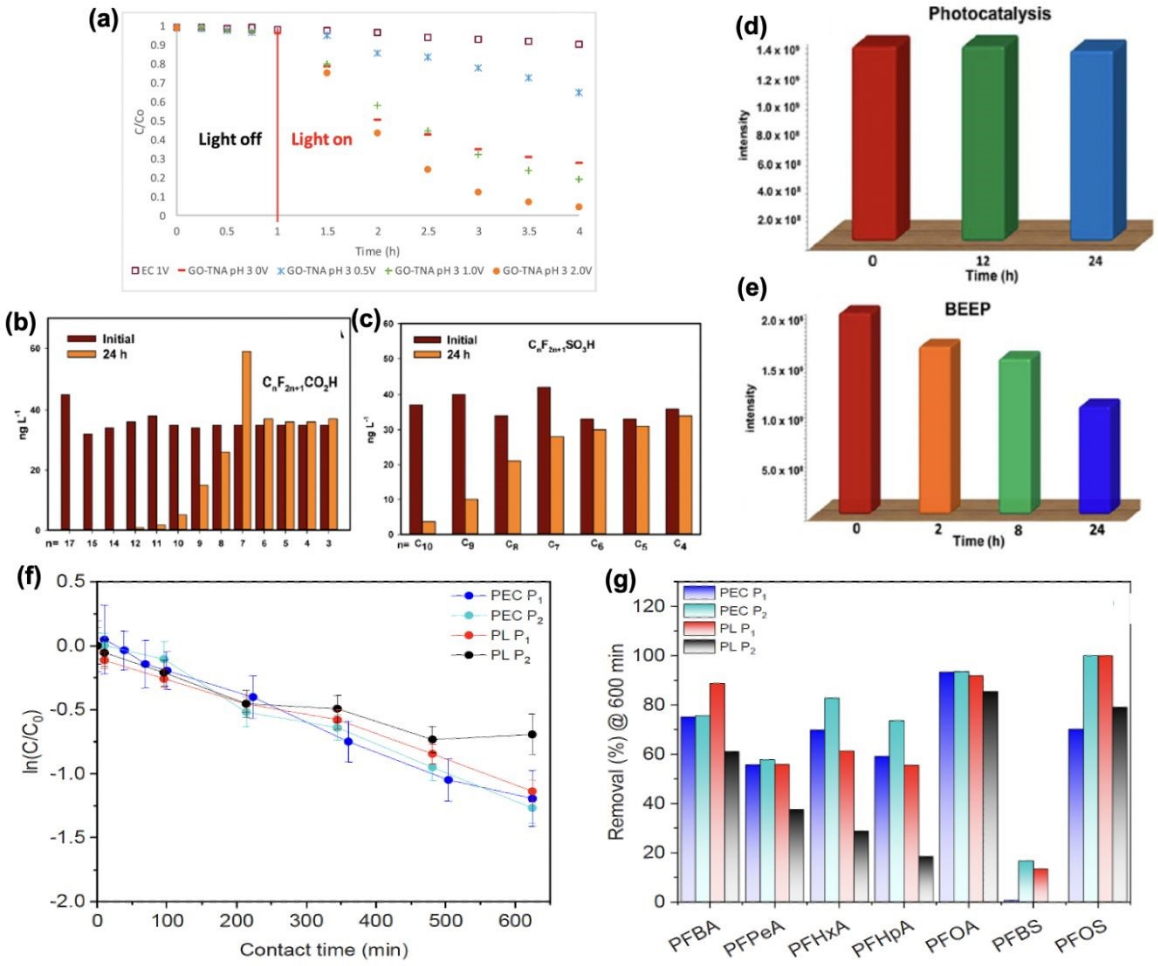

Figure 15. (a) Photoelectrocatalytic degradation of PFOA on GO/TNAs under UV light was tested with external bias from 0 to 2.0 V. Degradation increased with applied potential due to enhanced electron transfer from TNAs to graphene oxide sheets Reproduced from reference [294] with permission from Elsevier BV, copyright 2018 [294]; Photocatalytic degradation of PFAS using the BEEP reactor: (b) Concentration changes of 42 PFCAs after 24 h, showing complete removal of long chains (C12–C17) and progressive breakdown of shorter chains (C8–C12) into smaller intermediates, (c) Removal of PFSAs, with the longest PFDS (C10) achieving 90% degradation, while shorter chains (C7–C9) show lower removal, (d) Mass spectra of PFTeDA (C14) during BEEP treatment, illustrating stepwise decarboxylation and formation of smaller PFCAs ($[C8F17]^-$ and $[C6F13]^-$), (e) MS spectra of PFOS (C8) showing ~30% removal and 15% defluorination after 24 h, highlighting BEEP's efficiency in degrading both long- and short-chain PFAS, including resistant compounds like PFOS and PFOA Reproduced from reference [295] with permission from Royal Society of Chemistry, copyright 2025 [295]; Effect of UV power and PFAS chain length on removal efficiency: (f) Influence of UV intensity on PFOA removal: in photolysis (PL), reducing power from P1 to P2 decreased removal from 68% to 50%, whereas in photoelectrocatalysis (PEC), removal remained high (65–72%) due to the catalytic activity of the TiO_2-coated mesh. (g) Removal of PFAS with different chain lengths under PL and PEC: in PL at P2, removal increased with decreasing chain length (PFHpA 18.5% → PFBA 61%), while at P1, removal ranged 55–61% for PFHpA, PFHxA, PFPeA and 89% for PFBA. In PEC, removal rates at P2 were equal or higher than at P1, demonstrating efficient degradation across all chain lengths Reproduced from reference [296] with permission from Elsevier BV, copyright 2025.

View Article Online
DOI: 10.1039/D5MA01247C

Photoelectrocatalysis (PEC) and bias-enhanced electrochemical photocatalysis (BEEP) demonstrate significant advantages over conventional photocatalysis for PFAS degradation. PEC improves photocatalytic performance by applying an external bias to semiconductor photocatalysts, enhancing e^--h^+ separation, accelerating surface redox reactions, and promoting radical-mediated oxidation and defluorination [291–293]. Laboratory studies using graphene oxide-deposited TiO_2 nanotube arrays (GO/TNAs) showed that defluorination efficiency depends on initial PFOA concentration and surface pH, with maximum degradation (~83 %) at pH 3. Increasing the temperature from 25 °C to 75 °C accelerated degradation kinetics from 0.34 h^{-1} (83 % in 4 h) to 1.63 h^{-1} (complete degradation in 2.5 h). Applying a 2 V external bias further improved removal efficiency to 97 % by promoting charge separation, enhancing OH radical generation, and enabling anodic oxidation, although higher pH reduced efficiency due to competing OH^- adsorption (**Fig. 15a**) [294]. Similarly, bias-enhanced electrochemical photocatalysis (BEEP) demonstrates significant PFAS degradation [295]. BEEP combining UVA irradiation with a 2 V bias, enabled complete mineralization of long-chain PFCAs (C13–C17) within 24 h, with shorter-chain intermediates progressively degraded (**Fig. 15b** and **Fig. 15c**). Sulfonamide-containing PFAS were fully removed, while PFOS and PFOA showed measurable defluorination (~15% for PFOS in 24 h). Mass spectrometry confirmed PFOS degradation, with decreased molecular ion intensity during photocatalysis (**Fig. 15d**) and under BEEP treatment (**Fig. 15e**), providing molecular-level evidence of PFAS breakdown. The enhanced performance results from reduced e^--h^+ recombination, accelerated redox kinetics, and electrostatic attraction of PFAS to the biased TiO_2 surface, highlighting BEEP as an energy-efficient, scalable alternative to conventional treatments.

Field-relevant PEC studies further support these findings. In groundwater from the Veneto Region, Italy, site of one of the largest PFAS environmental disasters in Europe, a total of 48 PFAS species, including long- and short-chain compounds, were monitored, with up to 9 species detected in the wells. PEC achieved overall PFAS reductions of 63 % in well 1 and 65 % in well 2, with individual removal efficiencies ranging from 96 % (PFOA) to 1 % (PFBS) [296]. The average degradation order followed PFOA > PFHpA > PFHxA > PFPeA > PFBA for PFCAs and PFOS > PFHpS for PFSAs. Laboratory tests in ideal PFOA solutions confirmed that PEC degradation proceeds via decarboxylation followed by stepwise CF_2-unit loss, with transient formation of shorter-chain intermediates. Laboratory comparisons between photolysis (PL) and PEC under two UV lamp power settings (P1 = higher, P2 = lower) illustrate the advantages of bias-assisted PEC: as shown in **Fig. 15f**, reducing UV intensity from P1 to P2 decreased PL removal from 68 % to 50 %, while PEC removal remained stable or slightly increased, ranging from 65 % to 72 % [296]. **Fig. 15g** shows that for individual PFCAs, PL removal strongly depended on chain length and light intensity, whereas PEC maintained consistent or higher removal across all chain lengths regardless of UV power. These results indicate that PEC is less dependent on radiation density and that bias-assisted charge separation is a key driver of robust kinetics. In terms of operational efficiency, PEC was more energy-efficient than PL: EEO values were 36 kWh m^{-3} for PEC versus 46–59 kWh m^{-3} for PL, outperforming most other advanced oxidation processes and showing comparable performance to plasma and advanced reduction processes. PEC, including advanced configurations such as BEEP, has shown potential for both laboratory and field-relevant PFAS-

View Article Online
DOI: 10.1039/D5MA01247C

contaminated waters, enabling high removal and defluorination rates while maintaining energy efficiency and stability under varying UV conditions. These studies also indicate the importance of non-target analyses to further elucidate reaction pathways and identify by-products, as well as the potential value of pilot-scale reactors for evaluating energy consumption and process feasibility.

6.4.2. TiO_2-Based Advanced Oxidation Processes (AOPs)

TiO_2 photocatalysis has been combined with Advanced Oxidation Processes (AOPs) to achieve higher pollutant removal efficiencies than TiO_2 alone [297-300]. In these hybrid systems, the addition of oxidants such as H_2O_2, O_3, peroxymonosulfate (PMS), or related species promotes the formation of reactive oxygen species, leading to accelerated degradation and improved mineralization of persistent contaminants.

Photocatalytic ozonation represents a highly effective TiO_2-AOP strategy [301,302]. Pairing TiO_2 with ozone generates additional $^{\bullet}OH$, complementing photocatalytic oxidation. Using this approach, 99.1% PFOA degradation and 44.3% defluorination were achieved within 4 h (**Fig. 16a**) [303]. TiO_2/PMS systems were evaluated for PFOA degradation under both visible and UV light [304]. Under optimized conditions (0.25 g L^{-1} TiO_2, 0.75 g L^{-1} PMS, pH 3, 300 W visible light), 50 mg L^{-1} PFOA was degraded nearly completely within 8 h (**Fig. 16b**), with a pseudo-first-order rate constant of 0.310 h^{-1}, approximately 11× higher than TiO_2 alone (0.028 h^{-1}). Scavenger studies indicated that sulfate radicals ($SO_4^{\bullet -}$) from PMS and photogenerated holes (h^+) from TiO_2 were the primary reactive species. In real wastewater, PFOA removal decreased to 65% (influent) and 82% (effluent) in 8 h (k = 0.136 and 0.070 h^{-1}) due to coexisting organic compounds, highlighting matrix effects (**Fig. 16c**). Under UV light (254 and 185 nm, 32 W), degradation reached nearly 100% within 1.5 h, reflecting higher catalyst absorbance and stronger photon energy. For comparison with other TiO_2-based systems, TiO_2/PMS exhibits the highest apparent kinetics (k = 1.09 h^{-1}) [304], followed by Pt-modified TiO_2 (k = 0.726 h^{-1}) and Pd-modified TiO_2 (k = 0.438 h^{-1}), while Ag-modified TiO_2 shows the lowest reaction rate (k = 0.126 h^{-1}) [225]. This comparison reflects differences in kinetic performance among TiO_2-based systems when evaluated strictly by apparent rate constants.

View Article Online
DOI: 10.1039/D5MA01247C

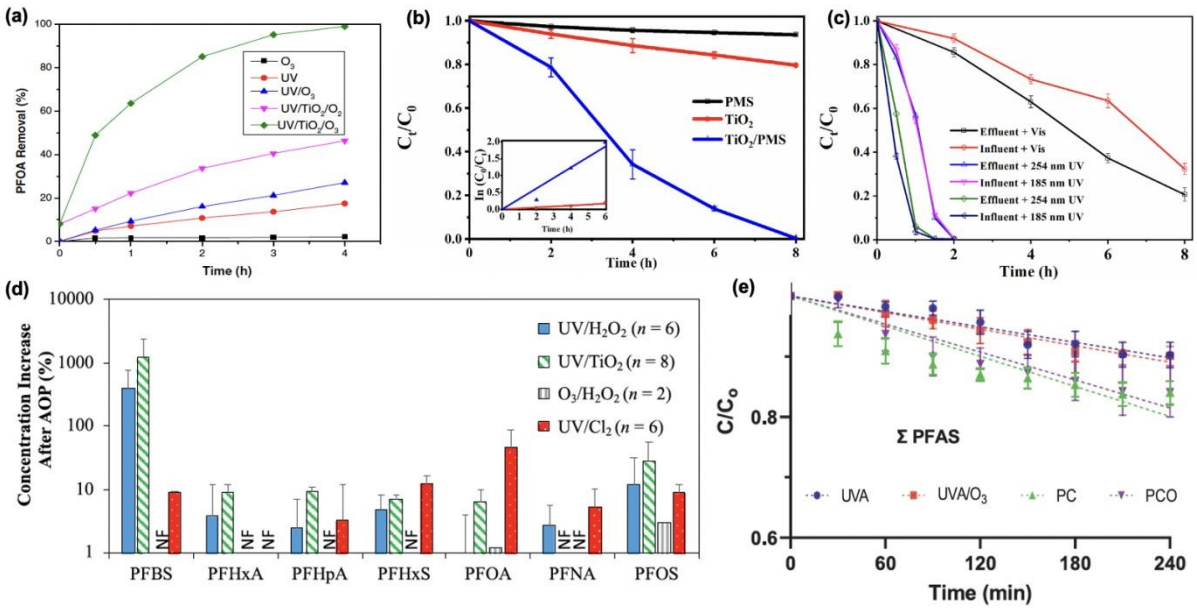

Figure 16. (a) PFOA degradation and defluorination over 4 h under different treatments. Sole ozonation: 0.5% F defluorination; direct UV photolysis: 17.5% decomposition, 8.3% defluorination; TiO_2 photocatalysis ($UV/TiO_2/O_2$): 46.4% decomposition; UV/O_3: 27.1% decomposition, 10.6% defluorination; photocatalytic ozonation ($UV/TiO_2/O_3$) achieved 99.1% decomposition and 44.3% C–F cleavage, highlighting strong synergistic effects Reproduced from reference [303] with permission from Elsevier BV, copyright 2016; Photocatalytic degradation of PFOA (50 mg L^{-1}) using TiO_2/PMS: (b) Under weak visible light (30 W) or darkness, PMS, TiO_2, and TiO_2/PMS showed negligible removal. Under powerful visible light (300 W), TiO_2 alone removed ~20% of PFOA, PMS alone was ineffective, and TiO_2/PMS achieved nearly 100% degradation within 8 h, demonstrating a strong synergistic effect, (c) In real wastewater samples, TiO_2/PMS under 300 W visible light degraded 65–82% of PFOA within 8 h (k = 0.136 h^{-1} for influent, 0.070 h^{-1} for effluent), lower than in pure water (k = 0.310 h^{-1}) due to coexisting organics. UV light (254 and 185 nm) maintained degradation efficiency comparable to pure water, showing stable photocatalytic performance in complex matrices Reproduced from reference [304] with permission from Elsevier BV, copyright 2020; (d) Fate of PFASs in pilot-scale AOP systems. Most targeted PFASs showed no significant removal, except PFHxA and PFHxS, which decreased by 7% and 11%, respectively, in the O_3/H_2O_2 effluent at Site 3. All other PFASs increased after treatment, with PFBS rising by 405% and PFOA/PFOS increasing by 14% and 13%, respectively. Variations between AOP technologies and sites reflect differences in precursor composition and source water quality Reproduced from reference [305] with permission from Elsevier BV, copyright 2022; (e) PFAS degradation after 4 h under different treatments. Photocatalysis and photocatalytic ozonation showed significantly higher removal of total PFAS, PFOA, PFHxS, and 6:2 FTS compared to photolysis ($p < 0.05$). Ozonation alone removed only ~4% and was not statistically different from adsorption Reproduced from reference [306] with permission from Elsevier BV, copyright 2022.

Venkatesan et al. [305] evaluated seven pilot-scale AOPs for PFAS and 1,4-dioxane removal in New York groundwater, including UV/TiO_2. While these AOPs transformed PFAS precursors, complete mineralization was not achieved, and concentrations of individual PFAS often increased due to precursor conversion. Specifically, average increases were observed for PFBS (≈405%, range 0–1220%), PFOA (≈14%, 0–48%), PFOS (≈13%, 3–25%), PFHxA (≈1%, −7–9%), PFHpA (≈3.8%, 0–9.5%), PFHxS (≈3.3%, −11–13%), and PFNA (≈2%, 0–5.2%) (**Fig. 16d**). These increases were dependent on UV and oxidant dose, indicating that hydroxyl radical-based AOPs primarily

View Article Online
DOI: 10.1039/D5MA01247C

facilitated precursor transformation rather than full degradation. Importantly, at one site, PFOA concentrations exceeded the New York State drinking water standard (10 ng/L) after treatment, highlighting the importance of considering AOP-induced PFAS formation when designing treatment systems. These findings highlight the challenges associated with AOPs, including limited removal efficiency and the potential for increasing certain PFAS concentrations, which complicates water treatment and regulatory compliance.

Photocatalytic ozonation, combining WO_3/TiO_2 catalysts with ozone under UVA-visible light, has been applied for the removal of five PFAS (PFOA, PFHxS, PFBS, 6:2 FTS, GenX) from water [306]. Four catalysts with varying WO_3 content (0, 1, 3, 5 wt%) were synthesized and the 5 wt% WO_3/TiO_2 catalyst (TW5) exhibited optimal properties and achieved 82% methylene blue removal in model tests. PFAS degradation after 4 h remained low (ΣPFAS removal ≈16%, range 4–26%), with photocatalytic ozonation only marginally improving removal compared to photocatalysis alone (**Fig. 16e**). Photolysis and ozone photolysis were less effective, and ozonation alone had negligible effect. These results demonstrate both the potential and current limitations of AOPs for PFAS removal, highlighting the need to optimize catalyst design and treatment conditions across multiple PFAS types.

6.4.3. TiO_2 Nanotube Arrays (TNAs) with Molecularly Imprinted Polymers (MIPs)

In environmental remediation, selectivity is critical when targeting trace pollutants in complex matrices containing multiple chemical species. While advanced technologies such as photocatalysis, adsorption, and membrane separation perform efficiently under laboratory conditions, their effectiveness often declines in real waters due to interference from coexisting compounds [307-312]. Components such as natural organic matter (NOM), dyes, pharmaceuticals, or metal ions can occupy active sites, scavenge reactive species, or alter solution chemistry, particularly when target pollutants are present at trace levels. To address these challenges, molecularly imprinted polymers (MIPs) have been employed for selective adsorption. For example, MIPs tailored for diclofenac achieved nearly 100% removal within 3 min at 5 mg/L, with high adsorption capacity (160 mg/g) and selectivity over structurally similar pharmaceuticals [313]. Hydrophilic MIPs synthesized via bulk polymerization removed ~90% of diclofenac in 10 min using only 5 mg of material, compared to 8% removal by a non-imprinted polymer [314]. These studies demonstrate that molecular recognition-based materials can efficiently remove trace pollutants even in chemically complex environments.

Similarly, research has applied MIPs for selective PFAS removal. One strategy involves modifying TiO_2 nanotube arrays with MIPs, using PFAS molecules (e.g., PFOA) as templates. The imprinted cavities selectively capture target PFAS near the TiO_2 surface, facilitating localized photocatalytic degradation [315]. Wu et al. demonstrated that MIP-TiO_2 NTs selectively degrade PFOA in real secondary effluent. The material showed higher degradation efficiency for PFOA than for PFHA, PFOS, or 2,4-D, with apparent rate constants significantly greater for PFOA. In secondary effluent (TOC 10.2 mg/L, pH 7.2), MIP-TiO_2 NTs achieved 81.1% PFOA removal in 8 h, comparable to 84% in pure water, whereas non-imprinted TiO_2 NTs reached only 50.2%. Further, surface-molecularly imprinted TiO_2 nanotubes (S-MIP-TiO_2 NTs) have been studied for enhanced photocatalytic

View Article Online
DOI: 10.1039/D5MA01247C

degradation of PFAS in secondary municipal wastewater effluents [316]. S-MIP-TiO_2 NTs achieved significantly higher PFOA degradation under 8 h UV irradiation compared to TiO_2 NTs and non-imprinted controls, with defluorination efficiency markedly improved. Adsorption studies indicate selective binding driven by functional group recognition and electrostatic interactions at pH 4–6. Photocatalytic reactions follow Langmuir-Hinshelwood kinetics, resulting in rate constants exceeding those of NIP-TiO_2 NTs. This study demonstrated that S-MIP-TiO_2 NTs can selectively and efficiently degrade multiple short- and long-chain PFCs from real wastewater effluents at environmentally relevant concentrations. Complementing nanostructured MIP-TiO_2 systems, 3D-printed TiO_2-polylactic acid (PLA) composites was developed for pilot-scale PFAS treatment in landfill leachate [317]. Customized 3D-printed tiles containing 20 wt% TiO_2 achieved over 80% PFAS removal, including PFOS, PFNA, PFDA, and PFOSAm, within 24 h, with even higher efficiency upon extended retention. This study highlighted the potential of additive manufacturing for creating scalable and efficient photocatalytic systems adaptable to real-world PFAS remediation.

Table 1. Comparative performance of modified TiO_2 photocatalysts (doped, composite, and immobilized systems) for PFAS degradation, highlighting design strategies, efficiency, and stability.

Material	PFAS studied	Amount of PC; amount of PFAS; Solution volume	Light used	Rate constant	Degradation/ defluorination, time	Cycle	Ref.
Pristine TiO_2 Photocatalysis							
TiO_2	HFBA, TFA, PFPA, NFPA, PFOA, NFBS, HFOS	2 g/L; 1.5-6 mM; 50 mL	UV light, 75 W, 1.4-7.2 mW/cm²	0.0024 - 0.0123 h^{-1}	CO_2: 12–54%, F^-: 15–64% (60 h)	-	[184]
TiO_2	PFOA, PFDA, PFNA	0.66 g/L; 48-120 uM, with 0.15 M $HClO_4$; -	UVC light, 16 W, 0.45 mW/cm²	0.1-0.94 h^{-1}	decomposition: 86-100%, 7h, mineralization: 30-54 %, (7-48 h)	-	[185]
TiO_2 (commercial RdH; sol–gel; sonication-assisted)	PFOA (120 µM)	0.66 g/L; 120 µM; 2-3 L	UV light, 8 -16 W	0.0342 h^{-1} (RdH), 0.1309 h^{-1} (Sol-gel) with ultrasound	degradation: 22%, 7 h (RdH); ~40%, 7 h Sol-gel; ~64%, 8 h (Sol–gel + ultrasound)		[186]
TiO_2	PFOA + intermediates	0.5 g/L; 24 µM; 500 mL	UV light, 23 W	1.16×10^{-2} min^{-1}	degradation: 86.7%, 3h; defluorination: 16.5%, 3h	-	[187]
TiO_2 (Biosynthesized)	PFOS	- ; 200 µg/L; 50 mL	UV light	–	degradation: 95.6 %, 2.5 h; defluorination: 56.1 %, 2.5 h	-	[195]
TiO_2	PFOS	1.45 g/L; 100 µg/L; 100 mL	UV light, 250 W	0.64 h^{-1}	degradation: 86%, 8 h	-	[197]
TiO_2	PFOA	0.66–1.0 g/L; 0.0040-0.0120 M; 1 L	UV light, 500 W, 75-95 W/m²	0.0332 - 0.0572 h^{-1}	mineralization: 32 %, 4 h; F^-: 29%, 6 h	-	[192]
TiO_2	PFOA	1.5 wt%; 5 mM; 0.1 L	UV light, 600 mW/cm²	–	8.6×10^{-2} dm^3/h, 4 h	-	[200]
TiO_2	PFBA, PFHxA, PFOA, PFHxS, PFOS; precursors: 6:2/8:2 diPAP, 6:2/8:2 FTSA, 6:2/8:2 FTCA, PFOSA, N-EtFOSAA	430 mg/L;100 µg/L; Solution: 1 L	UV/TiO_2 (PhotoTOP), Pyrex glass, ~60 °C steady state	-	degradation (of precursors):100 %, 2-4 h	-	[203]

TiO_2	PFOA	0.5 g/L; 60 mg/L; 120 mL	UV light, 125 W, 5.3 mW/cm²	0.058 h^{-1}	degradation: 31.1%, 7 h; defluorination: 3.3%, 7 h	-	[225]
TiO_2 (mesoporous)	PFOA	0.25 g/L; 10 ppm; 20 mL	UV light, 4W	6.3×10^{-3} min^{-1}	degradation: 55.9 %, 2h	-	[238]
TiO_2	PFOA	0.1-0.2 g/L; 10 mg/L; 160 mL	UV light, 30 W; Xe lamp, 300 W	-	degradation: 18%, 8h	-	[234]
TiO_2	PFOA + intermediates PFHpA, PFHxA, PFPeA, PFBA	0.05-0.5g/L; 0.24 mmol/L; 0.8 L	Mercury lamp 200–600 nm		degradation: 24 ± 11%, 12 h	-	[265]
TiO_2	PFOA	0.1 g/L; 0.24 mmol/L; 0.8 L	UV-A/B/C, visible, 150 W	0.018 h^{-1}	-	-	[266]
P25	PFOA	200 mg L^{-1}; 20 µM; 50 mL	UV (Hg lamp), 254 nm, 20 mW cm^{-2}	–	30%, F^- 9%; 16 h	-	[282]
TiO_2 nanoparticles	PFPA	0.5 g/L; 10 mg/L; Solution: n/a	UV light, 8 h	–	TiO_2: 48.4% defluorination;		[283]
TiO_2	PFOA	0.33–0.66 g/L; 10 mg/L; 21 mL	UV light, 15 W	0.0068 h^{-1}	-	-	[267]
TiO_2	PFOA	0.1 g/L; 100 µg/L; 100 mL	UV light, Visible light	-	UV: degradation: 41 %, defluorination: 21.8 %; Visible: degradation: 24 %; defluorination: 11.6 %	-	
TiO_2	PFOA	1 g/L; 100 µg/L; 100 mL	UV light, 4 × 16 W; Visible light, 200 W	-	defluorination: 11.6% (Visible), 23.2% (UV)	-	[291]
TiO_2	Short-chain PFCAs (C3–C6)	1 g/L; 100 µg/L each; 100 mL	UV light, 4 × 16 W; Visible light, 200 W	–	defluorination: 4.2% (Visible), 5.1% (UV)	-	[291]
TiO_2	PFOA	30 mg; 20 mg/L; 150 mL	UV light	-	Degradation: 41.6 %, defluorination: 5–20 %, 9 h	-	[291]
UV/TiO_2 pilot system	PFBS, PFHxA, PFHpA, PFHxS, PFOA, PFOS, PFNA	TiO_2 slurry; PFAS 0.3–8.2 ng/L; Flow 26.5 L/min	32 low-pressure UV lamps (7 kW)	Not reported	PFAS increase with UV power; ΣPFAS up to 103% at Site 2	1 Phase	[305]

Doped-TiO_2 Systems							
Fe:Nb-TiO_2	PFOA	0.5 g/L; 0.1 mM; 600 mL	MP mercury lamp 150 W,	–	stepwise degradation to shorter PFCAs (C6, C5, C4), fluoride ions released	-	[222]
Fe–TiO_2	PFOA	0.5 g/L; 50 mg/L; 1 L	UV light, 400 W, 120,000 lux	0.0015 min^{-1}	degradation: 69%, 12 h; defluorination: 9%, 12 h	-	[223]
Cu–TiO_2	PFOA	0.5 g/L; 50 mg/L; 1 L	UV light, 400 W, 120,000 lux	0.0031 min^{-1}	degradation: 91%, 12 h; defluorination:19%, 12 h	-	[223]
Pt–TiO_2	PFOA	0.5 g/L; 60 mg/L; 120 mL	UV light, 125 W, 5.3 mW/cm^2	0.7267 h^{-1}	degradation: 100%. 7 h; defluorination: 34.8%, 7 h	-	[225]
Pd–TiO_2	PFOA	0.5 g/L; 60 mg/L; 120 mL	UV light, 125 W, 5.3 mW/cm^2	0.4369 h^{-1}	degradation: 94.2%, 7 h; defluorination: 25.9%, 7 h	-	[225]
Ag–TiO_2	PFOA	0.5 g/L; 60 mg/L; 120 mL	UV light, 125 W, 5.3 mW/cm^2	0.1257 h^{-1}	degradation: 57.7%, 7 h; defluorination: 8.1%, 7 h	-	[225]
Pb–TiO_2	PFOA	0.5 g/L; 50 mg/L; 1.1 L	UV light	0.5136 h^{-1}	degradation: 99.9%, 7 h; defluorination: 22.4%, $t_{1/2}$ 1.3 h	-	[228]
TiO_2-Pb	PFOA	0.33–0.66 g/L; 10 mg/L; 21 mL	UV light, 15 W	0.0571 h^{-1}	-	-	[267]
Single-Atom Catalysis (SACs) on TiO_2							
Facet-engineered TiO_2 / PtNP/facet-engineered TiO_2 / Pt1/facet-engineered TiO_2	PFOA	0.25 g/L; 100 µM; 80 mL	UV light, 5 W, 7.87 mW/cm^2	Negligible / NA / 15× PtNP	Significant	10	[51]
N/Cl-Bi/TiO_2 variants	PFOA	0.2 g/L; 10 mg/L; 100 mL	UV light,30/300 W	–	defluorination: 55–85%	4	[234]
TiO_2 Coupled with Other Semiconductors or Oxide							
1-10 %-Sb_2O_3/TiO_2,	PFOA	0.25 g/L; 10 ppm; 20 mL	UV light, 4W	12.6×10^{-3} min^{-1}	degradation: 10-81.8%, 2 h	5	[238]

$BiOCl/TiO_2$	PFOA	0.1-0.2 g/L; 10 mg/L; 160 mL	UV light, 30 W, Xe lamp, 300 W	-	degradation: 96 %, 8h defluorination: 82%, 8h	4	[234]
$BiOBr/TiO_2$	PFOA	0.1-0.2 g/L; 10 mg/L; 160 mL	UV light, 30 W; Xe lamp, 300 W	-	degradation: 100%, 8h defluorination: 65%, 8h	-	[234]
$BiOI/TiO_2$	PFOA	0.1-0.2 g/L; 10 mg/L; 160 mL	UV light, 30 W; Xe lamp, 300 W	-	degradation, 88%, 8h defluorination: ~20%, 8h	-	[234]
Carbon-Based Hybrid Photocatalysts							
TiO_2–MWCNT composites	PFOA	1.6 g/L; 30 mg/L; 250 mL	UV light, 300 W	–	degradation: 94-100%, 8 h		[264]
TNTs@AC	PFOA	1.0 g/L; 100 µg/L; 40 mL	UV light, 21 mW/cm^2		degradation: 23.8%, 4 h	-	[254]
Fe/TNTs@AC	PFOA	1.0 g/L; 100 µg/L; 40 mL	UV light, 21 mW/cm^2	0.918 h^{-1}	degradation: 90%, 4 h; defluorination: ~62%, 4 h	6	[254]
TNTs@AC	PFOA	4 g/L; 400 µg/L; 10 mL	UV light, 2.28 mW/cm^2	-	degradation: 68.7%, 4 h	–	[260]
In/TNTs@AC (non-calcined)	PFOA	4 g/L; 400 µg/L; 10 mL	UV light, 2.28 mW/cm^2	-	degradation: 68.7%, 4 h	–	[260]
In/TNTs@AC (calcined)	PFOA	4 g/L; 400 µg/L; 10 mL	UV light, 2.28 mW/cm^2	-	degradation: 100 %, 4 h; defluorination: 60%, 4 h	4	[260]
TiO_2-rGO (5 wt% rGO)	PFOA	0.1 g/L; 0.24 mmol/L; 0.8 L	UV-A/B/C, visible, 150 W	0.211 h^{-1}	degradation: 86%, 8 h; defluorination: 30%, 8 h	-	[266]
TiO_2/rGO	PFOA	0.33–0.66 g/L; 10 mg/L; 21 mL	UV light, 15 W	0.0410 h^{-1}	-	-	[267]
TiO_2-Pb/rGO composite	PFOA	0.33–0.66 g/L; 10 mg/L; 21 mL	UV light, 15 W	0.2193 h^{-1}	degradation: 98%, 24 h; defluorination: 32%, 24 h	-	[267]

3D SG-TiO_2 QDa	PFOA,	0.30 mmol/L; 4.8 mg/200 mL; 200 mL	UV light, 150 W	1.898×10^{-4}/s	-	-	[269]
3D SG-TiO_2 QDb	PFOA	0.30 mmol/L; 4.8 mg/200 mL; 200 mL	UV light	1.530×10^{-4}/s	-	-	[269]
3D SG-TiO_2 NP	PFOA	0.30 mmol/L; 4.8 mg/200 mL; 200 mL	UV light	9.283×10^{-5}/s	-	-	[269]
MCQD/TiO_2	PFOA	0.1 g/L; 100 µg/L; 100 mL	UV light, Visible light	-	UV: degradation: 29 %; Visible: degradation: 20 %	-	[274]
Exfol.CQD/TiO_2	PFOA	0.1 g/L; 100 µg/L; 100 mL	UV light, Visible light	-	UV: degradation: 69 %, defluorination: 34.5 %; Visible: degradation: 50 %; defluorination: 32.0 %	-	[274]
Exfol.CQD/TiO_2	PFHxA, PFPeA, PFBA, PFPrA	0.1 g/L; 100 µg/L; 100 mL	Visible light	-	PFHxA: degradation: 40 %, defluorination: 5.6 %; PFPeA: degradation: 35 %, defluorination: 5.6 %; PFBA: degradation: 31.6 %, defluorination: 5.6 %. PFPrA: degradation: 21.6 %, defluorination: 5.6 %	-	[274]
PCQD/TiO_2	PFOA	1 g/L; 100 µg/L; 100 mL	UV light, 4×16 W; Visible light, 200 W	-	defluorination: 56.2% (UV), 46.6% (Visible)	-	[275]
PCQD/TiO_2	Short-chain PFCAs (C3–C6)	1 g/L; 100 µg/L each; 100 mL	UV light, 4×16 W; Visible light, 200 W	–	defluorination: 10.9% (Visible), 12.9% (UV)	-	[275]
Emerging Hybrid Systems							
MXene/TiO_2	PFOA	20 mg; 20 -100 mg/L; 150 mL	UV light	0.3296-0.1135 $\mathbf{h^{-1}}$	Degradation: 62.97 - 94.64 %; defluorination: 58.4 %, 9h	-	[281]

Ti_3C_2/TiO_2–80, Ti_3C_2-HF/TiO_2, P25	PFOA	200 mg L^{-1}; 20 µM; 50 mL	UV (Hg lamp), 254 nm, 20 mW cm^{-2}	–	>99.9% degraded, F^- 49%,16h	4	[282]
Ti_3C_2-HF/TiO_2, P25	PFOA	200 mg L^{-1}; 20 µM; 50 mL	UV (Hg lamp), 254 nm, 20 mW cm^{-2}	–	22%, F^- 12%,16 h; 4	-	[282]
TiO_2/zeolite nanocomposite	PFPA	0.5 g/L; 10 mg/L; Solution: n/a	UV light, 8 h	–	TiO_2/zeolite: 54.5%; RS model predicted 60.2%, experimental 58.7%	-	[283]
F-TiO2@MIL-125	PFOA, PFHpA, PFHxA, PFPeA	Amount n/a; PFAS: PFOA 185.151 µmol/g, PFHpA 155.932, PFHxA 106.509, PFPeA 57.902; Solution: n/a	Visible light	1.221 × 10^{-4}/s	PFOA degraded stepwise to CO_2 + F^-; adsorption equilibrium ~200 s; photocatalysis slower; High stability after multiple cycles (~96.7% regeneration)	multiple cycles	[65]
Photoelectrocatalysis (PEC)							
GO/TNA	PFOA	5×5 cm^2; 0.121–2.42 mM; 1.4 L	UV light, 8 W; UV light + external bias (0–2 V)	0.34 h^{-1} (25 °C, UV); 1.63 h^{-1} (75 °C, UV); – (PEC)	UV only: 83% in 4 h; PEC (2 V): 99.5%	3;-	[294]
TiO_2 nanoporous (BEEP photoreactor)	PFTeDA (C14), PFNA (C9), PFOS, 42 PFAS mixture	TiO_2 grown on inner Ti tube; PFAS 100 ppm (single analyte) / 42 PFAS mixture; 2 L solution	UVA 365 nm LED + 2 V bias (BEEP)	Not reported	PFTeDA: below detection in 12 h; PFOS: ~15% defluorination in 24 h; 42 PFAS: longer chains fully degraded in 24 h; smaller chains formed	-	[295]
TiO_2 photoanode (Plasma Electrolytic Oxidation on Ti mesh; anatase 58%, rutile 42%)	PFOA, PFHpA, PFHxA, PFPeA, PFBA, PFOS, PFHpS, PFHxS, PFBS	TiO_2 mesh; PFOA 2 µg/L in ultrapure water; groundwater: 873–1604 ng/L total PFAS; reactor volume 1 L	UV (two lamp powers, P1 and P2); photoelectrocatalysis (PEC)	PFOA: 0.00461–0.00652 min^{-1} (PEC P1); PFHpA: 0.00242–0.00428 min^{-1}; PFHxA: 0.00142–0.00309 min^{-1}; PFPeA: 0.00139–0.00315 min^{-1};	PFOA 96%, PFHpA 73%, PFHxA 75%, PFPeA 69%, PFBA 77%, PFOS 68%, PFHpS 40%, PFBS 1% @ 600 min	2	[296]

				PFBA: 0.00224–0.00292 min^{-1}; PFOS: 0.00261 min^{-1}; PFHpS: 0.00134 min^{-1}			
TiO_2 Nanotube Arrays (TNAs) with Molecularly Imprinted Polymers (MIPs)							
S-MIP-TiO_2 NTs, NIP-TiO_2 NTs, TiO_2 NTs	PFBA, PFPeA, PFHxA, PFHpA, PFOA	Active area: 400 cm^2/L; 10–109 ng/L, Wastewater: 10 µg/L; Solution: 300 mL (adsorption)	UV light, 8 W	TiO_2 NTs 0.0225, NIP-TiO_2 NTs 0.0316, S-MIP-TiO_2 NTs 0.0732 min^{-1}	S-MIP-TiO_2 NTs > NIP-TiO_2 NTs > TiO_2 NTs	5	[316]
TiO_2 NTs, NIP-TiO_2 NTs, MIP-TiO_2 NTs	PFOA, PFHA, PFOS,	-; 50 µmol/L; Competitive: PFOA 50 µmol/L + other PFAS 25 µmol/L;-	UV light	TiO_2 NTs 0.0011, NIP-TiO_2 NTs 0.0022, MIP-TiO_2 NTs 0.0036	TiO_2 NTs 41%, NIP-TiO_2 NTs 67%, MIP-TiO_2 NTs 84%; Secondary effluent: UV 18%, NIP-TiO_2 NTs 50.2%, MIP-TiO_2 NTs 81.1%; F^- release after 8 h: photolysis 5.4%, TiO_2 NTs 9.7%, NIP-TiO_2 NTs 15.7%, MIP-TiO_2 NTs 30.2%; TOC removal by MIP-TiO_2 NTs ~46%; -		[315]
PLA/TiO_2 composite tiles	PFOS, PFOA, PFHxA, PFBA, PFNA, PFDA, PFOSAm	14.7 wt% TiO_2; 850 cm^2 chamber surface; PFOS 130 ng/L, PFOA 1100–1500 ng/L, PFHxA 2900 ng/L, PFBA 2500 ng/L, PFNA 29 ng/L, PFDA 92 ng/L, PFOSAm 18 ng/L; PFUnDA/PFDOA near detection limit; -	UV light, ~0.34 W/m^2; cumulative 0.086–0.129 MJ/m^2	–	Mass removal rates: PFOS 2962–3072 ng/m^2/day; PFOA, PFHxA, PFPeA, PFBA >20,000 ng/m^2/day; Degradation: PFOS 91–95%, PFNA 89–93%, PFDA 86–95%, PFOSAm 89–92%, PFOA 39–78%; Short-chain PFAS increased due to longer-chain degradation; HRT 24 h vs 36 h; better removal at 36 h		[317]

Hybrid Advanced Oxidation Processes (AOPs)							
TiO_2 (P25)	PFOA	0.2-0.3 g/L; 10 mg/L; 0.8-1 L	UV light, 28 W	–	using O_3: 99.1% degradation, 44.3% C–F/4 h; using O_2: 46.4%		[303]
TiO_2/PMS	PFOA	0.25 g/L; 50 mg/L; 200 mL	300 W, 400–770 nm	0.310 h^{-1}	100%, 8 h	-	[304]
TiO_2/PMS	PFOA	0.25 g/L; 50 mg/L; 200 mL	32 W, 254 nm	1.09 h^{-1}	98%, 1.5 h	-	[304]

View Article Online
DOI: 10.1039/D5MA01247C

7. Critical Assessment of Parameters, Mechanisms, and Modifications

Table 1 summarizes the comparative performance of modified TiO_2 photocatalysts, including doped, composite, and immobilized systems, for PFAS degradation, highlighting key design strategies, degradation efficiencies, and operational stability. A critical comparative evaluation of these systems reveals clear performance hierarchies. Pristine TiO_2 (including P25) exhibits low degradation efficiency and defluorination (<30%), serving mainly as a benchmark [185,192,238]. Noble-metal-modified TiO_2 (Pt–TiO_2) achieves complete PFOA degradation in 7 h with high kinetics (0.727 h^{-1}) and substantial defluorination (~35%) [51,225]. Heterojunctions such as BiOBr/TiO_2 provide high defluorination (~65%) and full degradation in 8 h [234]. Carbon-supported hybrids (Fe/TNTs@AC) combine fast kinetics, high degradation (~90%), and excellent stability [254,260]. Emerging MXene/TiO_2 systems deliver up to 94.6% degradation and ~58% defluorination, providing scalable, noble-metal-free alternatives [281,282]. Photoelectrocatalytic TiO_2 systems achieve the highest overall performance (~99.5% degradation, 1.63 h^{-1}) though requiring applied bias and more complex reactors [295,296].

A comprehensive understanding of TiO_2-based PFAS photocatalysis necessitates the simultaneous evaluation of operational parameters, mechanistic pathways, and structural modifications (**Fig. 17**). These factors collectively determine degradation efficiency, selectivity, and stability. In this section, we critically assess the influence of key operational parameters, elucidate mechanistic insights into reactive species generation and C–F bond cleavage, and examine how structural and compositional modifications enhance charge separation and photocatalytic reactivity.

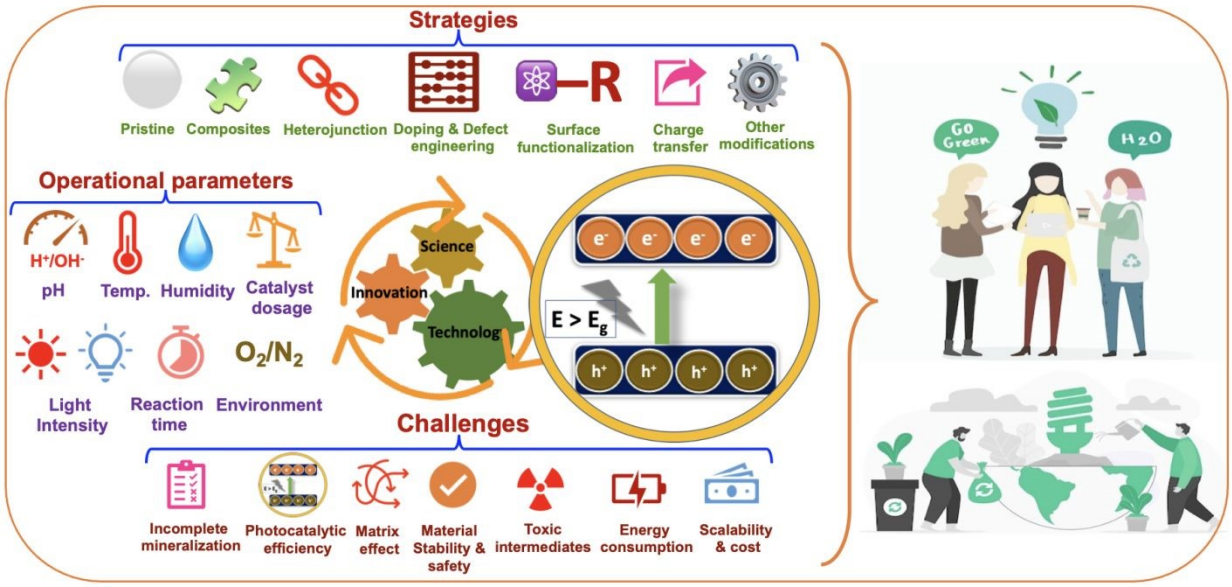

Figure 17. Overview of strategies, operational parameters, and remaining challenges involved in TiO_2-based photocatalysis. NOTE: a few parts of this figure are adapted from open sources like Freepik (https://www.freepik.com/) and Pixabay (https://pixabay.com/).

View Article Online
DOI: 10.1039/D5MA01247C

7.1. Influence of Operational Parameters

***pH and Surface Charge Effects*:** Photocatalytic performance of TiO_2-based photocatalysts in PFAS degradation is strongly governed by solution pH and the associated surface charge of the catalyst, which control PFAS adsorption, interfacial electron transfer, and reactive species generation. Acidic conditions favor degradation by protonating the catalyst surface, enhancing electrostatic attraction toward anionic PFAS molecules, and promoting the formation of reactive species such as $^{\bullet}OH$ and h^+ [184,185,195,197]. At higher pH, surface deprotonation occurs, and OH^- ions compete with PFAS for adsorption, reducing surface interactions and limiting photocatalytic activity. This behavior is directly related to the point of zero charge (pH_{pzc}) of the catalyst, which defines the pH at which the surface has a net neutral charge. When the solution pH exceeds pH_{pzc}, the surface becomes negatively charged, decreasing the adsorption of anionic PFAS and hindering subsequent photocatalytic reactions. To overcome these pH-dependent limitations, various surface modifications and composite strategies have been employed. In Fe/TNTs@AC composites, for instance, pH-related limitations are mitigated through surface modification. Pristine TNTs (pH_{pzc} = 2.57) show negligible PFOA adsorption due to their negative charge. Incorporation of Fe_2O_3 raises pH_{pzc} from 3.8 to 5.2, reducing repulsion and enhancing anionic PFOA adsorption. α-Fe_2O_3 (pH_{pzc} = 6.7) attracts PFOA's carboxylate head ($p_{Ka} \leq 3$) via electrostatic and Lewis acid–base interactions, while AC supports hydrophobic and anion–π interactions with the perfluorinated tail. This cooperative adsorption aligns PFOA for efficient hole-driven decarboxylation at the α-Fe_2O_3/TNTs interface. The composite achieves ~99% PFOA adsorption (pH 4–11) and ~61% defluorination at pH 4–8, declining to 56.8%, 42.7%, and 36.1% at pH 9–11. Other TiO_2 composites show similar adaptability: Fe:Nb–TiO_2 maintains activity from pH 4.3–9 via Fe-induced bandgap narrowing and Nb-assisted charge separation [22], In/TNTs@AC supports hole-driven decarboxylation over pH 4–11 [260], TiO_2-Pb/rGO sustains ROS-dominated degradation (h^+, $^{\bullet}O_2^-$, $^1O_2$) in pH 4.5–7.5 [267] and TiO_2-assisted photocatalytic ozonation achieves 99.1% PFOA removal and 44.3% defluorination under UV across pH 3-9 [303]. These advances extend TiO_2's operational pH window, enhancing its practicality for PFAS remediation.

Catalyst Loading and Atmosphere: Catalyst dosage also plays a dual role, moderate TiO_2-based photocatalysis loadings optimize UV light absorption and active site availability, while excessive loading leads to light scattering and reduced photon penetration, resulting in decreased degradation efficiency [185,192,238]. For example, in the Sb_2O_3/TiO_2 heterojunction system, an optimal 3 wt% Sb_2O_3 content achieved 81.8% PFOA degradation within 120 min, but higher catalyst concentrations suppressed activity due to agglomeration and recombination losses [238]. The type of oxidizing atmosphere further dictates reaction kinetics, oxygen-rich conditions favor reactive oxygen species (ROS) formation, while N_2 atmospheres can enhance reductive degradation pathways involving $CO_2^{\bullet-}$ radicals, particularly in the presence of organic electron donors like oxalic acid [187].

Temperature and Light Effects: Temperature and light conditions introduce additional complexity. While TiO_2 typically operates efficiently at ambient temperature (~25-30 °C), elevated temperatures can increase reaction rates up to an optimal limit before desorption

View Article Online
DOI: 10.1039/D5MA01247C

effects dominate [192,203]. The wavelength and intensity of illumination directly affect photon utilization, UV-C (254 nm) irradiation remains the most effective for initiating C–F bond scission, yet visible-light-responsive systems, achieved through metal or nonmetal modification, are gaining attention [222,234,275]. Temperature also influences charge carrier dynamics and radical generation. For instance, TiO_2/zeolite nanocomposites demonstrated enhanced PFPA degradation, where defluorination efficiency increased from 47.1% at 25 °C to 48.4% at 85 °C, with optimal performance below 100 °C to prevent thermal interference with photocatalytic pathways [283]. Elevated temperature promoted •OH radical formation and accelerated surface oxidation by improving charge carrier mobility and reducing recombination losses. These findings demonstrate that fine-tuning operational parameters is crucial for balancing adsorption, photon flux, and charge transfer dynamics in TiO_2-driven PFAS degradation systems.

7.2. Mechanistic Insights

A commonly proposed degradation pathway for PFOA begins with photoinduced oxidative decarboxylation, producing perfluoroalkyl radicals ($^{\bullet}C\square F_2\square_{+1}$). These radicals then undergo reactions with O_2 or H_2O to form perfluoroalcohol intermediates, which subsequently yield shorter-chain PFCAs through β-scission and hydrolysis. The chain-shortening continues stepwise until CO_2 and F^- are released. This mechanism has been supported by LC-MS and ion chromatography analyses, revealing time-dependent decreases in PFOA and corresponding increases in fluoride ions [185,187,238]. While oxidative routes dominate under oxygen-rich conditions, reductive pathways have also been recognized as critical for effective defluorination, especially under UV irradiation in the presence of organic hole scavengers (e.g., methanol or oxalic acid). The conduction band electrons in TiO_2 can react with O_2 to form $O_2^{\bullet-}$ or directly attack the carbon-fluorine bonds via hydrated electrons (e_{aq}^-) or $CO_2^{\bullet-}$ intermediates, enabling partial reduction of highly stable PFASs [187]. This dual-pathway mechanism, where oxidative and reductive routes operate concurrently, explains why systems with balanced oxygen availability and sacrificial donors often exhibit superior degradation rates compared to purely oxidative setups [51].

Moreover, the crystal phase and exposed facets of TiO_2 critically influence charge separation and reactive oxygen species (ROS) generation. Anatase TiO_2 typically exhibits superior photocatalytic activity compared to rutile, owing to its higher surface area and lower e^--h^+ recombination rates [36,51,222]. Surface modifications, such as fluorination or oxygen vacancies (TiO_{2-x}), further enhance electron trapping and extend carrier lifetimes, promoting •OH radical formation and effective C–F bond cleavage [234,275]. Incorporation of carbon-based materials, including graphene oxide or MWCNTs, improves electron conductivity and facilitates π–π interactions with PFAS molecules, enhancing charge transfer and radical-mediated degradation [264].

The reaction kinetics of PFAS degradation generally follow a pseudo-first-order model, highlighting the importance of electron transfer between TiO_2 and adsorbed PFAS molecules. Degradation rates can be influenced by PFAS chain length, surface adsorption, and operational

View Article Online
DOI: 10.1039/D5MA01247C

conditions such as pH, dissolved oxygen, light intensity, temperature, and the presence of co-contaminants. Short-chain PFASs may degrade more slowly due to weaker adsorption, whereas long-chain PFASs, despite stronger initial adsorption, often undergo slower complete mineralization. These insights underscore the need to optimize both the interplay of surface adsorption and e^--h^+ utilization and the operational parameters to achieve efficient defluorination and total organic carbon removal in TiO_2-based PFAS remediation systems.

7.3. Structural and Compositional Modifications

Bandgap Engineering via Doping and Decoration: Transition-metal doping and noble-metal decoration have two recurring effects: narrowing the optical bandgap or introducing midgap states that extend light absorption toward visible wavelengths and acting as electron traps that reduce recombination. Cu- and Fe-doped TiO_2 systems outperformed bare TiO_2 in PFOA decomposition, with Cu doping particularly effective at lowering the bandgap and enhancing e^- trapping [223]. Noble metals (Pt, Pd, Ag) act as efficient electron sinks and promote hole-driven oxidation; the ordering Pt > Pd > Ag > TiO_2 observed in one comparative study evidences the benefit of strong electron trapping and Schottky junction formation for enhanced h_{vb}^+ activity and intermediate PFCA formation (PFHpA–PFPrA) leading toward CO_2 + F^- [225]. Most striking mechanistic advances come from single-atom catalysts: a facet-engineered TiO_2 with atomically dispersed Pt (Pt_1) not only improved charge separation but uniquely enabled both oxidative ($^\bullet$OH generation) and reductive (H spillover and hydrodefluorination) routes; the study reported substantial Ti–F surface binding (≈58% of fluorine associated with Ti–F), underscoring strong surface-mediated defluorination and single-atom stability via Pt–O coordination [51]. These single-atom platforms therefore broaden the mechanistic toolkit from purely oxidative chain-shortening toward hybrid oxidative–reductive defluorination, an important step for challenging C–F bond cleavage.

Heterojunctions for Enhanced Photocatalysis: Creating intimate interfaces between TiO_2 and other semiconductors (BiOX, ReS_2, BN, Sb_2O_3, etc.) enhances spatial charge separation and tailors the dominant ROS. BiOX/TiO_2 heterojunctions follow the trend BiOCl/TiO_2 > BiOBr/TiO_2 > BiOI/TiO_2 in activity, reflecting band alignment and carrier transport differences; in these systems h^+ and $O_2^{\bullet-}$ jointly drive stepwise decarboxylation [234]. S-scheme heterostructures such as ReS_2–TiO_2 introduce an internal electric field and oxygen vacancies that selectively retain high-energy electrons and holes at appropriate sites, thereby increasing $^\bullet O_2^-$ and $^\bullet$OH formation and producing measurable gains in PFAS degradation over bare TiO_2 [246]. Sb_2O_3 loading is another demonstrable success: an optimized 3 wt% Sb_2O_3/TiO_2 composition achieved ~81.8% PFOA degradation in 120 min with good reusability (~88% retained after five cycles), while excessive loadings were detrimental due to light attenuation and recombination, illustrating the criticality of tuning interfacial content to balance light harvesting and charge dynamics [238].

Conductive Carbon Supports for Enhanced PFAS Photocatalysis: Incorporation of conductive carbon supports, rGO, MWCNTs, CQDs, and graphene oxide, fulfills multiple roles: electron conductivity to prolong charge carrier lifetimes, light absorption extension, and in some cases adsorption enhancement that localizes PFAS near reactive sites. Quantitatively, rGO decoration

View Article Online
DOI: 10.1039/D5MA01247C

reduced the TiO_2 bandgap from 3.25 to 2.94 eV and improved photocatalytic performance, while MWCNT/TiO_2 composites with an optimal 10:1 ratio combined adsorption with efficient electron storage to suppress recombination and drive stepwise CF_2 cleavage [264,265,266]. Exfoliated CQD/TiO_2 composites demonstrated markedly superior PFOA degradation (69% under UVC, 50% under visible) compared to bare TiO_2 (41%/24%), linking improved interparticle electron transfer and reduced aggregation to measurable gains in both conversion and defluorination stability [274]. These results collectively show that conductive carbon frameworks are among the most practical routes to visible-light activity and suppressed recombination without relying solely on scarce noble metals.

Adsorptive and 2D Supports for PFAS Photocatalysis: Adsorptive enrichment increases local PFAS concentration at photocatalytic sites and can convert dilute, hard-to-treat streams into effectively treatable loads. Fe/TNTs@AC and In/TNTs@AC exemplify this strategy: low Fe loadings (~1 wt%) on TNTs@AC enabled robust adsorption followed by h^+-dominated Kolbe-like decarboxylation, producing stepwise C–F cleavage with reduced energy consumption compared to bulk aqueous approaches [254,260]. Zeolite supports with 10% TiO_2 achieved 54.5% defluorination at 85 °C and pH 13 (0.5 g L^{-1} catalyst), highlighting that support choice and operating pH are decisive for defluorination yields [283]. Molecularly imprinted polymer coatings (MIP-TiO_2 NTs) provide an additional level of selectivity for low-concentration PFAS in complex matrices, improving capture and subsequent photocatalytic turnover (S-MIP and MIP devices showed selectivity orders such as PFOA > PFOS > PFHA), though attention must be paid to the risk of concentrating toxic intermediates if mineralization is incomplete [316, 315]. MXene/TiO_2 composites (Ti_3C_2/TiO_2) and related 2D supports have emerged as powerful synergies of adsorption and electron transport. Intercalation strategies (e.g., DES-assisted $NaBF_4$ intercalation) enlarge MXene spacing to favor TiO_2 growth and intimate contact, producing composites that outperform P25 in adsorption/photocatalysis and that display stable, reusable behavior (optimal $NaBF_4$ ~80 mM; pzc ≈ 5.8) [282]. MXene-based composites often report the active species order $^{\bullet}OH$ > $^{\bullet}O_2^-$ > h^+ and optimal pH values around 5.2, but like other high-adsorption supports they must be carefully dosed to avoid aggregation and UV scattering [281,282].

Reactor and hybrid process engineering: Beyond material chemistry, reactor innovation (PEC, applied bias, photoelectrocatalytic meshes, 3D-printed TiO_2 tiles) materially affects scalability and energy efficiency. Applied bias in nanoporous arrays (BEEP technology) enhanced charge separation sufficiently to operate across salinity ranges (0–35 g L^{-1}) and to preferentially degrade longer-chain PFAS first, generating short-chain intermediates that can then be further treated in downstream units [295]. Photoelectrocatalytic treatment of groundwater in Veneto achieved ~63–65% removal across mixed PFAS compounds with lower energy input than photolysis at higher lamp power, illustrating that process integration (PEC vs PL) can lower EEO while maintaining comparable efficacy [296]. Hybrid oxidant strategies coupling TiO_2 with PMS or O_3 represent another practical path: TiO_2/PMS delivered 100% PFOA removal under 300 W visible light (0.25/0.75 g L^{-1} TiO_2/PMS at pH 3) and UV/TiO_2/O_3 reached 99.1% degradation with 44.3% defluorination under acidic conditions, highlighting that radical type ($SO_4^{\bullet-}$ vs $^{\bullet}OH$) and oxidant dosing strategy critically determine both conversion and defluorination efficacy [303,304].

View Article Online
DOI: 10.1039/D5MA01247C

8. Challenges and Knowledge Gaps

Despite the remarkable progress summarized above, the practical application of TiO_2-based photocatalytic systems for PFAS degradation remains constrained by a combination of scientific, engineering, and environmental challenges (**Fig. 17**). These challenges extend beyond catalytic activity alone and encompass incomplete mineralization, energy efficiency, reactor scalability, matrix effects, catalyst stability, and mechanistic uncertainty. Addressing these interconnected limitations is essential for translating laboratory-scale successes into viable water treatment technologies.

8.1. Incomplete Mineralization and Transformation Limitations

The foremost limitation of TiO_2-based PFAS photocatalysis is incomplete mineralization, even when high apparent degradation efficiencies are reported. In many systems, the disappearance of parent PFAS compounds does not correspond to full defluorination or conversion to CO_2 and inorganic fluoride. Instead, short-chain perfluorinated intermediates, particularly C_2–C_5 perfluorocarboxylates, tend to accumulate, some of which are equally or more recalcitrant and mobile than their long-chain precursors [185,303]. This behavior arises from the exceptionally high C–F bond dissociation energy and the reduced adsorption affinity of short-chain PFASs toward TiO_2 surfaces. Consequently, extended irradiation times or secondary treatment stages are often required, underscoring that achieving selective and complete defluorination, rather than partial molecular transformation, remains a central mechanistic and catalyst-design challenge.

8.2. Material Stability and Environmental Safety

Material stability and environmental safety represent critical challenges for the practical deployment of modified TiO_2 photocatalysts. Under prolonged irradiation, surface processes such as Ti–F bond accumulation can occur, leading to active-site passivation and suppression of further photocatalytic reactions. In parallel, leaching of dopant metals (e.g., Cu, Fe, Sb, Pb) or the release of nanoscale catalyst fragments during operation poses risks of secondary contamination and long-term performance deterioration [238,282]. Although several modified TiO_2 systems exhibit acceptable recyclability over five to ten laboratory cycles with minimal activity loss, extended aging, fouling, mechanical integrity, and durability under realistic continuous-flow conditions remain largely uncharacterized. Beyond catalytic performance, comprehensive evaluation of toxicity and environmental compatibility is essential prior to large-scale implementation. Modified TiO_2 systems must be assessed for the formation of potentially harmful transformation by-products, metal ion release, and long-term ecological impacts under realistic water treatment conditions. Life-cycle considerations, including material synthesis, operational stability, and end-of-life disposal, remain largely overlooked in current photocatalysis studies but are critical for ensuring sustainable deployment.

View Article Online
DOI: 10.1039/D5MA01247C

Emerging composite materials further complicate stability and safety considerations. For example, MXene–TiO_2 hybrids are susceptible to surface oxidation and structural degradation in aqueous and oxidative environments [318], particularly under prolonged illumination and in the presence of dissolved oxygen. Such degradation can reduce electrical conductivity, disrupt interfacial charge transfer, impair photocatalytic efficiency, and increase the likelihood of metal species release. Consequently, systematic long-term stability, leaching, toxicity, and environmental impact assessments under realistic operational conditions are required before modified TiO_2 catalysts, especially advanced composite systems, can be considered viable for sustained PFAS remediation.

8.3. Water Matrix Effects and Process Complexity

Matrix effects represent a significant challenge for the real-world application of photocatalytic systems. Constituents commonly present in natural and wastewater matrices, such as bicarbonates, chlorides, natural organic matter (NOM), and competing inorganic anions, can substantially suppress photocatalytic activity by scavenging reactive oxygen species (ROS) or occupying active surface sites [319,320]. Suspended solids, colored components, natural antioxidants, and mixed pollutants in real water matrices can further reduce photon penetration and pollutant–catalyst contact, exacerbating activity losses relative to idealized laboratory conditions. Beyond reducing degradation rates, these matrix components can alter reaction pathways and shift product distributions. Laboratory experiments conducted under idealized aqueous conditions often overestimate performance compared to complex environmental matrices. Dissolved oxygen (DO) is a critical chemical factor that interacts with water matrix effects. DO can enhance PFAS degradation in systems dominated by holes (h^+) by suppressing electron–hole recombination and promoting hydroxyl radical formation (e.g., Pb-TiO_2: ~25% PFOA removal under N_2 vs. ~95–98% at 1.6–7.1 mg/L DO [228]). Conversely, in systems where electron-mediated or direct photolysis pathways are dominant, high DO can suppress degradation efficiency. Matrix components and DO together influence real-water photocatalytic performance, affecting both reaction rates and pathways. Therefore, standardized testing protocols that incorporate realistic water chemistry, including DO levels, are essential for meaningful cross-study comparisons and scalable reactor design.

8.4. Energy Efficiency and Practical Considerations

The energy required for PFAS photocatalytic degradation is a critical factor in evaluating the feasibility of treatment technologies [124]. Photocatalytic systems relying on UV-C irradiation or high-intensity mercury lamps may exhibit high electrical energy per order (EE/O) values when photon utilization is inefficient, potentially limiting large-scale implementation unless reactor design and irradiance are carefully optimized [321]. Despite its importance, EE/O is not reported consistently across studies, complicating direct techno-economic comparisons. Some studies have considered energy consumption metrics to evaluate and compare system performance. For example, BN/TiO_2 composites have been reported to achieve lower EE/O values than bare TiO_2, with lamp output-based EE/O values of ~102 kWh m^{-3} $order^{-1}$ under 254-nm irradiation and ~253 kWh m^{-3} $order^{-1}$ under 365-nm irradiation [36]. A TiO_2-Pb/rGO system achieved 98% PFOA

View Article Online
DOI: 10.1039/D5MA01247C

removal with an EE/O of 4.05 kWh m^{-3} [267]. PEC generally requires lower energy than PL, with EEO ranges of 20–150 kWh m^{-3} (PEC) and 60–240 kWh m^{-3} (PL) [296]. In ultrapure water, PEC EEO values for PFOA (35.8–62.6 kWh m^{-3}) are much lower than sonolysis and photochemical oxidation and comparable to plasma and advanced reduction processes. Higher energy demand in groundwater is due to matrix complexity and lower PFAS concentrations.

8.5. Hybrid Photocatalytic Systems and Operational Complexity

Hybrid photocatalytic systems, including TiO_2/PMS and TiO_2/O_3, have been widely investigated for the enhanced degradation of persistent pollutants such as PFAS by combining direct photocatalytic oxidation with radical-mediated pathways [322,323]. Although these systems often outperform standalone photocatalysis under laboratory conditions, their practical implementation remains constrained by chemical complexity and operational limitations. A major challenge is the formation of undesirable transformation products. The generation of reactive oxygen species (e.g., $^{\bullet}OH$ and $SO_4^{\bullet-}$) can promote rapid pollutant degradation, but competing side reactions are common in real water matrices [324]. In the presence of nitrate or nitrite, reactive nitrogen species may form and induce nitration reactions, leading to nitrogen-containing by-products that can be more persistent and toxic than the parent compounds. As a result, high removal efficiencies do not necessarily correspond to reduced environmental risk, highlighting the importance of transformation product analysis and toxicity evaluation alongside conventional performance metrics.

Scalability is further limited by operational complexity. Hybrid systems depend on external oxidants such as persulfate, ozone, or hydrogen peroxide, which increase energy consumption, chemical usage, and process cost. Precise control of oxidant dosing and reaction conditions is required to avoid inefficiencies, secondary reactions, or residual oxidant release. Alternative hybrid configurations, such as photocatalysis combined with adsorption, membrane processes, or photoelectrocatalysis, can improve specific aspects of performance but introduce additional challenges related to reactor design, mass transfer, fouling, and material stability [325,326].

8.6. Engineering Challenges and Scalability Considerations

TiO_2-based photocatalysis for PFAS degradation is still largely at the laboratory research stage, with most studies conducted under controlled, ideal conditions. While these studies demonstrate the significant potential for photocatalyst, translating laboratory-scale findings into continuous-flow or field applications faces multiple engineering, operational, and scalability challenges.

Photocatalyst Immobilization and Stability: Immobilization remains a major bottleneck. Suspended or slurry-phase photocatalysts offer high surface areas but complicate separation, recovery, reuse, and containment [321,327]. Immobilized configurations, including porous coatings, supported membranes, structured reactors, and 3D-printed monoliths, enhance retention, operational safety, and continuous-flow capability while minimizing secondary contamination. However, long-term stability under prolonged irradiation and in complex water matrices remains poorly understood. Immobilization can introduce mass-transfer limitations and

View Article Online
DOI: 10.1039/D5MA01247C

reduced active-site accessibility, while activity losses may arise from surface deactivation, fluoride accumulation, photocorrosion, dopant leaching, or adsorption of intermediates. Prolonged operation may induce surface restructuring and active-site passivation, contributing to gradual performance decline.

Flow Reactor Design and Mass Transfer: Most lab studies employ batch reactors, which do not replicate continuous-flow conditions [328,329]. Scaling up requires optimization of hydrodynamics, residence time, photon delivery, and pollutant–catalyst contact. Optical non-uniformities and mass-transfer limitations may arise upon scale-up [321]. Hybridized systems combining membranes, cross-flow configurations, or adsorption–photocatalysis approaches can mitigate fouling, enhance catalyst utilization, and improve operational flexibility.

LED and Solar-Assisted Light Sources: LED- and solar-assisted systems offer improved energy efficiency, wavelength tunability, and operational safety [330]. Limited light penetration and non-uniform photon distribution remain critical, especially in large-volume or continuous-flow reactors. UV reactors often rely on mercury-vapor lamps, with associated environmental issues, whereas visible-light-active composites enable LED use, though fabrication still involves rare earth elements [331]. Strategies to improve photon distribution include optimized LED arrays, reflective optics, thin-film or immobilized catalysts, and solar-assisted hybrid operation.

9. Conclusions and Perspectives

TiO_2-based photocatalysis has emerged as a versatile and promising strategy for PFAS remediation, offering sustainable pathways to break the highly resilient C–F bond. Advances in material modification, heterojunction engineering, and integration with conductive or carbonaceous supports have enhanced charge separation, light harvesting, and reactive species generation, leading to significant progress in PFAS degradation, and establishing TiO_2 as a leading and well-studied photocatalytic platform for PFAS treatment. In summary, this review not only highlighted recent advances in TiO_2-based photocatalysis for PFAS remediation but also critically assessed the influence of operational parameters, mechanistic pathways, structural and compositional modifications, hybrid and system-level strategies, and associated engineering and environmental challenges, providing a comprehensive overview of opportunities and remaining mechanistic gaps.

Looking forward, future research should prioritize hybrid and system-level strategies to improve efficiency and scalability. Photoelectrocatalytic configurations under low external biases can enhance charge separation, improve defluorination, and reduce energy consumption; coupling TiO_2 with conductive or tailored carbon materials such as graphene, carbon nitride, or MXenes can facilitate interfacial charge transport, lower overpotentials, and improve catalyst stability; and S-scheme heterojunctions help maintain strong redox potentials and suppress charge recombination. Integrated “concentrate-and-destroy” approaches, where TiO_2-coated adsorbents capture PFAS from dilute streams followed by in situ photodegradation, may overcome mass-transfer limitations and minimize secondary waste. To bridge laboratory innovation with field-scale application, future efforts must emphasize environmental

View Article Online
DOI: 10.1039/D5MA01247C

compatibility, sustainability, and safety, with rigorous evaluation of catalyst toxicity, transformation byproducts, and life-cycle impacts, combined with durable, scalable reactor designs and energy-efficient operation. Coordinated advances across materials science, process engineering, and policy frameworks, guided by molecular design principles and data-driven discovery, can transform TiO_2-based photocatalysis from a promising research platform into a field-ready solution for one of today's most persistent forever chemicals.

Author Contributions

Avtar Singh: Conceptualization, Investigation, Methodology, Visualization, Writing - original draft, Writing - review & editing, Supervision; Thiagarajan Soundappan: Writing - review & editing.

Conflicts of interest

There are no conflicts to declare.

Data availability

No primary research results, software or code have been included, and no new data were generated or analyzed as part of this review.

Acknowledgment

The authors express their gratitude to Dr. Yogesh Singla, Navajo Technical University (NTU), NM, USA, alongside their other collaborators and peers for their invaluable insights in shaping this manuscript. The authors also extend their appreciation to the publishers for granting permission to reproduce figures used in this publication.

References

1. Cousins, I. T.; Ng, C. A.; Wang, Z.; Scheringer, M. Why Is High Persistence Alone a Major Cause of Concern? Environ. Sci.: Processes Impacts 2019, 21 (5), 781–792. https://doi.org/10.1039/C8EM00515J.
2. Jensen, S.; Johnels, A.; Olsson, M.; Otterlind, G. DDT and PCB in Marine Animals from Swedish Waters. Nature 1969, 224, 247–250. https://doi.org/10.1038/224247a0.
3. Kaushik, A.; Singh, A.; Gupta, V. K.; Mishra, Y. K. Nano/Micro-Plastic, an Invisible Threat Getting into the Brain. Chemosphere 2024, 361, 142380. https://doi.org/10.1016/j.chemosphere.2024.142380.
4. Butzlaff, A. H.; Deighton, J.; Le, T.; Nguyen, K.; Bonilla, C.; Chen, Z.; Kirshner, M.; Shikuma, N.; Peccia, J.; McNeill, K.; Higgins, C. P. PFAS, 6-PPD-Q, and Microplastics in Urban Sewer Overflows: Co-Occurrence and High-Rate Treatment Assessment. npj Emerg. Contam. 2025, 1, 5. https://doi.org/10.1038/s44454-025-00010-4.

View Article Online
DOI: 10.1039/D5MA01247C

5. Schymanski, E. L.; Zhang, J.; Thiessen, P. A.; Chirsir, P.; Kondic, T.; Bolton, E. E. Per- and Polyfluoroalkyl Substances (PFAS) in PubChem: 7 Million and Growing. Environ. Sci. Technol. 2023, 57 (44), 16918–16928. https://doi.org/10.1021/acs.est.3c04855.
6. Tokranov, A. K.; Hopkins, Z. R.; Lindsey, B. D.; Jurgens, B. C. PFAS Are Widespread, Not Ubiquitous: Clarifying Misconceptions About the Prevalence of "Forever Chemicals." Environ. Sci. Technol. 2025, 59 (24), 11947–11949. https://doi.org/10.1021/acs.est.5c03878.
7. Boettger, J. D.; DeLuca, N. M.; Zurek-Ost, M. A.; Miller, K. E.; Fuller, C.; Bradham, K. D.; Ashley, P.; Friedman, W.; Pinzer, E. A.; Cox, D. C.; Dewalt, G.; Isaacs, K. K.; Hubal, E. A. C.; McCord, J. P. Emerging Per- and Polyfluoroalkyl Substances in Tap Water from the American Healthy Homes Survey II. Environ. Sci. Technol. 2025, 59 (5), 2686–2698. https://doi.org/10.1021/acs.est.4c08037.
8. Ríos-Bonilla, K. M.; Aga, D. S.; Lee, J.; König, M.; Qin, W.; Cristobal, J. R.; Atilla-Gokcumen, G. E.; Escher, B. I. Neurotoxic Effects of Mixtures of Perfluoroalkyl Substances (PFAS) at Environmental and Human Blood Concentrations. Environ. Sci. Technol. 2024, 58 (38), 16774–16784. https://doi.org/10.1021/acs.est.4c06017.
9. Gaines, L. G. T. Historical and Current Usage of Per- and Polyfluoroalkyl Substances (PFAS): A Literature Review. Am. J. Ind. Med. 2023, 66, 353–378. https://doi.org/10.1002/ajim.23362.
10. O'Hagan, D. Understanding Organofluorine Chemistry: An Introduction to the C–F Bond. Chem. Soc. Rev. 2008, 37, 308–319. https://doi.org/10.1039/B711844A. 10b-Jeon, S.; Lee, E.; Min, T.; Lee, Y.; Lee, G.; Kim, A.; Yoon, H. Efficient Removal of Short-Chain Perfluoroalkyl Substances (PFAS) Using Asymmetric Membrane Capacitive Deionization. Sep. Purif. Technol. 2024, 348, 127728. https://doi.org/10.1016/j.seppur.2024.127728.
11. Leter, G.; Consales, C.; Eleuteri, P.; Uccelli, R.; Specht, I. O.; Toft, G.; Moccia, T.; Budillon, A.; Jönsson, B. A. G.; Lindh, C. H.; Giwercman, A.; Pedersen, H. S.; Ludwicki, J. K.; Zviezdai, V.; Heederik, D.; Bonde, J. P. E.; Spanò, M. Exposure to Perfluoroalkyl Substances and Sperm DNA Global Methylation in Arctic and European Populations. Environ. Mol. Mutagen. 2014, 55, 591–600. https://doi.org/10.1002/em.21874.
12. Fenton, S. E.; Ducatman, A.; Boobis, A.; DeWitt, J. C.; Lau, C.; Ng, C.; Smith, J. S.; Roberts, S. M. Per- and Polyfluoroalkyl Substance Toxicity and Human Health Review: Current State of Knowledge and Strategies for Informing Future Research. Environ. Toxicol. Chem. 2021, 40 (3), 606–630. https://doi.org/10.1002/etc.4890.
13. He, Y.; Cheng, X.; Gunjal, S. J.; Zhang, C. Advancing PFAS Sorbent Design: Mechanisms, Challenges, and Perspectives. ACS Mater. Au 2024, 4 (2), 108–114. https://doi.org/10.1021/acsmaterialsau.3c00066.
14. Pauletto, P. S.; Bandosz, T. J. Activated Carbon versus Metal–Organic Frameworks: A Review of Their PFAS Adsorption Performance. J. Hazard. Mater. 2022, 425, 127810. https://doi.org/10.1016/j.jhazmat.2021.127810.
15. Loukopoulos, E.; Marugán-Benito, S.; Raptis, D.; Tylianakis, E.; Froudakis, G. E.; Mavrandonakis, A.; Platero-Prats, A. E. Chemically Tailored Metal–Organic Frameworks for Enhanced Capture of Short- and Long-Chain Per- and Polyfluoroalkyl Substances from Water. Adv. Funct. Mater. 2024, 34, 2409932. https://doi.org/10.1002/adfm.202409932.

View Article Online
DOI: 10.1039/D5MA01247C

16. Liang, R.-R.; Xu, S.; Han, Z.; Yang, Y.; Wang, K.-Y.; Huang, Z.; Rushlow, J.; Cai, P.; Samorì, P.; Zhou, H.-C. Exceptionally High Perfluorooctanoic Acid Uptake in Water by a Zirconium-Based Metal–Organic Framework through Synergistic Chemical and Physical Adsorption. J. Am. Chem. Soc. 2024, 146 (14), 9811–9818. https://doi.org/10.1021/jacs.3c14487.
17. Mukhopadhyay, R.; Sarkar, B.; Palansooriya, K. N.; Dar, J. Y.; Bolan, N. S.; Parikh, S. J.; Sonne, C.; Ok, Y. S. Natural and Engineered Clays and Clay Minerals for the Removal of Poly- and Perfluoroalkyl Substances from Water: State-of-the-Art and Future Perspectives. Adv. Colloid Interface Sci. 2021, 297, 102537. https://doi.org/10.1016/j.cis.2021.102537.
18. Luft, C. M.; Schutt, T. C.; Shukla, M. K. Properties and Mechanisms for PFAS Adsorption to Aqueous Clay and Humic Soil Components. Environ. Sci. Technol. 2022, 56 (14), 10053–10061. https://doi.org/10.1021/acs.est.2c00499.
19. Gomri, C.; Benkhaled, B. T.; Cretin, M.; Semsarilar, M. Adsorbent Material Used for the Treatment of Per- and Poly-Fluoroalkyl Substances (PFAS): A Short Review. Macromol. Chem. Phys. 2024, 225, 2400012. https://doi.org/10.1002/macp.202400012.
20. Smith, S. J.; Lauria, M.; Ahrens, L.; McCleaf, P.; Hollman, P.; Seroka, S. B.; Hamers, T.; Arp, H. P. H.; Wiberg, K. Electrochemical Oxidation for Treatment of PFAS in Contaminated Water and Fractionated Foam,A Pilot-Scale Study. ACS ES&T Water 2023, 3 (4), 1201–1211. https://doi.org/10.1021/acsestwater.2c00660.
21. Bashir, Y.; Raj, R.; Ghangrekar, M. M.; Nema, A. K.; Das, S.; Zhang, L.; Si, C.; Zeng, F.; Duan, X.; Zhang, D.; Xu, W.; Shi, J. Critical Assessment of Advanced Oxidation Processes and Bio-Electrochemical Integrated Systems for Removing Emerging Contaminants from Wastewater. RSC Sustainability 2023, 1, 1912–1931. https://doi.org/10.1039/D3SU00112A.
22. Persulfate Activation for Efficient Remediation of Perfluorooctanoic Acid (PFOA) and Perfluorooctane Sulfonic Acid (PFOS) in Water: Mechanisms, Removal Efficiency, and Future Prospects. J. Environ. Chem. Eng. 2024, 12 (1), 111422. https://doi.org/10.1016/j.jece.2023.111422.
23. Cao, C.-S.; Wang, J.; Yang, L.; Wang, J.; Zhang, Y.; Zhu, L. A Review on the Advancement in Photocatalytic Degradation of Poly/Perfluoroalkyl Substances in Water: Insights into the Mechanisms and Structure–Function Relationship. Science of The Total Environment 2024, 946, 174137. https://doi.org/10.1016/j.scitotenv.2024.174137
24. Rosansky, S.; Al-Dirani, S. M.; Scheitlin, C. G.; Dasu, K.; Dzurnak, M.; Xia, X.; Orth, C.; McCauley, M.; Mullins, L. Field Demonstration of PFAS Destruction in Various Alcohol-Resistant AFFFs Using Supercritical Water Oxidation (SCWO). ACS ES&T Water 2024, 4 (10), 4486–4496. https://doi.org/10.1021/acsestwater.4c00499.
25. McDonough, J. T.; Kirby, J.; Bellona, C.; Quinnan, J. A.; Welty, N.; Follin, J.; Liberty, K. Validation of Supercritical Water Oxidation to Destroy Perfluoroalkyl Acids. Remediation 2022, 32, 75–90. https://doi.org/10.1002/rem.21711.
26. Skinner, J. P.; Raderstorf, A.; Rittmann, B. E.; Delgado, A. G. Biotransforming the “Forever Chemicals”: Trends and Insights from Microbiological Studies on PFAS. Environ. Sci. Technol. 2025, 59 (11), 5417–5430. https://doi.org/10.1021/acs.est.4c04557.
27. LaFond, J. A.; Hatzinger, P. B.; Guelfo, J. L.; Millerick, K.; Jackson, W. A. Bacterial Transformation of Per- and Poly-Fluoroalkyl Substances: A Review for the Field of

View Article Online
DOI: 10.1039/D5MA01247C

Bioremediation. Environ. Sci.: Adv. 2023, 2, 1019–1041. https://doi.org/10.1039/D3VA00031A.

28. Wackett, L. P. Nothing Lasts Forever: Understanding Microbial Biodegradation of Polyfluorinated Compounds and Perfluorinated Alkyl Substances. Microb. Biotechnol. 2022, 15 (3), 773–792. https://doi.org/10.1111/1751-7915.14018.
29. Nau-Hix, C.; Multari, N.; Singh, R. K.; Richardson, S.; Kulkarni, P.; Anderson, R. H.; Holsen, T. M.; Thagard, S. M. Field Demonstration of a Pilot-Scale Plasma Reactor for the Rapid Removal of Poly- and Perfluoroalkyl Substances in Groundwater. ACS ES&T Water 2021, 1 (3), 680–687. https://doi.org/10.1021/acsestwater.0c00170.
30. Singh, R. K.; Multari, N.; Nau-Hix, C.; Woodard, S.; Nickelsen, M.; Mededovic Thagard, S.; Holsen, T. M. Removal of Poly- and Per-Fluorinated Compounds from Ion Exchange Regenerant Still Bottom Samples in a Plasma Reactor. Environ. Sci. Technol. 2020, 54 (21), 13973–13980. https://doi.org/10.1021/acs.est.0c02158.
31. Kim, N.; Elbert, J.; Shchukina, E.; et al. Integrating Redox-Electrodialysis and Electrosorption for the Removal of Ultra-Short- to Long-Chain PFAS. Nat. Commun. 2024, 15, 8321. https://doi.org/10.1038/s41467-024-52630-w.
32. Liu, C.; Zhao, X.; Faria, A. F.; Deliz Quiñones, K. Y.; Zhang, C.; He, Q.; Ma, J.; Shen, Y.; Zhi, Y. Evaluating the Efficiency of Nanofiltration and Reverse Osmosis Membrane Processes for the Removal of Per- and Polyfluoroalkyl Substances from Water: A Critical Review. Sep. Purif. Technol. 2022, 302, 122161. https://doi.org/10.1016/j.seppur.2022.122161.
33. Awoyemi, O. S.; Naidu, R.; Fang, C. Advancements on Ultrasonic Degradation of Per- and Polyfluoroalkyl Substances (PFAS): Toward Hybrid Approaches. Environments 2024, 11, 187. https://doi.org/10.3390/environments11090187.
34. Chen, X.; Yuan, T.; Yang, X.; Ding, S.; Ma, M. Insights into Photo/Electrocatalysts for the Degradation of Per- and Polyfluoroalkyl Substances (PFAS) by Advanced Oxidation Processes. *Catalysts* 2023, *13* (9), 1308. https://doi.org/10.3390/catal13091308.
35. Kim, T.-H.; Lee, S.-H.; Kim, H. Y.; Doudrick, K.; Yu, S.; Kim, S. D. Decomposition of Perfluorooctane Sulfonate (PFOS) Using a Hybrid Process with Electron Beam and Chemical Oxidants. *Chem. Eng. J.* 2019, *361*, 1363–1370. https://doi.org/10.1016/j.cej.2018.10.195.
36. Duan, L.; Wang, B.; Heck, K. N.; Clark, C. A.; Wei, J.; Wang, M.; Metz, J.; Wu, G.; Tsai, A.-L.; Guo, S.; Arredondo, J.; Mohite, A. D.; Senftle, T. P.; Westerhoff, P.; Alvarez, P.; Wen, X.; Song, Y.; Wong, M. S. Titanium Oxide Improves Boron Nitride Photocatalytic Degradation of Perfluorooctanoic Acid. *Chem. Eng. J.* 2022, *448,* 137735. https://doi.org/10.1016/j.cej.2022.137735.
37. Guin, J. P.; Sullivan, J. A.; Thampi, K. R. Challenges Facing Sustainable Visible Light Induced Degradation of Poly- and Perfluoroalkyls (PFA) in Water: A Critical Review. ACS Eng. Au 2022, 2 (3), 134–150. https://doi.org/10.1021/acsengineeringau.1c00031.
38. Liu, F.; Guan, X.; Xiao, F. Photodegradation of Per- and Polyfluoroalkyl Substances in Water: A Review of Fundamentals and Applications. J. Hazard. Mater. 2022, 439, 129580. https://doi.org/10.1016/j.jhazmat.2022.129580.
39. Zhang, H.; Chen, J. X.; Qu, J. P.; Kang, Y. B. Photocatalytic Low-Temperature Defluorination of PFASs. Nature 2024, 635 (8039), 610–617. https://doi.org/10.1038/s41586-024-08179-1.

View Article Online
DOI: 10.1039/D5MA01247C

40. Hamza, M. A.; Keltie, A. J.; Matthews, R. K.; Day, M. L.; Shearer, C. J. $CdIn_2S_4$ Micro-Pyramids for Reductive Photocatalytic Degradation of Perfluorooctanesulfonic Acid. Small 2025, e04601. https://doi.org/10.1002/smll.202504601.
41. Moreira, R.; Esfahani, E. B.; Zeidabadi, A. F.; et al. Hybrid Graphenic and Iron Oxide Photocatalysts for the Decomposition of Synthetic Chemicals. Commun. Eng. 2024, 3, 114. https://doi.org/10.1038/s44172-024-00267-4.
42. Gates, K.; Rai, S.; Pramanik, A.; Kolawole, O. P.; Kundu, S.; Ucak-Astarlioglu, M.; Shukla, M. K.; Al-Ostaz, A.; Ray, P. C. Insight into the Photocatalytic Degradation Mechanism for "Forever Chemicals" PFNA by Reduced Graphene Oxide/WO_3 Nanoflower Heterostructures. ACS Omega 2025, 10 (10), 10675–10684. https://doi.org/10.1021/acsomega.5c00054.
43. Chowdhury, N.; Choi, H. Photocatalytic Degradation of Perfluorooctanoic Acid on Pb-Doped TiO_2 Coated with Reduced Graphene Oxide. Water Environ. Res. 2023, 95 (5), e10871. https://doi.org/10.1002/wer.10871.
44. Huang, K. E.; Lai, C. W.; Juan, J. C.; Pang, Y. L.; Khe, C. S.; Badruddin, I. A.; Gapsari, F.; Anam, K. Recent Advances in Titanium Dioxide Bio-Derived Carbon Photocatalysts for Organic Pollutant Degradation in Wastewater. iScience 2025, 28 (5), 112368. https://doi.org/10.1016/j.isci.2025.112368.
45. Anucha, C. B.; Altin, I.; Bacaksiz, E.; Stathopoulos, V. N. Titanium Dioxide (TiO_2)-Based Photocatalyst Materials Activity Enhancement for Contaminants of Emerging Concern (CECs) Degradation: In the Light of Modification Strategies. Chem. Eng. J. Adv. 2022, 10, 100262. https://doi.org/10.1016/j.ceja.2022.100262.
46. Daghrir, R.; Drogui, P.; Robert, D. Modified TiO_2 for Environmental Photocatalytic Applications: A Review. Ind. Eng. Chem. Res. 2013, 52 (10), 3581–3599. https://doi.org/10.1021/ie303468t.
47. Narasaiah, B. P.; Banoth, P.; Dominguez, A. G. B.; Mandal, B. K.; Kumar, C. K.; Barnes, C. H. W.; Valladares, L. D. L. S.; Kollu, P. Biogenic Photo-Catalyst TiO_2 Nanoparticles for Remediation of Environment Pollutants. ACS Omega 2022, 7 (30), 26174–26189. https://doi.org/10.1021/acsomega.2c01763.
48. Arun, J.; Nachiappan, S.; Rangarajan, G.; Alagappan, R. P.; Gopinath, K. P.; Lichtfouse, E. Synthesis and Application of Titanium Dioxide Photocatalysis for Energy, Decontamination and Viral Disinfection: A Review. *Environ. Chem. Lett.* 2023, *21* (1), 339–362. https://doi.org/10.1007/s10311-022-01503-z.
49. Singh, A.; Dhau, J.; Kumar, R.; Badru, R.; Singh, P.; Mishra, Y. K.; Kaushik, A. Tailored Carbon Materials (TCM) for Enhancing Photocatalytic Degradation of Polyaromatic Hydrocarbons. *Prog. Mater. Sci.* 2024, *144*, 101289. https://doi.org/10.1016/j.pmatsci.2024.101289.
50. Liu, L.; Chen, X. Titanium Dioxide Nanomaterials: Self-Structural Modifications. Chem. Rev. 2014, 114 (19), 9890–9918. https://doi.org/10.1021/cr400624r
51. Weon, S.; Suh, M.-J.; Chu, C.; Huang, D.; Stavitski, E.; Kim, J.-H. Site-Selective Loading of Single-Atom Pt on TiO2 for Photocatalytic Oxidation and Reductive Hydrodefluorination. ACS ES&T Eng. 2021, 1 (3), 512–522. https://doi.org/10.1021/acsestengg.0c00210.
52. Roy, N.; Sohn, Y.; Pradhan, D. Synergy of Low-Energy {101} and High-Energy {001} TiO_2 Crystal Facets for Enhanced Photocatalysis. ACS Nano 2013, 7 (3), 2532–2540. https://doi.org/10.1021/nn400041p

View Article Online
DOI: 10.1039/D5MA01247C

53. Lazzeri, M.; Vittadini, A.; Selloni, A. Structure and Energetics of Stoichiometric TiO_2 Anatase Surfaces. Phys. Rev. B 2001, 63 (15), 155409. https://doi.org/10.1103/PhysRevB.63.155409
54. Li, Z.; Wang, S.; Wu, J.; Zhou, W. Recent Progress in Defective TiO_2 Photocatalysts for Energy and Environmental Applications. Renewable Sustainable Energy Rev. 2022, 156, 111980. https://doi.org/10.1016/j.rser.2021.111980
55. Bak, T.; Li, W.; Nowotny, J.; Atanacio, A. J.; Davis, J. Photocatalytic Properties of TiO_2: Evidence of the Key Role of Surface Active Sites in Water Oxidation. J. Phys. Chem. A 2015, 119 (36), 9465–9473. https://doi.org/10.1021/acs.jpca.5b05031
56. Chen, X.; Liu, L.; Huang, F. Black Titanium Dioxide (TiO_2) Nanomaterials. Chem. Soc. Rev. 2015, 44, 1861–1885. https://doi.org/10.1039/C4CS00330F
57. Qu, X.; Lin, J.; Qiang, W.; Chen, C.; Sun, D. Self-Doped Defect-Mediated TiO_2 with Disordered Surface for High-Efficiency Photodegradation of Various Pollutants. Chemosphere 2022, 308 (Part 2), 136239. https://doi.org/10.1016/j.chemosphere.2022.136239
58. Zhang, D.; Yang, M.; Dong, S. Hydroxylation of the Rutile TiO_2(110) Surface Enhancing Its Reducing Power for Photocatalysis. J. Phys. Chem. C 2015, 119 (3), 1451–1456. https://doi.org/10.1021/jp510427v
59. Teng, F.; Li, M.; Gao, C.; Zhang, G.; Zhang, P.; Wang, Y.; Chen, L.; Xie, E. Preparation of Black TiO_2 by Hydrogen Plasma Assisted Chemical Vapor Deposition and Its Photocatalytic Activity. Appl. Catal. B: Environ. 2014, 148–149, 339–343. https://doi.org/10.1016/j.apcatb.2013.11.015
60. Adhikari, S.; Sarkar, D.; Madras, G. Hierarchical Design of CuS Architectures for Visible Light Photocatalysis of 4-Chlorophenol. ACS Omega 2017, 2 (7), 4009–4021. https://doi.org/10.1021/acsomega.7b00669.
61. Wang, W.; Mukhopadhyay, S. M. Hierarchical Nanostructured Surface Design for Robust and Flexible Multifunctional Devices. Carbon Trends 2021, 5, 100096. https://doi.org/10.1016/j.cartre.2021.100096.
62. Yi, J.; Zhang, G.; Wang, Y.; Qian, W.; Wang, X. Recent Advances in Phase-Engineered Photocatalysts: Classification and Diversified Applications. Materials 2023, 16 (11), 3980. https://doi.org/10.3390/ma16113980.
63. Qiu, C.; Shen, J.; Lin, J.; Liu, D.; Li, D.; Zhang, J.; Zhang, Z.; Lin, H.; Wang, X.; Fu, X. Construction of the Rutile/Anatase Micro-Heterophase Junction Photocatalyst from Anatase by Liquid Nitrogen Quenching Method. ACS Appl. Energy Mater. 2021, 4 (9), 10172–10186. https://doi.org/10.1021/acsaem.1c02066.
64. Ahmed, M. A.; Mahmoud, S. A.; Mohamed, A. A. Interfacially Engineered Metal Oxide Nanocomposites for Enhanced Photocatalytic Degradation of Pollutants and Energy Applications. *RSC Adv.* 2025, *15*, 15561–15603. https://doi.org/10.1039/D4RA08780A.
65. Kong, Z.; Lu, L.; Zhu, C.; Xu, J.; Fang, Q.; Liu, R.; Shen, Y. Enhanced Adsorption and Photocatalytic Removal of PFOA from Water by F-Functionalized MOF with In-Situ-Growth TiO_2: Regulation of Electron Density and Bandgap. Sep. Purif. Technol. 2022, 297, 121449. https://doi.org/10.1016/j.seppur.2022.121449.
66. Fernandes, R. J. C.; Silva, A. R.; Cardoso, B. D.; Coutinho, P. J. G.; Pereira, L. Potential of Photocatalytic Nanomaterials for PFOA and PFOS Degradation: Challenges and

View Article Online
DOI: 10.1039/D5MA01247C

Opportunities. J. Environ. Chem. Eng. 2025, 13 (1), 115201. https://doi.org/10.1016/j.jece.2024.115201.

67. Thind, S. S.; Ryane, B. A.; Hayden, J. B.; Chagunda, I.; Paul, M.; McIndoe, J. S. Bias Enhanced Electro-Photocatalysis on TiO_2 Nanoporous Materials for Decomposition of Forever Chemicals in Saltwater. Environ. Sci.: Adv. 2025, 4, 1024–1034. https://doi.org/10.1039/D4VA00423J.
68. Verma, S.; Mezgebe, B.; Hejase, C. A.; Sahle-Demessie, E.; Nadagouda, M. N. Photodegradation and Photocatalysis of Per- and Polyfluoroalkyl Substances (PFAS): A Review of Recent Progress. Next Mater. 2024, 2, 100077. https://doi.org/10.1016/j.nxmate.2023.100077.
69. Veciana, A.; Steiner, S.; Tang, Q.; Pustovalov, V.; Llacer-Wintle, J.; Wu, J.; Chen, X.-Z.; Manyiwa, T.; Ultra, V. U., Jr.; Garcia-Cirera, B.; Puigmartí-Luis, J.; Franco, C.; Janssen, D. J.; Nyström, L.; Boulos, S.; Pané, S. Breaking the Perfluorooctane Sulfonate Chain: Piezocatalytic Decomposition of PFOS Using $BaTiO_3$ Nanoparticles. Small Sci. 2024, 4, 2400337. https://doi.org/10.1002/smsc.202400337.
70. Ebnesajjad, S. Discovery and History of Fluoropolymers. In *Introduction to Fluoropolymers*; Ebnesajjad, S., Ed.; William Andrew Publishing: Boston, 2013; pp 17–35. https://doi.org/10.1016/B978-1-4557-7442-5.00003-6.
71. American Physical Society. The History of Fluoropolymers. *APS News Archives*, April 2021. https://www.aps.org/archives/publications/apsnews/202104/history.cfm (accessed Aug 12, 2025).
72. Habib, Z.; Song, M.; Ikram, S.; Zahra, Z. Overview of Per- and Polyfluoroalkyl Substances (PFAS), Their Applications, Sources, and Potential Impacts on Human Health. *Pollutants* 2024, *4* (1), 136–152. https://doi.org/10.3390/pollutants4010009.
73. Glüge, J.; Scheringer, M.; Cousins, I. T.; DeWitt, J. C.; Goldenman, G.; Herzke, D.; Lohmann, R.; Ng, C. A.; Trier, X.; Wang, Z. An Overview of the Uses of Per- and Polyfluoroalkyl Substances (PFAS). *Environ. Sci.: Processes Impacts* 2020, *22*, 2345–2373. https://doi.org/10.1039/D0EM00291G.
74. Gao, C.; Drage, D. S.; Abdallah, M. A.-E.; Quan, F.; Zhang, K.; Hu, S.; Zhao, X.; Zheng, Y.; Harrad, S.; Qiu, W. Factors Influencing Concentrations of PFAS in Drinking Water: Implications for Human Exposure. *ACS ES&T Water* 2024, *4* (11), 4881–4892. https://doi.org/10.1021/acsestwater.4c00533.
75. Peritore, A. F.; Gugliandolo, E.; Cuzzocrea, S.; Crupi, R.; Britti, D. Current Review of Increasing Animal Health Threat of Per- and Polyfluoroalkyl Substances (PFAS): Harms, Limitations, and Alternatives to Manage Their Toxicity. *Int. J. Mol. Sci.* 2023, *24* (14), 11707. https://doi.org/10.3390/ijms241411707.
76. Wee, S. Y.; Aris, A. Z. Environmental Impacts, Exposure Pathways, and Health Effects of PFOA and PFOS. *Ecotoxicol. Environ. Saf.* 2023, *267*, 115663. https://doi.org/10.1016/j.ecoenv.2023.115663.
77. DeLuca, N. M.; Minucci, J. M.; Mullikin, A.; Slover, R.; Cohen Hubal, E. A. Human Exposure Pathways to Poly- and Perfluoroalkyl Substances (PFAS) from Indoor Media: A Systematic Review. *Environ. Int.* 2022, *162*, 107149. https://doi.org/10.1016/j.envint.2022.107149.

View Article Online
DOI: 10.1039/D5MA01247C

78. Mahoney, H.; Xie, Y.; Brinkmann, M.; Giesy, J. P. Next Generation Per- and Polyfluoroalkyl Substances: Status and Trends, Aquatic Toxicity, and Risk Assessment. *Eco Environ. Health* 2022, *1* (2), 117–131. DOI: 10.1016/j.eehl.2022.05.002.
79. Kirkwood-Donelson, K. I.; Minucci, J. M.; Mullikin, A.; Slover, R.; Cohen Hubal, E. A. Uncovering Per- and Polyfluoroalkyl Substances (PFAS) with Nontargeted Ion Mobility Spectrometry–Mass Spectrometry Analyses. *Sci. Adv.* 2023, *9*, eadj7048. https://doi.org/10.1126/sciadv.adj7048.
80. Itumoh, E. J.; Data, S.; Chen, J. L.-Y.; Kah, M.; Padhye, L. P.; Leitao, E. M. Addressing the Persistence of Per- and Polyfluoroalkyl Substances (PFAS): Current Challenges and Potential Solutions. *RSC Sustainability* 2024, *2*, 3183–3201. https://doi.org/10.1039/D4SU00152D.
81. Barzen-Hanson, K. A.; Roberts, S. C.; Choyke, S.; Oetjen, K.; McAlees, A.; Riddell, N.; McCrindle, R.; Ferguson, P. L.; Higgins, C. P.; Field, J. A. Discovery of 40 Classes of Per- and Polyfluoroalkyl Substances in Historical Aqueous Film-Forming Foams (AFFFs) and AFFF-Impacted Groundwater. *Environ. Sci. Technol.* 2017, *51* (4), 2047–2057. https://doi.org/10.1021/acs.est.6b05843
82. Chambers, W. S.; Hopkins, J. G.; Richards, S. M. A Review of Per- and Polyfluorinated Alkyl Substance Impairment of Reproduction. *Front. Toxicol.* 2021, *3*, 732436. https://doi.org/10.3389/ftox.2021.732436.
83. Evich, M. G.; Davis, M. J. B.; McCord, J. P.; Acrey, B.; Awkerman, J. A.; Knappe, D. R. U.; Lindstrom, A. B.; Speth, T. F.; Tebes-Stevens, C.; Strynar, M. J.; Wang, Z.; Weber, E. J.; Henderson, W. M.; Washington, J. W. Per- and Polyfluoroalkyl Substances in the Environment. *Science* 2022, *375* (6580), eabg9065. https://doi.org/10.1126/science.abg9065.
84. Su, A.; Cheng, Y.; Zhang, C.; Yang, Y.-F.; She, Y.-B.; Rajan, K. An Artificial Intelligence Platform for Automated PFAS Subgroup Classification: A Discovery Tool for PFAS Screening. *Sci. Total Environ.* 2024, *921*, 171229. https://doi.org/10.1016/j.scitotenv.2024.171229.
85. Yaghoobian, S.; Ramirez-Ubillus, M. A.; Zhai, L.; Hwang, J. H. A Perspective of Emerging Trends in Integrated PFAS Detection and Remediation Technologies with Data Driven Approaches. *Chem. Sci.* 2025, *16* (30), 13564–13573. https://doi.org/10.1039/d5sc01624j.
86. U.S. Environmental Protection Agency. PFAS Analytical Methods Development and Sampling Research. https://www.epa.gov/water-research/pfas-analytical-methods-development-and-sampling-research (accessed Aug 12, 2025).
87. Jovanović, M.; Müller, V.; Feldmann, J.; Leitner, E. Analysis of Per- and Polyfluoroalkyl Substances (PFAS) in Raw Materials Intended for the Production of Paper-Based Food Contact Materials,Evaluating LC-MS/MS versus Total Fluorine and Extractable Organic Fluorine. *Food Addit. Contam., Part A* 2024, *41* (5), 525–536. https://doi.org/10.1080/19440049.2024.2332334.
88. Kause, R.; van Leeuwen, S.; Krätschmer, K.; van Dooren, B.; Keppels, R.; Makarem, H.; Hoogenboom, L. R. A. P.; de Pagter-de Witte, L.; Berendsen, B. J. A. Development and Application of a Liquid Chromatography–Tandem Mass Spectrometry Method for the Analysis of 20 Perfluoroalkyl Substances in Fruit and Vegetables at Sub-Parts-per-Trillion Levels. *J. Agric. Food Chem.* 2024, *72* (33), 18731–18741. https://doi.org/10.1021/acs.jafc.4c01172.

View Article Online
DOI: 10.1039/D5MA01247C

89. Garnett, J.; Halsall, C.; Winton, H.; Joerss, H.; Mulvaney, R.; Ebinghaus, R.; Frey, M.; Jones, A.; Leeson, A.; Wynn, P. Increasing Accumulation of Perfluorocarboxylate Contaminants Revealed in an Antarctic Firn Core (1958–2017). *Environ. Sci. Technol.* 2022, *56* (16), 11246–11255. https://doi.org/10.1021/acs.est.2c02592.
90. Zhu, L.; Bossi, R.; Carvalho, P. N.; Rigét, F. F.; Christensen, J. H.; Weihe, P.; Bonefeld-Jørgensen, E. C.; Vorkamp, K. Suspect and Non-Target Screening of Chemicals of Emerging Arctic Concern in Biota, Air and Human Serum. *Environ. Pollut.* 2024, *360*, 124605. https://doi.org/10.1016/j.envpol.2024.124605.
91. Kause, R.; van Leeuwen, S.; Krätschmer, K.; van Dooren, B.; Keppels, R.; Makarem, H.; Hoogenboom, L. R. A. P.; de Pagter-de Witte, L.; Berendsen, B. J. A. Development and Application of a Liquid Chromatography–Tandem Mass Spectrometry Method for the Analysis of 20 Perfluoroalkyl Substances in Fruit and Vegetables at Sub-Parts-per-Trillion Levels. J. Agric. Food Chem. 2024, 72 (33), 18731–18741. https://doi.org/10.1021/acs.jafc.4c01172.
92. Lai, Y.; Koelmel, J. P.; Walker, D. I.; Price, E. J.; Papazian, S.; Manz, K. E.; Castilla-Fernández, D.; Bowden, J. A.; Nikiforov, V.; David, A.; Bessonneau, V.; Amer, B.; Seethapathy, S.; Hu, X.; Lin, E. Z.; Jbebli, A.; McNeil, B. R.; Barupal, D.; Cerasa, M.; Xie, H.; Kalia, V.; Nandakumar, R.; Singh, R.; Tian, Z.; Gao, P.; Zhao, Y.; Froment, J.; Rostkowski, P.; Dubey, S.; Coufalíková, K.; Seličová, H.; Hecht, H.; Liu, S.; Udhani, H. H.; Restituito, S.; Tchou-Wong, K.-M.; Lu, K.; Martin, J. W.; Warth, B.; Godri Pollitt, K. J.; Klánová, J.; Fiehn, O.; Metz, T. O.; Pennell, K. D.; Jones, D. P.; Miller, G. W. High-Resolution Mass Spectrometry for Human Exposomics: Expanding Chemical Space Coverage. Environ. Sci. Technol. 2024, 58 (29), 12784–12822. https://doi.org/10.1021/acs.est.4c01156.
93. Zahra, Z.; Song, M.; Habib, Z.; Ikram, S. Advances in Per- and Polyfluoroalkyl Substances (PFAS) Detection and Removal Techniques from Drinking Water, Their Limitations, and Future Outlooks. Emerg. Contam. 2025, 11 (1), 100434. https://doi.org/10.1016/j.emcon.2024.100434.
94. Poothong, S.; Papadopoulou, E.; Padilla-Sánchez, J. A.; Thomsen, C.; Haug, L. S. Multiple Pathways of Human Exposure to Poly- and Perfluoroalkyl Substances (PFASs): From External Exposure to Human Blood. Environ. Int. 2020, 134, 105244. https://doi.org/10.1016/j.envint.2019.105244.
95. DeLuca, N. M.; Minucci, J. M.; Mullikin, A.; Slover, R.; Cohen Hubal, E. A. Human Exposure Pathways to Poly- and Perfluoroalkyl Substances (PFAS) from Indoor Media: A Systematic Review. Environ. Int. 2022, 162, 107149. https://doi.org/10.1016/j.envint.2022.107149.
96. Dehghani, M. H.; Aghaei, M.; Bashardoust, P.; et al. An Insight into the Environmental and Human Health Impacts of Per- and Polyfluoroalkyl Substances (PFAS): Exploring Exposure Pathways and Their Implications. Environ. Sci. Eur. 2025, 37, 81. https://doi.org/10.1186/s12302-025-01122-9.
97. Steenland, K.; Fletcher, T.; Stein, C. R.; Bartell, S. M.; Darrow, L.; Lopez-Espinosa, M.-J.; Ryan, P. B.; Savitz, D. A. Review: Evolution of Evidence on PFOA and Health Following the Assessments of the C8 Science Panel. Environ. Int. 2020, 145, 106125. https://doi.org/10.1016/j.envint.2020.106125.
98. Boston, C.; Keck, S.; Naperala, A.; Collins, J. The Evolution of PFAS Epidemiology: New Scientific Developments Call into Question Alleged “Probable Links” between PFOA and

View Article Online
DOI: 10.1039/D5MA01247C

Kidney Cancer and Thyroid Disease. Front. Public Health 2025, 13, 1532277. https://doi.org/10.3389/fpubh.2025.1532277.

99. Szilagyi, J. T.; Avula, V.; Fry, R. C. Perfluoroalkyl Substances (PFAS) and Their Effects on the Placenta, Pregnancy, and Child Development: A Potential Mechanistic Role for Placental Peroxisome Proliferator-Activated Receptors (PPARs). Curr. Environ. Health Rep. 2020, 7 (3), 222–230. https://doi.org/10.1007/s40572-020-00279-0.
100. Ho, T. C.; Wan, H. T.; Lee, W. K.; Lam, T. K. Y.; Lin, X.; Chan, T. F.; Lai, K. P.; Wong, C. K. C. Effects of In Utero PFOS Exposure on Epigenetics and Metabolism in Mouse Fetal Livers. Environ. Sci. Technol. 2023, 57 (40), 14892–14903. https://doi.org/10.1021/acs.est.3c05207.
101. Lai, T. T.; Eken, Y.; Wilson, A. K. Binding of Per- and Polyfluoroalkyl Substances to the Human Pregnane X Receptor. Environ. Sci. Technol. 2020, 54 (24), 15986–15995. https://doi.org/10.1021/acs.est.0c04651.
102. Holder, C.; Cohen Hubal, E. A.; Luh, J.; Lee, M. G.; Melnyk, L. J.; Thomas, K. Systematic Evidence Mapping of Potential Correlates of Exposure for Per- and Poly-Fluoroalkyl Substances (PFAS) Based on Measured Occurrence in Biomatrices and Surveys of Dietary Consumption and Product Use. Int. J. Hyg. Environ. Health 2024, 259, 114384. https://doi.org/10.1016/j.ijheh.2024.114384.
103. Dunder, L.; Salihovic, S.; Elmståhl, S.; et al. Associations between Per- and Polyfluoroalkyl Substances (PFAS) and Diabetes in Two Population-Based Cohort Studies from Sweden. J. Expo. Sci. Environ. Epidemiol. 2023, 33, 748–756. https://doi.org/10.1038/s41370-023-00529-x.
104. Dunn, F.; Paquette, S. E.; Pennell, K. D.; Plavicki, J. S.; Manz, K. E. Metabolomic Changes Following GenX and PFBS Exposure in Developing Zebrafish. Aquat. Toxicol. 2024, 271, 106908. https://doi.org/10.1016/j.aquatox.2024.106908.
105. Sinclair, G. M.; Long, S. M.; Singh, N.; Coggan, T. L.; Askeland, M. P. J.; Jones, O. A. H. Exposure to Environmentally Relevant Levels of PFAS Causes Metabolic Changes in the Freshwater Amphipod Austrochiltonia subtenuis. Metabolites 2022, 12, 1135. https://doi.org/10.3390/metabo12111135.
106. Ortiz-Villanueva, E.; Jaumot, J.; Martínez, R.; Navarro-Martín, L.; Piña, B.; Tauler, R. Assessment of Endocrine Disruptors Effects on Zebrafish (Danio rerio) Embryos by Untargeted LC-HRMS Metabolomic Analysis. Sci. Total Environ. 2018, 635, 156–166. https://doi.org/10.1016/j.scitotenv.2018.03.369.
107. Ning, J.; Ding, C.; Xu, H.; Liu, Z.; Guan, Q.; Xia, Y.; Xu, Q. Effect of Per- and Polyfluoroalkyl Substances on Neurodevelopment: Evidence-Based Risk Assessment in the TRAEC Strategy Context. Environ. Int. 2024, 191, 109003. https://doi.org/10.1016/j.envint.2024.109003.
108. Brown-Leung, J. M.; Cannon, J. R. Neurotransmission Targets of Per- and Polyfluoroalkyl Substance Neurotoxicity: Mechanisms and Potential Implications for Adverse Neurological Outcomes. Chem. Res. Toxicol. 2022, 35 (8), 1312–1333. https://doi.org/10.1021/acs.chemrestox.2c00072.
109. Hu, X. C.; Andrews, D. Q.; Lindstrom, A. B.; Bruton, T. A.; Schaider, L. A.; Grandjean, P.; Lohmann, R.; Carignan, C. C.; Blum, A.; Balan, S. A.; Higgins, C. P.; Sunderland, E. M. Detection of Poly- and Perfluoroalkyl Substances (PFASs) in U.S. Drinking Water Linked to

View Article Online
DOI: 10.1039/D5MA01247C

Industrial Sites, Military Fire Training Areas, and Wastewater Treatment Plants. Environ. Sci. Technol. Lett. 2016, 3 (10), 344–350. https://doi.org/10.1021/acs.estlett.6b00260.

110. Gezahegn, A.; Merga, L. B.; Mammo, S. Industrial Effluents Caused Environmental Pollution and Its Potential Ecological and Human Health Impacts in Ethiopia: A Review. Waste Manage. Bull. 2025, 100240. https://doi.org/10.1016/j.wmb.2025.100240.
111. Wang, F.; Xiang, L.; Leung, K. S.-Y.; Elsner, M.; Zhang, Y.; Guo, Y.; Pan, B.; Sun, H.; An, T.; Ying, G.; Brooks, B. W.; Hou, D.; Helbling, D. E.; Sun, J.; Qiu, H.; Vogel, T. M.; Zhang, W.; Gao, Y.; Simpson, M. J.; Luo, Y.; Chang, S. X.; Su, G.; Wong, B. M.; Fu, T.-M.;, D.; Jobst, K. J.; Ge, C.; Coulon, F.; Harindintwali, J. D.; Zeng, X.; Wang, H.; Fu, Y.; Wei, Z.; Lohmann, R.; Chen, C.; Song, Y.; Sanchez-Cid, C.; Wang, Y.; El-Naggar, A.; Yao, Y.; Huang, Y.; Law, J. C.-F.; Gu, C.; Shen, H.; Gao, Y.; Qin, C.; Li, H.; Zhang, T.; Corcoll, N.; Liu, M.; Alessi, D. S.; Li, H.; Brandt, K. K.; Pico, Y.; Gu, C.; Guo, J.; Su, J.; Corvini, P.; Ye, M.; Rocha-Santos, T.; He, H.; Yang, Y.; Tong, M.; Zhang, W.; Suanon, F.; Brahushi, F.; Wang, Z.; Hashsham, S. A.; Virta, M.; Yuan, Q.; Jiang, G.; Tremblay, L. A.; Bu, Q.; Wu, J.; Peijnenburg, W.; Topp, E.; Cao, X.; Jiang, X.; Zheng, M.; Zhang, T.; Luo, Y.; Zhu, L.; Li, X.; Barceló, D.; Chen, J.; Xing, B.; Amelung, W.; Cai, Z.; Naidu, R.; Shen, Q.; Zhu, Y.-G.; Schaeffer, A.; Rillig, M. C.; Wu, F.; Yu, G.; Tiedje, J. M. Emerging Contaminants: A One Health Perspective. Innovation 2024, 5 (4), 100612. https://doi.org/10.1016/j.xinn.2024.100612.
112. Zenobio, J. E.; Nzeribe, B. N.; Hilyard, M.; DiGuiseppi, B. Deciphering PFAS in Rainwater: Sources, Distribution, and Environmental Impact. Remediat. J. 2025, 35, e70029. https://doi.org/10.1002/rem.70029.
113. Li, W.-L.; Hung, H.; Kasperkiewicz, A.; Shunthirasingham, C.; Chisamore, J.; Rabu, M.; Park, R.; Huo, C.-Y.; Lee, P.; Dryfhout-Clark, H. Assessing the Shifts in Atmospheric Per- and Polyfluoroalkyl Substances (PFAS) Levels in the Great Lakes and Implications for the Environmental Transport and Fate. ACS ES&T Air ASAP. https://doi.org/10.1021/acsestair.5c00121.
114. Zhang, L.; Zhang, Y.; Gong, Q.; Yang, Z.; Sun, D. Uncovering the Effects of the North Pacific Subtropical Gyre on Per- and Polyfluoroalkyl Substances Distribution in the Tropical Western Pacific. J. Hazard. Mater. 2025, 494, 138631. https://doi.org/10.1016/j.jhazmat.2025.138631.
115. Lohmann, R.; Abass, K.; Bonefeld-Jørgensen, E. C.; Bossi, R.; Dietz, R.; Ferguson, S.; Fernie, K. J.; Grandjean, P.; Herzke, D.; Houde, M.; Lemire, M.; Letcher, R. J.; Muir, D.; De Silva, A. O.; Ostertag, S. K.; Rand, A. A.; Søndergaard, J.; Sonne, C.; Sunderland, E. M.; Vorkamp, K.; Wilson, S.; Weihe, P. Cross-Cutting Studies of Per- and Polyfluorinated Alkyl Substances (PFAS) in Arctic Wildlife and Humans. Sci. Total Environ. 2024, 954, 176274. https://doi.org/10.1016/j.scitotenv.2024.176274.
116. Yan, P.-F.; Dong, S.; Pennell, K. D.; Cápiro, N. L. A Review of the Occurrence and Microbial Transformation of Per- and Polyfluoroalkyl Substances (PFAS) in Aqueous Film-Forming Foam (AFFF)-Impacted Environments. *Sci. Total Environ.* 2024, *927*, 171883. https://doi.org/10.1016/j.scitotenv.2024.171883.
117. Ruyle, B. J.; Thackray, C. P.; Butt, C. M.; LeBlanc, D. R.; Tokranov, A. K.; Vecitis, C. D.; Sunderland, E. M. Centurial Persistence of Forever Chemicals at Military Fire Training Sites. Environ. Sci. Technol. 2023, 57 (21), 8096–8106. https://doi.org/10.1021/acs.est.3c00675.

View Article Online
DOI: 10.1039/D5MA01247C

118. Salvatore, D.; Mok, K.; Garrett, K. K.; Poudrier, G.; Brown, P.; Birnbaum, L. S.; Goldenman, G.; Miller, M. F.; Patton, S.; Poehlein, M.; Varshavsky, J.; Cordner, A. Presumptive Contamination: A New Approach to PFAS Contamination Based on Likely Sources. Environ. Sci. Technol. Lett. 2022, 9 (11), 983–990. https://doi.org/10.1021/acs.estlett.2c00502.
119. Filipovic, M.; Woldegiorgis, A.; Norström, K.; Bibi, M.; Lindberg, M.; Österås, A.-H. Historical Usage of Aqueous Film Forming Foam: A Case Study of the Widespread Distribution of Perfluoroalkyl Acids from a Military Airport to Groundwater, Lakes, Soils and Fish. Chemosphere 2015, 129, 39–45. https://doi.org/10.1016/j.chemosphere.2014.09.005.
120. Ateia, M.; Buren, J. V.; Barrett, W.; Martin, T.; Back, G. G. Sunrise of PFAS Replacements: A Perspective on Fluorine-Free Foams. ACS Sustain. Chem. Eng. 2023, 11, 7986–7996. https://doi.org/10.1021/acssuschemeng.3c01124.
121. Paige, T.; De Silva, T.; Buddhadasa, S.; Prasad, S.; Nugegoda, D.; Pettigrove, V. Background Concentrations and Spatial Distribution of PFAS in Surface Waters and Sediments of the Greater Melbourne Area, Australia. Chemosphere 2024, 349, 140791. https://doi.org/10.1016/j.chemosphere.2023.140791.
122. EPA NSW. Regulation of PFAS Firefighting Foams. https://www.epa.nsw.gov.au/Your-environment/Chemicals/PFAS-in-NSW/Regulation-of-PFAS-firefighting-foams.
123. ECHA. ECHA Publishes Updated PFAS Restriction Proposal. https://echa.europa.eu/-/echa-publishes-updated-pfas-restriction-proposal.
124. Tshangana, C. S.; Nhlengethwa, S. T.; Glass, S.; et al. Technology Status to Treat PFAS-Contaminated Water and Limiting Factors for Their Effective Full-Scale Application. npj Clean Water 2025, 8, 41. https://doi.org/10.1038/s41545-025-00457-3.
125. Smith, S. J.; Lauria, M.; Ahrens, L.; McCleaf, P.; Hollman, P.; Bjälkefur Seroka, S.; Hamers, T.; Arp, H. P.; Wiberg, K. Electrochemical Oxidation for Treatment of PFAS in Contaminated Water and Fractionated Foam–A Pilot-Scale Study. ACS ES&T Water 2023, 3 (4), 1201–1211. https://doi.org/10.1021/acsestwater.2c00660.
126. Hussain, H. N.; Jilani, M. I.; Imtiaz, F.; Ahmed, T.; Arshad, M. B.; Mudassar, M.; Sharif, M. N. Advances in the Removal of Polyfluoroalkyl Substances (PFAS) from Water Using Destructive and Non-Destructive Methods. Green Anal. Chem. 2025, 12, 100225. https://doi.org/10.1016/j.greeac.2025.100225.
127. Ren, Z.; Bergmann, U.; Leiviskä, T. Reductive Degradation of Perfluorooctanoic Acid in Complex Water Matrices Using the UV/Sulfite Process. *Water Res.* 2021, *205*, 117676.
128. Kang, Y.-G.; Birch, Q. T.; Nadagouda, M. N.; Dionysiou, D. D. Advanced destruction technologies for PFAS in soils: Progress and challenges. *Curr. Opin. Environ. Sci. Health* 2023, *33*, 100459. https://doi.org/10.1016/j.coesh.2023.100459.
129. Grimison, C.; Knight, E. R.; Nguyen, T. M. H.; Nagle, N.; Kabiri, S.; Bräunig, J.; Navarro, D. A.; Kookana, R. S.; Higgins, C. P.; McLaughlin, M. J.; Mueller, J. F. The efficacy of soil washing for the remediation of per- and poly-fluoroalkyl substances (PFASs) in the field. *J. Hazard. Mater.* 2023, *445*, 130441. https://doi.org/10.1016/j.jhazmat.2022.130441
130. Napoli, R.; Fazzino, F.; Vagliasindi, F. G. A.; Falciglia, P. P. Sustainable remediation strategies and technologies of per- and polyfluoroalkyl substances (PFAS)-contaminated soils: A critical review. *Sustainability* 2025, *17* (14), 6635. https://doi.org/10.3390/su17146635.
131. Alinezhad, A.; Sasi, P. C.; Zhang, P.; Yao, B.; Kubátová, A.; Golovko, S. A.; Golovko, M. Y.; Xiao, F. An investigation of thermal air degradation and pyrolysis of per- and polyfluoroalkyl

View Article Online
DOI: 10.1039/D5MA01247C

substances and aqueous film-forming foams in soil. ACS ES&T Eng. 2022, 2 (2), 198–209. https://doi.org/10.1021/acsestengg.1c00335.

132. Wang, J.; Lin, Z.; He, X.; Song, M.; Westerhoff, P.; Doudrick, K.; Hanigan, D. Critical review of thermal decomposition of per- and polyfluoroalkyl substances: Mechanisms and implications for thermal treatment processes. Environ. Sci. Technol. 2022, 56 (9), 5355–5370. https://doi.org/10.1021/acs.est.2c02251.
133. Mahinroosta, R.; Senevirathna, L. A review of the emerging treatment technologies for PFAS contaminated soils. J. Environ. Manage. 2020, 255, 109896. https://doi.org/10.1016/j.jenvman.2019.109896.
134. Wang, F.; Lu, X.; Li, X.-y.; Shih, K. Effectiveness and mechanisms of defluorination of perfluorinated alkyl substances by calcium compounds during waste thermal treatment. Environ. Sci. Technol. 2015, 49 (9), 5672–5680. https://doi.org/10.1021/es506234b.
135. Duchesne, A. L.; Brown, J. K.; Patch, D. J.; Major, D.; Weber, K. P.; Gerhard, J. I. Remediation of PFAS-contaminated soil and granular activated carbon by smoldering combustion. Environ. Sci. Technol. 2020, 54 (19), 12631–12640. https://doi.org/10.1021/acs.est.0c03058.
136. Hao, S.; Choi, Y. J.; Deeb, R. A.; Strathmann, T. J.; Higgins, C. P. Application of hydrothermal alkaline treatment for destruction of per- and polyfluoroalkyl substances in contaminated groundwater and soil. Environ. Sci. Technol. 2022, 56 (10), 6647–6657. https://doi.org/10.1021/acs.est.2c00654.
137. Turner, L. P.; Kueper, B. H.; Jaansalu, K. M.; Patch, D. J.; Battye, N.; El-Sharnouby, O.; Mumford, K. G.; Weber, K. P. Mechanochemical remediation of perfluorooctanesulfonic acid (PFOS) and perfluorooctanoic acid (PFOA) amended sand and aqueous film-forming foam (AFFF) impacted soil by planetary ball milling. Sci. Total Environ. 2021, 765, 142722. https://doi.org/10.1016/j.scitotenv.2020.142722.
138. Battye, N. J.; Patch, D. J.; Roberts, D. M. D.; O'Connor, N. M.; Turner, L. P.; Kueper, B. H.; Hulley, M. E.; Weber, K. P. Use of a horizontal ball mill to remediate per- and polyfluoroalkyl substances in soil. Sci. Total Environ. 2022, 835, 155506. https://doi.org/10.1016/j.scitotenv.2022.155506.
139. Yan, Y.; Wei, Z.; Duan, X.; Long, M.; Spinney, R.; Dionysiou, D. D.; Xiao, R.; Alvarez, P. J. J. Merits and limitations of radical vs. nonradical pathways in persulfate-based advanced oxidation processes. Environ. Sci. Technol. 2023, 57 (33), 12153–12179. https://doi.org/10.1021/acs.est.3c05153.
140. DiGuiseppi, W. H.; Newell, C. J.; Carey, G.; Kulkarni, P. R.; Xia, Z.; Stults, J.; Maher, T. L.; Houtz, E. F.; Mora, R.; Wice, R.; Tomiczek, P. W.; Richardson, S. D.; Xiong, J.; Hale, J.; Hnatko, J. P.; McGregor, R.; McDonough, J. T.; Oka, A.; Thomas, R.; … Hatton, J. Available and emerging liquid treatment technologies for PFASs. Remediation 2024, 34 (2), e21782. https://doi.org/10.1002/rem.21782.
141. Smith, S. J.; Lauria, M.; Ahrens, L.; McCleaf, P.; Hollman, P.; Seroka, S. B.; Hamers, T.; Arp, H. P. H.; Wiberg, K. Electrochemical oxidation for treatment of PFAS in contaminated water and fractionated foam–A pilot-scale study. ACS ES&T Water 2023, 3 (4), 1201–1211. https://doi.org/10.1021/acsestwater.2c00660.

View Article Online
DOI: 10.1039/D5MA01247C

142. Sörengård, M.; Niarchos, G.; Jensen, P. E.; Ahrens, L. Electrodialytic per- and polyfluoroalkyl substances (PFASs) removal mechanism for contaminated soil. Chemosphere 2019, 232, 224–231. https://doi.org/10.1016/j.chemosphere.2019.05.088.
143. Kavusi, E.; Khalaf Ansar, B. S.; Ebrahimi, S.; Sharma, R.; Ghoreishi, S. S.; Nobaharan, K.; Abdoli, S.; Dehghanian, Z.; Lajayer, B. A.; Senapathi, V.; Price, G. W.; Astatkie, T. Critical review on phytoremediation of polyfluoroalkyl substances from environmental matrices: Need for global concern. Environ. Res. 2023, 217, 114844. https://doi.org/10.1016/j.envres.2022.114844.
144. Bhattacharya, A.; Fathima, J.; Varghese, S.; Chatterjee, P.; Gadhamshetty, V. Advances in bioremediation strategies for PFAS-contaminated water and soil. Soil Environ. Health 2025, 3 (1), 100126. https://doi.org/10.1016/j.seh.2024.100126.
145. Nason, S. L.; Thomas, S.; Stanley, C.; Silliboy, R.; Blumenthal, M.; Zhang, W.; Liang, Y.; Jones, J. P.; Zuverza-Mena, N.; White, J. C.; Haynes, C. L.; Vasiliou, V.; Timko, M. P.; Berger, B. W. A comprehensive trial on PFAS remediation: Hemp phytoextraction and PFAS degradation in harvested plants. Environ. Sci.: Adv. 2024, 3, 304–313. https://doi.org/10.1039/D3VA00340J.
146. Zhang, W.; Cao, H.; Subramanya, S. M.; Savage, P.; Liang, Y. Destruction of perfluoroalkyl acids accumulated in Typha latifolia through hydrothermal liquefaction. ACS Sustainable Chem. Eng. 2020, 8 (25), 9257–9262. https://doi.org/10.1021/acssuschemeng.0c03249.
147. Rahman, M. H.-U.; Sikder, R.; Tonmoy, T. A.; Hossain, M. M.; Ye, T.; Aich, N.; Gadhamshetty, V. Transforming PFAS Management: A Critical Review of Machine Learning Applications for Enhanced Monitoring and Treatment. *J. Water Process Eng.* 2025, *70*, 106941. https://doi.org/10.1016/j.jwpe.2025.106941.
148. Hosseinzadeh, A.; Altaee, A.; Li, X.; Zhou, J. L. Machine Learning-Based Modeling and Analysis of Perfluoroalkyl and Polyfluoroalkyl Substances Controlling Systems in Protecting Water Resources. *Curr. Opin. Chem. Eng.* 2023, *42*, 100983. https://doi.org/10.1016/j.coche.2023.100983.
149. Caldas Ramos, M.; Collison, C. J.; White, A. D. A Review of Large Language Models and Autonomous Agents in Chemistry. *Chem. Sci.* 2025, *16*, 2514–2572. https://doi.org/10.1039/D4SC03921A.
150. Olawade, D. B.; Ijiwade, J. O.; Fapohunda, O.; Ige, A. O.; Olajoyetan, D. O.; Wada, O. Z. Predictive Modeling of PFAS Behavior and Degradation in Novel Treatment Scenarios: A Review. *Process Saf. Environ. Prot.* 2025, *196*, 106869. https://doi.org/10.1016/j.psep.2025.106869.
151. Yang, L.; Chen, Z.; Goult, C. A.; Schlatzer, T.; Paton, R. S.; Gouverneur, V. Phosphate-Enabled Mechanochemical PFAS Destruction for Fluoride Reuse. *Nature* 2025, *640* (8057), 100–106. https://doi.org/10.1038/s41586-025-08698-5.
152. Glass, S.; Santiago-Cruz, H. A.; Chen, W.; et al. Merits, Limitations and Innovation Priorities for Heterogeneous Catalytic Platforms to Destroy PFAS. *Nat. Water* 2025, *3*, 644–654. https://doi.org/10.1038/s44221-025-00433-8.
153. Miklos, D. B.; et al. Evaluation of Advanced Oxidation Processes for Water and Wastewater Treatment,A Critical Review. *Water Res.* 2018, *139*, 118–131. https://doi.org/10.1016/j.watres.2018.03.042.

View Article Online
DOI: 10.1039/D5MA01247C

154. Wang, Y.; Warner, M.; Li, K.; Hawkins, G. L.; Huang, Q. Assessing Explicit Models of Per- and Polyfluoroalkyl Substances Adsorption on Anion Exchange Resins by Rapid Small-Scale Column Tests. *Chemosphere* 2022, *300*, 134547. https://doi.org/10.1016/j.chemosphere.2022.134547.
155. Liu, L.; Chen, X. Titanium Dioxide Nanomaterials: Self-Structural Modifications. Chem. Rev. 2014, 114 (19), 9890–9918. https://doi.org/10.1021/cr400624r
156. Yang, X.; Wang, D. Photocatalysis: From Fundamental Principles to Materials and Applications. *ACS Appl. Energy Mater.* 2018, *1* (12), 6657–6693. https://doi.org/10.1021/acsaem.8b01345.
157. Mu, C.; Lv, C.; Meng, X.; Sun, J.; Tong, Z.; Huang, K. In Situ Characterization Techniques Applied in Photocatalysis: A Review. *Adv. Mater. Interfaces* 2023, *10*, 2201842. https://doi.org/10.1002/admi.202201842.
158. Nosaka, Y.; Nosaka, A. Y. *Generation and Detection of Reactive Oxygen Species in Photocatalysis.* Chemical Reviews 2017, *117* (17), 11302–11336. https://doi.org/10.1021/acs.chemrev.7b0016
159. Wilsey, M. K.; Taseska, T.; Meng, Z.; Yu, W.; Müller, A. M. Advanced Electrocatalytic Redox Processes for Environmental Remediation of Halogenated Organic Water Pollutants. *Chem. Commun.* 2023, 59, 11895–11922. https://doi.org/10.1039/D3CC03176D.
160. Wang, S.; Yang, Q.; Chen, F.; Sun, J.; Luo, K.; Yao, F.; Wang, X.; Wang, D.; Li, X.; Zeng, G. Photocatalytic Degradation of Perfluorooctanoic Acid and Perfluorooctane Sulfonate in Water: A Critical Review. *Chem. Eng. J.* 2017, *328*, 927–942. https://doi.org/10.1016/j.cej.2017.07.076.
161. Bertucci, S.; Lova, P. Exploring Solar Energy Solutions for Per- and Polyfluoroalkyl Substances Degradation: Advancements and Future Directions in Photocatalytic Processes. *Sol. RRL* 2024, *8*, 2400116. https://doi.org/10.1002/solr.202400116
162. Arana Juve, J.-M.; Donoso Reece, J. A.; Wong, M. S.; Wei, Z.; Ateia, M. Photocatalysts for Chemical-Free PFOA Degradation – What We Know and Where We Go from Here? *J. Hazard. Mater.* 2024, *462*, 132651. https://doi.org/10.1016/j.jhazmat.2023.132651
163. Qi, Y.; Cao, H.; Pan, W.; Wang, C.; Liang, Y. The Role of Dissolved Organic Matter during Per- and Polyfluorinated Substance (PFAS) Adsorption, Degradation, and Plant Uptake: A Review. *J. Hazard. Mater.* 2022, *436*, 129139. https://doi.org/10.1016/j.jhazmat.2022.129139
164. Verma, S.; Varma, R. S.; Nadagouda, M. N. Remediation and Mineralization Processes for Per- and Polyfluoroalkyl Substances (PFAS) in Water: A Review. *Sci. Total Environ.* 2021, *794*, 148987. https://doi.org/10.1016/j.scitotenv.2021.148987
165. Park, H.; Vecitis, C. D.; Cheng, J.; Choi, W.; Mader, B. T.; Hoffmann, M. R. Reductive Defluorination of Aqueous Perfluorinated Alkyl Surfactants: Effects of Ionic Headgroup and Chain Length. *J. Phys. Chem. A* 2009, *113* (4), 690–696. https://doi.org/10.1021/jp807116q
166. Kutsuna, S.; Nagaoka, Y.; Takeuchi, K.; Hori, H. TiO_2-Induced Heterogeneous Photodegradation of a Fluorotelomer Alcohol in Air. *Environ. Sci. Technol.* 2006, *40* (21), 6824–6829. https://doi.org/10.1021/es060852
167. Gong, X.-Q.; Selloni, A. Reactivity of Anatase TiO_2 Nanoparticles: The Role of the Minority (001) Surface. *J. Phys. Chem. B* 2005, *109* (42), 19560–19562. https://doi.org/10.1021/jp055311g

View Article Online
DOI: 10.1039/D5MA01247C

168. Liu, C.; Qin, Y.; Guo, W.; Shi, Y.; Wang, Z.; Yu, Y.; Wu, L. Visible-Light-Driven Photocatalysis over Nano-TiO_2 with Different Morphologies: From Morphology through Active Site to Photocatalytic Performance. *Appl. Surf. Sci.* 2022, *580*, 152262. https://doi.org/10.1016/j.apsusc.2021.152262.
169. Janković, I. A.; Saponjić, Z. V.; Džunuzović, E. S.; Nedeljković, J. M. New Hybrid Properties of TiO_2 Nanoparticles Surface Modified with Catecholate Type Ligands. *Nanoscale Res. Lett.* 2009, *5* (1), 81–88. https://doi.org/10.1007/s11671-009-9447-y.
170. Wypych, A.; Bobowska, I.; Tracz, M.; Opasinska, A.; Kadlubowski, S.; Krzywania-Kaliszewska, A.; Grobelny, J.; Wojciechowski, P. Dielectric Properties and Characterisation of Titanium Dioxide Obtained by Different Chemistry Methods. *J. Nanomater.* 2014, 124814, 9 pages. https://doi.org/10.1155/2014/124814.
171. Reghunath, S.; Pinheiro, D.; Devi, S. K. R. A Review of Hierarchical Nanostructures of TiO_2: Advances and Applications. *Appl. Surf. Sci. Adv.* 2021, *3*, 100063. https://doi.org/10.1016/j.apsadv.2021.100063.
172. Singh, A.; Goyal, V.; Singh, J.; Rawat, M. Structural, Morphological, Optical and Photocatalytic Properties of Green Synthesized TiO_2 NPs. *Curr. Res. Green Sustain. Chem.* 2020, *3*, 100033. https://doi.org/10.1016/j.crgsc.2020.100033.
173. Nakata, K.; Fujishima, A. TiO_2 Photocatalysis: Design and Applications. *J. Photochem. Photobiol., C* 2012, *13* (3), 169–189. https://doi.org/10.1016/j.jphotochemrev.2012.06.001.
174. Nemiwal, M.; Zhang, T. C.; Kumar, D. Recent Progress in g-C_3N_4, TiO_2 and ZnO Based Photocatalysts for Dye Degradation: Strategies to Improve Photocatalytic Activity. *Sci. Total Environ.* 2021, *767*, 144896. https://doi.org/10.1016/j.scitotenv.2020.144896.
175. Etafo, N. O.; Bamidele, M. O.; Bamisaye, A.; Alli, Y. A. Revolutionizing Photocatalysis: Unveiling Efficient Alternatives to Titanium (IV) Oxide and Zinc Oxide for Comprehensive Environmental Remediation. *J. Water Process Eng.* 2024, *62*, 105369. https://doi.org/10.1016/j.jwpe.2024.105369
176. Liu, L.; Zhao, H.; Andino, J. M.; Li, Y. Photocatalytic CO_2 Reduction with H_2O on TiO_2 Nanocrystals: Comparison of Anatase, Rutile, and Brookite Polymorphs and Exploration of Surface Chemistry. ACS Catal. 2012, 2 (8), 1817–1828. https://doi.org/10.1021/cs300273q.
177. Eddy, D. R.; Sheha, G. A. N.; Permana, M. D.; Saito, N.; Takei, T.; Kumada, N.; Irkham; Rahayu, I.; Abe, I.; Sekine, Y.; Oyumi, T.; Izumi, Y. Study on Triphase of Polymorphs TiO_2 (Anatase/Rutile/Brookite) for Boosting Photocatalytic Activity of Metformin Degradation. Chemosphere 2024, 351, 141206. https://doi.org/10.1016/j.chemosphere.2024.141206.
178. Di Paola, A.; Bellardita, M.; Palmisano, L. Brookite, the Least Known TiO_2 Photocatalyst. Catalysts 2013, 3, 36–73. https://doi.org/10.3390/catal3010036.
179. El Mchaouri, M.; Mallah, S.; Abouhajjoub, D.; Boumya, W.; Elmoubarki, R.; Essadki, A.; Barka, N.; Elhalil, A. Engineering TiO_2 Photocatalysts for Enhanced Visible-Light Activity in Wastewater Treatment Applications. Tetrahedron Green Chem. 2025, 6, 100084. https://doi.org/10.1016/j.tgchem.2025.100084
180. Alabdallah, N. M.; Alluqmani, S. M.; Almarri, H. M.; Al-Zahrani, A. A. Physical, Chemical, and Biological Routes of Synthetic Titanium Dioxide Nanoparticles and Their Crucial Role in Temperature Stress Tolerance in Plants. Heliyon 2024, 10 (4), e26537. https://doi.org/10.1016/j.heliyon.2024.e26537.

View Article Online
DOI: 10.1039/D5MA01247C

181. Wu, J.; Bai, G. R.; Eastman, J. A.; et al. Synthesis of TiO_2 Nanoparticles Using Chemical Vapor Condensation. MRS Online Proc. Libr. 2005, 879, Z7.12. https://doi.org/10.1557/PROC-879-Z7.12.
182. Cargnello, M.; Gordon, T. R.; Murray, C. B. Solution-Phase Synthesis of Titanium Dioxide Nanoparticles and Nanocrystals. Chem. Rev. 2014, 114 (19), 9319–9345. https://doi.org/10.1021/cr500170p.
183. Öztürk, U.; Çitak, A. S. Synthesis of Titanium Dioxide Nanoparticles with Renewable Resources and Their Applications: Review. Turk. J. Chem. 2022, 46 (5), 1345–1357. https://doi.org/10.55730/1300-0527.3443.
184. Dillert, R.; Bahnemann, D.; Hidaka, H. Light-Induced Degradation of Perfluorocarboxylic Acids in the Presence of Titanium Dioxide. Chemosphere 2007, 67 (4), 785–792. https://doi.org/10.1016/j.chemosphere.2006.10.023.
185. Panchangam, S. C.; Lin, A. Y.-C.; Shaik, K. L.; Lin, C.-F. Decomposition of Perfluorocarboxylic Acids (PFCAs) by Heterogeneous Photocatalysis in Acidic Aqueous Medium. Chemosphere 2009, 77 (2), 242–248. https://doi.org/10.1016/j.chemosphere.2009.07.003.
186. Panchangam, S. C.; Lin, A. Y.-C.; Tsai, J.-H.; Lin, C.-F. Sonication-Assisted Photocatalytic Decomposition of Perfluorooctanoic Acid. Chemosphere 2009, 75 (5), 654–660. https://doi.org/10.1016/j.chemosphere.2008.12.065.
187. Wang, Y.; Zhang, P. Photocatalytic Decomposition of Perfluorooctanoic Acid (PFOA) by TiO2 in the Presence of Oxalic Acid. J. Hazard. Mater. 2011, 192 (3), 1869–1875. https://doi.org/10.1016/j.jhazmat.2011.07.026.
188. Surdhar, P. S.; Mezyk, S. P.; Armstrong, D. A. Reduction Potential of the CO_2^- Radical Anion in Aqueous Solutions. J. Phys. Chem. 1989, 93, 3360–3363.
189. Li, Y.; Wasgestian, F. Photocatalytic Reduction of Nitrate Ions on TiO_2 by Oxalic Acid. J. Photochem. Photobiol., A 1998, 112, 255–259.
190. Perissinotti, L. L.; Brusa, M. A.; Grela, M. A. Yield of Carboxyl Anion Radicals in the Photocatalytic Degradation of Formate over TiO_2 Particles. Langmuir 2001, 17, 8422–8427.
191. Gatto, S.; Sansotera, M.; Persico, F.; Gola, M.; Pirola, C.; Panzeri, W.; Navarrini, W.; Bianchi, C. L. Surface Fluorination on TiO2 Catalyst Induced by Photodegradation of Perfluorooctanoic Acid. Catal. Today 2015, 241 (Part A), 8–14. https://doi.org/10.1016/j.cattod.2014.04.031.
192. Sansotera, M.; Persico, F.; Rizzi, V.; Panzeri, W.; Pirola, C.; Bianchi, C. L.; Mele, A.; Navarrini, W. The Effect of Oxygen in the Photocatalytic Oxidation Pathways of Perfluorooctanoic Acid. *J. Fluor. Chem.* 2015, *179*, 159–168. https://doi.org/10.1016/j.jfluchem.2015.06.019.
193. Peydayesh, M.; Bagnani, M.; Soon, W. L.; Mezzenga, R. Turning Food Protein Waste into Sustainable Technologies. Chem. Rev. 2023, 123 (5), 2112–2154. https://doi.org/10.1021/acs.chemrev.2c00236.
194. Ghareeb, A.; Fouda, A.; Kishk, R. M.; et al. Unlocking the Potential of Titanium Dioxide Nanoparticles: An Insight into Green Synthesis, Optimizations, Characterizations, and Multifunctional Applications. Microb. Cell Fact. 2024, 23, 341. https://doi.org/10.1186/s12934-024-02609-5.
195. Saheed, M.; Jimoh Oladejo, T.; Rabi, E.; Muhammed Binin, E.; Azeezah Taiwo, A.; Damola Taye, S.; Abdulmumuni, S.; Adekunle Jelili, O.; Hassana Ladio, A.; Saka Abdulkareem, A.; et al. Photocatalytic Degradation and Defluorination of Per- and Poly-Fluoroalkyl Substances

View Article Online
DOI: 10.1039/D5MA01247C

(PFASs) Using Biosynthesized TiO2 Nanoparticles under UV–Visible Light. Eng. Proc. 2023, 37, 114. https://doi.org/10.3390/ECP2023-14630.

196. Murgolo, S.; Yargeau, V.; Gerbasi, R.; Visentin, F.; El Habra, N.; Ricco, G.; Lacchetti, I.; Carere, M.; Curri, M. L.; Mascolo, G. A New Supported TiO_2 Film Deposited on Stainless Steel for the Photocatalytic Degradation of Contaminants of Emerging Concern. Chem. Eng. J. 2017, 318, 103–111. https://doi.org/10.1016/j.cej.2016.05.125.
197. Furtado, R. X. de S.; Sabatini, C. A.; Zaiat, M.; Azevedo, E. B. Perfluorooctane Sulfonic Acid (PFOS) Degradation by Optimized Heterogeneous Photocatalysis (TiO2/UV) Using the Response Surface Methodology (RSM). J. Water Process Eng. 2021, 41, 101986. https://doi.org/10.1016/j.jwpe.2021.101986.
198. Sansotera, M.; Persico, F.; Pirola, C.; Navarrini, W.; Di Michele, A.; Bianchi, C. L. Decomposition of Perfluorooctanoic Acid Photocatalyzed by Titanium Dioxide: Chemical Modification of the Catalyst Surface Induced by Fluoride Ions. Appl. Catal. B: Environ. 2014, 148–149, 29–35. https://doi.org/10.1016/j.apcatb.2013.10.038.
199. Gao, Y.-q.; Zhong, X.-m.; Ren, X.-t.; Tian, F.-x.; Gao, N.-y.; Li, C. Synergistic Mechanism and Toxicity Reduction Potential in Medium-Pressure UV/Chlorine/TiO_2 System for Metronidazole Removal. J. Water Process Eng. 2024, 65, 105903. https://doi.org/10.1016/j.jwpe.2024.105903.
200. Ochiai, T.; Iizuka, Y.; Nakata, K.; Murakami, T.; Tryk, D. A.; Koide, Y.; Morito, Y.; Fujishima, A. Efficient Decomposition of Perfluorocarboxylic Acids in Aqueous Suspensions of a TiO2 Photocatalyst with Medium-Pressure Ultraviolet Lamp Irradiation under Atmospheric Pressure. Ind. Eng. Chem. Res. 2011, 50 (19), 10943–10947. https://doi.org/10.1021/ie1017496.
201. Hori, H.; Hayakawa, E.; Einaga, H.; Kutsuna, S.; Koike, K.; Ibusuki, T.; Kiatagawa, H.; Arakawa, R. Decomposition of Environmentally Persistent Perfluorooctanoic Acid in Water by Photochemical Approaches. Environ. Sci. Technol. 2004, 38, 6118.
202. Zhao, B.; Zhang, P. Photocatalytic Decomposition of Perfluorooctanoic Acid with β-Ga_2O_3 Wide Bandgap Photocatalyst. Catal. Commun. 2009, 10, 1184.
203. Zweigle, J.; Bugsel, B.; Capitain, C.; Zwiener, C. PhotoTOP: PFAS Precursor Characterization by UV/TiO2 Photocatalysis. Environ. Sci. Technol. 2022, 56 (22), 15728–15736. https://doi.org/10.1021/acs.est.2c05652.
204. Janda, J.; Nodler, K.; Scheurer, M.; Happel, O.; Nurenberg, G.; Zwiener, C.; Lange, F. T. Closing the gap,Inclusion of ultrashort-chain perfluoroalkyl carboxylic acids in the total oxidizable precursor (TOP) assay protocol. *Environ. Sci. Process Impacts* 2019, 21 (11), 1926–1935.
205. Houtz, E. F.; Sedlak, D. L. Oxidative conversion as a means of detecting precursors to perfluoroalkyl acids in urban runoff. *Environ. Sci. Technol.* 2012, 46 (17), 9342–9349.
206. Jiang, M.; Nozaki, K.; Mokudai, T.; Nakano, Y.; Uo, M.; Yamashita, K.; Ohara, S.; Wakabayashi, N. Enhancing the Photocatalytic Activity and Antibacterial Efficiency of TiO2 Nanosheets via Doping with Ag, Cu, or Ce. ACS Appl. Nano Mater. 2025, 8 (22), 11568–11581. https://doi.org/10.1021/acsanm.5c01768.
207. Etacheri, V.; Di Valentin, C.; Schneider, J.; Bahnemann, D.; Pillai, S. C. Visible-Light Activation of TiO_2 Photocatalysts: Advances in Theory and Experiments. J. Photochem. Photobiol. C: Photochem. Rev. 2015, 25, 1–29. https://doi.org/10.1016/j.jphotochemrev.2015.08.003

View Article Online
DOI: 10.1039/D5MA01247C

208. Thambiliyagodage, C.; Usgodaarachchi, L. Photocatalytic Activity of N, Fe and Cu Co-Doped TiO2 Nanoparticles under Sunlight. Curr. Res. Green Sustain. Chem. 2021, 4, 100186. https://doi.org/10.1016/j.crgsc.2021.100186.
209. Khlyustova, A.; Sirotkin, N.; Kusova, T.; Kraev, A.; Titov, V.; Agafonov, A. Doped TiO2: The Effect of Doping Elements on Photocatalytic Activity. Mater. Adv. 2020, 1, 1193–1201. https://doi.org/10.1039/D0MA00171F.
210. Mathew, S.; John, B. K.; Abraham, T.; Mathew, B. Metal-Doped Titanium Dioxide for Environmental Remediation, Hydrogen Evolution and Sensing: A Review. ChemistrySelect 2021, 6, 12742.
211. Kumar, S. G.; Gomathi Devi, L. Review on Modified TiO_2 Photocatalysis under UV/Visible Light: Selected Results and Related Mechanisms on Interfacial Charge Carrier Transfer Dynamics. J. Phys. Chem. A 2011, 115 (46), 13211–13241. https://doi.org/10.1021/jp204364a.
212. He, C.; Yu, Y.; Hu, X.; Larbot, A. Influence of Silver Doping on the Photocatalytic Activity of Titania Films. Appl. Surf. Sci. 2002, 200, 239–247. https://doi.org/10.1016/S0169-4332(02)00927-3.
213. Xu, A.-W.; Gao, Y.; Liu, H.-Q. The Preparation, Characterization, and Their Photocatalytic Activities of Rare-Earth-Doped TiO_2 Nanoparticles. J. Catal. 2002, 207, 151–157. https://doi.org/10.1006/jcat.2002.3539.
214. Saqib, N. U.; Adnan, R.; Shah, I. A. A Mini-Review on Rare Earth Metal-Doped TiO_2 for Photocatalytic Remediation of Wastewater. Environ. Sci. Pollut. Res. 2016, 23, 15941–15951. https://doi.org/10.1007/s11356-016-6984-7.
215. Yang, L.; Zhang, J.; Tong, H.; Li, X.; Zhao, D.; Lan, K. Synthesis of Mesoporous Titania Nanomaterials for Evolving Photocatalytic Applications. Adv. Energy Mater. 2025, e02405. https://doi.org/10.1002/aenm.202502405.
216. Watthanaarun, J.; Pavarajarn, V.; Supaphol, P. Titanium (IV) Oxide Nanofibers by Combined Sol–Gel and Electrospinning Techniques: Preliminary Report on Effects of Preparation Conditions and Secondary Metal Dopant. Sci. Technol. Adv. Mater. 2005, 6, 240–245. https://doi.org/10.1016/j.stam.2005.02.002.
217. Shah, R.; Khan, D.; Al-Anazi, A.; Ahmad, W.; Ullah, I.; Shah, N. S.; Khan, J. A. Non-Metal Doped ZnO and TiO_2 Photocatalysts for Visible Light Active Degradation of Pharmaceuticals and Hydrogen Production: A Review. Appl. Catal., Open 2025, 204, 207043. https://doi.org/10.1016/j.apcato.2025.207043.
218. Basavarajappa, P. S.; Patil, S. B.; Ganganagappa, N.; Raghava Reddy, K.; Raghu, A. V.; Venkata Reddy, C. Recent Progress in Metal-Doped TiO_2, Non-Metal Doped/Co-Doped TiO_2 and TiO_2 Nanostructured Hybrids for Enhanced Photocatalysis. Int. J. Hydrogen Energy 2020, 45 (13), 7764–7778. https://doi.org/10.1016/j.ijhydene.2019.07.241.
219. Di Valentin, C.; Pacchioni, G.; Selloni, A.; Livraghi, S.; Giamello, E. Characterization of Paramagnetic Species in N-Doped TiO_2 Powders by EPR Spectroscopy and DFT Calculations. J. Phys. Chem. B 2005, 109 (23), 11414–11419. https://doi.org/10.1021/jp051756t.
220. FengHui, F.; ChengBu, C. DFT Description on Electronic Structure and Optical Absorption Properties of Anionic S-Doped Anatase TiO_2. J. Phys. Chem. B 2006, 110 (36), 17866–17871. https://doi.org/10.1021/jp0635462.

View Article Online
DOI: 10.1039/D5MA01247C

221. Daghrir, R.; Drogui, P.; Robert, D. Modified TiO_2 for Environmental Photocatalytic Applications: A Review. Ind. Eng. Chem. Res. 2013, 52 (10), 3581–3599. https://doi.org/10.1021/ie303468t.
222. Estrellan, C. R.; Salim, C.; Hinode, H. Photocatalytic Decomposition of Perfluorooctanoic Acid by Iron and Niobium Co-Doped Titanium Dioxide. J. Hazard. Mater. 2010, 179 (1–3), 79–83. https://doi.org/10.1016/j.jhazmat.2010.02.060.
223. Chen, M.-J.; Lo, S.-L.; Lee, Y.-C.; Huang, C.-C. Photocatalytic Decomposition of Perfluorooctanoic Acid by Transition-Metal Modified Titanium Dioxide. J. Hazard. Mater. 2015, 288, 168–175. https://doi.org/10.1016/j.jhazmat.2015.02.004.
224. Vohra, M. S.; Kim, S.; Choi, W. Effects of Surface Fluorination of TiO_2 on the Photocatalytic Degradation of Tetramethylammonium. J. Photochem.
225. Li, M.; Yu, Z.; Liu, Q.; Sun, L.; Huang, W. Photocatalytic Decomposition of Perfluorooctanoic Acid by Noble Metallic Nanoparticles Modified TiO2. Chem. Eng. J. 2016, 286, 232–238. https://doi.org/10.1016/j.cej.2015.10.037.
226. Vanlalhmingmawia, C.; Lee, S. M.; Tiwari, D. Plasmonic Noble Metal Doped Titanium Dioxide Nanocomposites: Newer and Exciting Materials in the Remediation of Water Contaminated with Micropollutants. J. Water Process Eng. 2023, 51, 103360. https://doi.org/10.1016/j.jwpe.2022.103360.
227. Zhan, F.; Qi, J.; Li, R.; Zhao, H.; Liu, Y.; La, P. Synthesis, Photocatalytic Applications and Future Prospects of Noble Metal-Modified Semiconductors Fabricated via Photodeposition. Phys. Chem. Chem. Phys. 2025, 27, 13770–13792. https://doi.org/10.1039/D5CP01191D.
228. Chen, M.-J.; Lo, S.-L.; Lee, Y.-C.; Kuo, J.; Wu, C.-H. Decomposition of Perfluorooctanoic Acid by Ultraviolet Light Irradiation with Pb-Modified Titanium Dioxide. J. Hazard. Mater. 2016, 303, 111–118. https://doi.org/10.1016/j.jhazmat.2015.10.011.
229. Huang, B.; Wu, Z.; Zhou, H.; Li, J.; Zhou, C.; Xiong, Z.; Pan, Z.; Yao, G.; Lai, B. Recent Advances in Single-Atom Catalysts for Advanced Oxidation Processes in Water Purification. J. Hazard. Mater. 2021, 412, 125253. https://doi.org/10.1016/j.jhazmat.2021.125253.
230. Wei, T.; Zhou, J.; An, X. Recent Advances in Single-Atom Catalysts (SACs) for Photocatalytic Applications. Mater. Rep. Energy 2024, 4 (3), 100285. https://doi.org/10.1016/j.matre.2024.100285.
231. Wu, S.-M.; Schmuki, P. Single Atom Cocatalysts in Photocatalysis. Adv. Mater. 2025, 37, 2414889. https://doi.org/10.1002/adma.202414889.
232. Kerketta, U.; Tesler, A. B.; Schmuki, P. Single-Atom Co-Catalysts Employed in Titanium Dioxide Photocatalysis. Catalysts 2022, 12, 1223. https://doi.org/10.3390/catal12101223.
233. Sun, H.; Tang, R.; Huang, J. Considering Single-Atom Catalysts as Photocatalysts from Synthesis to Application. iScience 2022, 25 (5), 104232. https://doi.org/10.1016/j.isci.2022.104232.
234. Liu, X.; Gong, K.; Duan, X.; Wei, W.; Wang, T.; Chen, Z.; Zhang, L.; Ni, B.-J. Photo-Induced Bismuth Single Atoms on TiO2 for Highly Efficient Photocatalytic Defluorination of Perfluorooctanoic Acid: Ionization of the C–F Bond. ACS ES&T Eng. 2023, 3 (10), 1626–1636. https://doi.org/10.1021/acsestengg.3c00177.

View Article Online
DOI: 10.1039/D5MA01247C

235. Cui, Z.; Jafarzadeh, A.; Hao, Y.; Liu, L.; Li, L.; Zheng, Y. Prediction of the Decomposition Tendency of $C_5F_{10}O$ on Discharged Metal Surfaces. IEEE Trans. Dielectr. Electr. Insul. 2023, 30, 1365–1367. https://doi.org/10.1109/TDEI.2023.3260035.
236. Anucha, C. B.; Altin, I.; Bacaksiz, E.; Stathopoulos, V. N. Titanium Dioxide (TiO_2)-Based Photocatalyst Materials Activity Enhancement for Contaminants of Emerging Concern (CECs) Degradation: In the Light of Modification Strategies. Chem. Eng. J. Adv. 2022, 10, 100262. https://doi.org/10.1016/j.ceja.2022.100262.
237. Dahl, M.; Liu, Y.; Yin, Y. Composite Titanium Dioxide Nanomaterials. Chem. Rev. 2014, 114 (19), 9853–9889. https://doi.org/10.1021/cr400634p.
238. Yao, X.; Zuo, J.; Wang, Y.-J.; Song, N.-N.; Li, H.-H.; Qiu, K. Enhanced photocatalytic degradation of perfluorooctanoic acid by mesoporous Sb_2O_3/TiO_2 heterojunctions. Front. Chem. 2021, 9, 690520. https://doi.org/10.3389/fchem.2021.690520.
239. Chen, F.; He, A.; Wang, Y.; Yu, W.; Chen, H.; Geng, F.; Li, Z.; Zhou, Z.; Liang, Y.; Fu, J.; Zhao, L.; Wang, Y. Efficient Photodegradation of PFOA Using Spherical BiOBr Modified TiO2 via Hole-Remained Oxidation Mechanism. Chemosphere 2022, 298, 134176. https://doi.org/10.1016/j.chemosphere.2022.134176.
240. Li, X.; Zhang, P.; Jin, L.; Shao, T.; Li, Z.; Cao, J. Efficient Photocatalytic Decomposition of Perfluorooctanoic Acid by Indium Oxide and Its Mechanism. Environ. Sci. Technol. 2012, 46 (10), 5528–5534. https://doi.org/10.1021/es204279u.
241. Zhang, X.; Li, R.; Jia, M.; Wang, S.; Huang, Y.; Chen, C. Degradation of Ciprofloxacin in Aqueous Bismuth Oxybromide (BiOBr) Suspensions under Visible Light Irradiation: A Direct Hole Oxidation Pathway. Chem. Eng. J. 2015, 274, 290–297. https://doi.org/10.1016/j.cej.2015.03.077.
242. Fang, Y.-F.; Ma, W.-H.; Huang, Y.-P.; Cheng, G.-W. Exploring the Reactivity of Multicomponent Photocatalysts: Insight into the Complex Valence Band of BiOBr. Chem.–Eur. J. 2013, 19 (9), 3224–3229. https://doi.org/10.1002/chem.201202602.
243. Liang, L.; Gao, S.; Zhu, J.; Wang, L.; Xiong, Y.; Xia, X.; Yang, L. The Enhanced Photocatalytic Performance toward Carbamazepine by Nitrogen-Doped Carbon Dots Decorated on $BiOBr/CeO_2$: Mechanism Insight and Degradation Pathways. Chem. Eng. J. 2020, 391, 123599. https://doi.org/10.1016/j.cej.2019.123599.
244. Singh, B.; Kaur, G.; Singh, P.; Singh, K.; Sharma, J.; Kumar, M.; Bala, R.; Meena, R.; Sharma, S. K.; Kumar, A. Nanostructured $BN–TiO_2$ Composite with Ultra-High Photocatalytic Activity. New J. Chem. 2017, 41 (20), 11640–11646.
245. Duan, L.; Wang, B.; Heck, K.; Guo, S.; Clark, C. A.; Arredondo, J.; Wang, M.; Senftle, T. P.; Westerhoff, P.; Wen, X.; Song, Y.; Wong, M. S. Efficient Photocatalytic PFOA Degradation over Boron Nitride. Environmental Science & Technology Letters 2020, 7 (8), 613–619. https://doi.org/10.1021/acs.estlett.0c00434
246. Chen, A.; Ji, H.; Xu, Z.; Wang, Z.; Xie, H.; Zhang, L. Unique S-Scheme Structures in Electrostatic Self-Assembled $ReS_2–TiO_2$ for High-Efficiency Perfluorooctanoic Acid Removal. *J. Colloid Interface Sci.* 2025, *681*, 63–70. https://doi.org/10.1016/j.jcis.2024.11.164.
247. Yang, C.; Zhang, G.; Meng, Y.; Pan, G.; Ni, Z.; Xia, S. Direct Z-Scheme CeO_2@LDH Core–Shell Heterostructure for Photodegradation of Rhodamine B by Synergistic Persulfate Activation. J. Hazard. Mater. 2021, 408, 124908. https://doi.org/10.1016/j.jhazmat.2020.124908.

View Article Online
DOI: 10.1039/D5MA01247C

248. Du, Y.; Meng, Y.; Pan, G. X.; Shen, H.; Yao, Y. Y.; Xie, B.; Ni, Z. M.; Xia, S. J. Comparison of Performance and Mechanism for Single and Double Vacancies MoS_2 Catalyzing Water Gas Shift Reaction. Int. J. Hydrogen Energy 2023, 48, 24628–24639. https://doi.org/10.1016/j.ijhydene.2022.06.198.
249. Kong, E. D. H.; Lai, C. W.; Juan, J. C.; Pang, Y. L.; Khe, C. S.; Badruddin, I. A.; Gapsari, F.; Anam, K. Recent Advances in Titanium Dioxide Bio-Derived Carbon Photocatalysts for Organic Pollutant Degradation in Wastewater. *iScience* 2025, *28* (5), 112368. https://doi.org/10.1016/j.isci.2025.112368.
250. Xia, B.; Cao, P.; Tang, X.; Shi, Q.; Lv, Y.; Zhang, X. Promoting Interfacial Charge Separation for Efficient Photocatalysis of Organic Dyes Using ESM-Solidified TiO_2-Based Coupling Materials. *Mater. Today Commun.* 2025, *45*, 112436. https://doi.org/10.1016/j.mtcomm.2025.112436.
251. Meirelles, M. R.; Giroto, A. S.; Furukawa, K.; Gonçalves, M. Valorization of Lignocellulosic Biomass for Photocatalytic Applications: Development of Activated Carbon–TiO_2 Composites. *ACS Sustainable Resour. Manag.* 2025, *2* (3), 524–535. https://doi.org/10.1021/acssusresmgt.4c00512.
252. Dong, X.; Li, H.; Guo, Y.; Ge, C.; Zha, J. Construction of Hierarchical Black TiO_2/Carbon Fiber: Enhanced Photocatalytic Activity Based on Schottky Heterojunctions. *ACS Appl. Bio Mater.* 2024, *7* (8), 5397–5410. https://doi.org/10.1021/acsabm.4c00572.
253. Padmanabhan, N. T.; Thomas, N.; Louis, J.; Mathew, D. T.; Ganguly, P.; John, H.; Pillai, S. C. Graphene Coupled TiO_2 Photocatalysts for Environmental Applications: A Review. *Chemosphere* 2021, *271*, 129506. https://doi.org/10.1016/j.chemosphere.2020.129506
254. Li, F.; Wei, Z.; He, K.; Blaney, L.; Cheng, X.; Xu, T.; Liu, W.; Zhao, D. A Concentrate-and-Destroy Technique for Degradation of Perfluorooctanoic Acid in Water Using a New Adsorptive Photocatalyst. Water Res. 2020, 185, 116219. https://doi.org/10.1016/j.watres.2020.116219.
255. Xu, T.; Ji, H.; Gu, Y.; Tong, T.; Xia, Y.; Zhang, L.; Zhao, D. Enhanced Adsorption and Photocatalytic Degradation of Perfluorooctanoic Acid in Water Using Iron (Hydr)oxides/Carbon Sphere Composite. Chem. Eng. J. 2020, 388, 124230. https://doi.org/10.1016/j.cej.2020.124230.
256. Wei, Z.; Luo, S.; Xiao, R.; Khalfin, R.; Semiat, R. Characterization and Quantification of Chromate Adsorption by Layered Porous Iron Oxyhydroxide: An Experimental and Theoretical Study. J. Hazard. Mater. 2017, 338, 472–481. https://doi.org/10.1016/j.jhazmat.2017.05.049.
257. Zhu, Y.; Xu, T.; Zhao, D.; Li, F.; Liu, W.; Wang, B.; An, B. Adsorption and Solid-Phase Photocatalytic Degradation of Perfluorooctane Sulfonate in Water Using Gallium-Doped Carbon-Modified Titanate Nanotubes. *Chem. Eng. J.* 2021, *421* (Part 1), 129676. https://doi.org/10.1016/j.cej.2021.129676.
258. Yu, Q.; Zhang, R.; Deng, S.; Huang, J.; Yu, G. Sorption of Perfluorooctane Sulfonate and Perfluorooctanoate on Activated Carbons and Resin: Kinetic and Isotherm Study. Water Res. 2009, 43 (4), 1150–1158. https://doi.org/10.1016/j.watres.2008.12.001.
259. Wibowo, N.; Setyadhi, L.; Wibowo, D.; Setiawan, J.; Ismadji, S. Adsorption of Benzene and Toluene from Aqueous Solutions onto Activated Carbon and Its Acid and Heat Treated

View Article Online
DOI: 10.1039/D5MA01247C

Forms: Influence of Surface Chemistry on Adsorption. J. Hazard. Mater. 2007, 146, 237–242. https://doi.org/10.1016/j.jhazmat.2006.12.011.

260. Arana Juve, J.-M.; Li, F.; Zhu, Y.; Liu, W.; Ottosen, L. D. M.; Zhao, D.; Wei, Z. Concentrate and Degrade PFOA with a Photo-Regenerable Composite of In-Doped TNTs@AC. *Chemosphere* 2022, *300*, 134495. https://doi.org/10.1016/j.chemosphere.2022.134495.
261. Gayen, R. N.; Hussain, S.; Bhar, R.; Pal, A. K. Synthesis and Characterization of Indium Phosphide Films Prepared by Co-Evaporation Technique. Vacuum 2012, 86, 1240–1247. https://doi.org/10.1016/j.vacuum.2011.11.005.
262. Detweiler, Z. M.; Wulfsberg, S. M.; Frith, M. G.; Bocarsly, A. B.; Bernasek, S. L. The Oxidation and Surface Speciation of Indium and Indium Oxides Exposed to Atmospheric Oxidants. Surf. Sci. 2016, 648, 188–195. https://doi.org/10.1016/j.susc.2015.10.026.
263. Kosmulski, M. Pristine Points of Zero Charge of Gallium and Indium Oxides. J. Colloid Interface Sci. 2001, 238, 225–227. https://doi.org/10.1006/jcis.2001.7484.
264. Song, C.; Chen, P.; Wang, C.; Zhu, L. Photodegradation of Perfluorooctanoic Acid by Synthesized TiO_2–MWCNT Composites under 365 nm UV Irradiation. *Chemosphere* 2012, *86* (8), 853–859. https://doi.org/10.1016/j.chemosphere.2011.11.034.
265. Gomez-Ruiz, B.; Ribao, P.; Diban, N.; Rivero, M. J.; Ortiz, I.; Urtiaga, A. Photocatalytic Degradation and Mineralization of Perfluorooctanoic Acid (PFOA) Using a Composite TiO_2–rGO Catalyst. *J. Hazard. Mater.* 2018, *344*, 950–957. https://doi.org/10.1016/j.jhazmat.2017.11.048.
266. Rivero, M. J.; Ribao, P.; Gomez-Ruiz, B.; Urtiaga, A.; Ortiz, I. Comparative Performance of TiO_2–rGO Photocatalyst in the Degradation of Dichloroacetic and Perfluorooctanoic Acids. *Sep. Purif. Technol.* 2020, *240*, 116637. https://doi.org/10.1016/j.seppur.2020.116637.
267. Chowdhury, N.; Choi, H. Photocatalytic Degradation of Perfluorooctanoic Acid on Pb-Doped TiO_2 Coated with Reduced Graphene Oxide. *Water Environ. Res.* 2023, *95* (5), e10871. https://doi.org/10.1002/wer.10871.
268. Li, W.; Zhuang, C.; Li, Y.; Gao, C.; Jiang, W.; Sun, Z.; Qi, K. Anchoring Ultra-Small TiO_2 Quantum Dots onto Ultra-Thin and Large-Sized MXene Nanosheets for Highly Efficient Photocatalytic Water Splitting. *Ceram. Int.* 2021, *47* (15), 21769–21776. https://doi.org/10.1016/j.ceramint.2021.04.192.
269. Dimitriou, C.; Belles, L.; Boukos, N.; Deligiannakis, Y. {TiO_2/TiO_2(B)} Quantum Dot Hybrids: A Comprehensible Route toward High-Performance [>0.1 mol g^{-1} h^{-1}] Photocatalytic H_2 Production from H_2O. *ACS Catal.* 2024, *14* (23), 17919–17934. https://doi.org/10.1021/acscatal.4c05001
270. Ikram, M.; Ul Haq, M. A.; Haider, A.; Haider, J.; Ul-Hamid, A.; Shahzadi, I.; Bari, M. A.; Ali, S.; Goumri-Said, S.; Kanoun, M. B. The Enhanced Photocatalytic Performance and First-Principles Computational Insights of Ba Doping-Dependent TiO_2 Quantum Dots. *Nanoscale Adv.* 2022, *4* (18), 3996–4008. https://doi.org/10.1039/d2na00361a
271. Zhu, C.; Xu, J.; Song, S.; Wang, J.; Li, Y.; Liu, R.; Shen, Y. TiO_2 Quantum Dots Loaded Sulfonated Graphene Aerogel for Effective Adsorption-Photocatalysis of PFOA. *Sci. Total Environ.* 2020, *698*, 134275. https://doi.org/10.1016/j.scitotenv.2019.134275.
272. Pechnikova, N. A.; Domvri, K.; Porpodis, K.; Istomina, M. S.; Iaremenko, A. V.; Yaremenko, A. V. Carbon Quantum Dots in Biomedical Applications: Advances, Challenges, and Future Prospects. *Aggregate* 2025, *6*, e707. https://doi.org/10.1002/agt2.707

View Article Online
DOI: 10.1039/D5MA01247C

273. Akhtar, M. A.; Anum, J.; Ahmed, S. S.; Ahmed, M. A.; Khan, A. M.; Sayes, C. M.; Rahim, A. Eco-Friendly Synthesis of N-Doped Carbon Quantum Dots from *Bombax ceiba* Stem: A Photophysical Study with Exploratory Sensing of Fe^{3+}/Cd^{2+} and Dye Degradation. *J. Water Process Eng.* 2025, *78*, 108704. https://doi.org/10.1016/j.jwpe.2025.108704
274. Nejatpour, M.; Ünsür, A. M.; Yılmaz, B.; Gül, M.; Ozden, B.; Barisci, S.; Dükkancı, M. Enhanced Photodegradation of Perfluorocarboxylic Acids (PFCAs) Using Carbon Quantum Dots (CQDs) Doped TiO_2 Photocatalysts: A Comparative Study between Exfoliated Graphite and Mussel Shell-Derived CQDs. *J. Environ. Chem. Eng.* 2025, *13* (1), 115382. https://doi.org/10.1016/j.jece.2025.115382.
275. Ünsür, A. M.; Nejatpour, M.; Dükkancı, M.; Ozden, B.; Samai, S.; Parlak, C.; Barisci, S. Green Approach for Perfluorocarboxylic Acids (PFCAs) Removal with Density Functional Theory (DFT) Insights: Peanut-Shell Biomass-Based Carbon Quantum Dots (PCQDs) Coupled with TiO_2 Photocatalyst. *J. Hazard. Mater.* 2025, *495*, 139060. https://doi.org/10.1016/j.jhazmat.2025.139060.
276. Li, X.; Bai, Y.; Shi, X.; Su, N.; Nie, G.; Zhang, R.; Nie, H.; Ye, L. Applications of MXene ($Ti_3C_2T_x$) in Photocatalysis: A Review. Mater. Adv. 2021, 2 (5), 1570–1594. https://doi.org/10.1039/D0MA00938E.
277. Urso, M.; Bruno, L.; Dattilo, S.; Carroccio, S. C.; Mirabella, S. Band Engineering versus Catalysis: Enhancing the Self-Propulsion of Light-Powered MXene-Derived Metal–TiO_2 Micromotors To Degrade Polymer Chains. ACS Appl. Mater. Interfaces 2024, 16 (1), 1293–1307. https://doi.org/10.1021/acsami.3c13470.
278. Rostami, M.; Badiei, A.; Alijani, M.; Das, A.; Ziarani, G. M. Nanoarchitectonic MOF-Derived Materials for Enhanced Photocatalytic Activity in Organic Contaminant Removal: A Review. Alex. Eng. J. 2025, 126, 448–479. https://doi.org/10.1016/j.aej.2025.04.092.
279. Abánades Lázaro, I.; Szalad, H.; Valiente, P.; Albero, J.; García, H.; Martí-Gastaldo, C. Tuning the Photocatalytic Activity of Ti-Based Metal–Organic Frameworks through Modulator Defect-Engineered Functionalization. ACS Appl. Mater. Interfaces 2022, 14 (18), 21007–21017. https://doi.org/10.1021/acsami.2c02668.
280. Armaković, S. J.; Armaković, S. Zeolite-Supported TiO_2 for Enhanced Photocatalytic Performance in Environmental Applications: A Review. Catalysts 2025, 15 (2), 174. https://doi.org/10.3390/catal15020174.
281. Zhang, K.; Li, C.; Xu, L.; He, Z.; Zhang, Z.; Sumita, J.; Ghumro, J. A.; Dong, K. MXene and Its Composites Combined with Photocatalytic Degradation of Perfluorooctanoic Acid: Efficiency and Active Species Study. Environ. Res. 2025, 278, 121690. https://doi.org/10.1016/j.envres.2025.121690.
282. Song, H.; Wang, Y.; Ling, Z.; Zu, D.; Li, Z.; Shen, Y.; Li, C. Enhanced Photocatalytic Degradation of Perfluorooctanoic Acid by Ti_3C_2 MXene-Derived Heterojunction Photocatalyst: Application of Intercalation Strategy in DESs. Sci. Total Environ. 2020, 746, 141009. https://doi.org/10.1016/j.scitotenv.2020.141009.
283. Halder, S.; Chou, F.-C.; Wan, T.-K.; Tsai, Y.-T.; Cheng, P.-C.; Lin, Y.-C. Enhanced Photodegradation of Pentafluoropropionic Acid (PFPA) via TiO_2–Synthetic Zeolite Composites: A Sustainable Approach for Effective Defluorination. J. Water Process Eng. 2024, 62, 105296. https://doi.org/10.1016/j.jwpe.2024.105296.

View Article Online
DOI: 10.1039/D5MA01247C

284. Chauke, N. M.; Raphulu, M. A Review: Simultaneous “One-Pot” Pollution Mitigation and Hydrogen Production from Industrial Wastewater Using Photoelectrocatalysis Process. *Mater. Today Catal.* 2024, *5*, 100052. https://doi.org/10.1016/j.mtcata.2024.100052
285. Dong, C.; Fang, W.; Yi, Q.; Zhang, J. A Comprehensive Review on Reactive Oxygen Species (ROS) in Advanced Oxidation Processes (AOPs). Chemosphere 2022, 308, 136205. https://doi.org/10.1016/j.chemosphere.2022.136205.
286. Tufail, A.; Price, W. E.; Hai, F. I. A Critical Review on Advanced Oxidation Processes for the Removal of Trace Organic Contaminants: A Voyage from Individual to Integrated Processes. Chemosphere 2020, 260, 127460. https://doi.org/10.1016/j.chemosphere.2020.127460.
287. Taoufik, N.; Boumya, W.; Achak, M.; Sillanpää, M.; Barka, N. Comparative Overview of Advanced Oxidation Processes and Biological Approaches for the Removal of Pharmaceuticals. J. Environ. Manage. 2021, 288, 112404. https://doi.org/10.1016/j.jenvman.2021.112404.
288. Luo, Y.; Feng, X.; Chen, Z.; Shen, X. Molecularly Imprinted Photocatalysts: Fabrication, Application and Challenges. Mater. Adv. 2022, 3, 8830–8847. https://doi.org/10.1039/D2MA00848C.
289. Kubiak, A.; Jaruga, M.; Lusina, A.; Nazim, T.; Sobańska, K.; Pietrzyk, P.; Cegłowski, M. Real-World Application of Molecularly Imprinted TiO_2-Graphite Photocatalysts: Efficient Pharmaceutical Removal under Energy-Optimized LED System. J. Water Process Eng. 2025, 69, 106894. https://doi.org/10.1016/j.jwpe.2024.106894.
290. Guo, M.; Hu, Y.; Wang, R.; Yu, H.; Sun, L. Molecularly Imprinted Polymer-Based Photocatalyst for Highly Selective Degradation of Methylene Blue. Environ. Res. 2021, 194, 110684. https://doi.org/10.1016/j.envres.2020.110684.
291. Yu, J.; González-Cobos, J.; Dappozze, F.; Vernoux, P.; Caravaca, A.; Guillard, C. Basic Comprehension and Recent Trends in Photoelectrocatalytic Systems. Green Chem. 2024, 26, 1682–1708. https://doi.org/10.1039/D3GC03371F.
292. Liu, D.; Wan, X.; Kong, T.; Han, W.; Xiong, Y. Single-Atom-Based Catalysts for Photoelectrocatalysis: Challenges and Opportunities. J. Mater. Chem. A 2022, 10, 5878–5888. https://doi.org/10.1039/D1TA08252C.
293. Fernandez-Ibanez, P.; McMichael, S.; Rioja Cabanillas, A.; Alkharabsheh, S.; Tolosana Moranchel, A.; Byrne, J. A. New Trends on Photoelectrocatalysis (PEC): Nanomaterials, Wastewater Treatment and Hydrogen Generation. Curr. Opin. Chem. Eng. 2021, 34, 100725. https://doi.org/10.1016/j.coche.2021.100725.
294. Park, K.; Ali, I.; Kim, J.-O. Photodegradation of Perfluorooctanoic Acid by Graphene Oxide-Deposited TiO_2 Nanotube Arrays in Aqueous Phase. J. Environ. Manage. 2018, 218, 333–339. https://doi.org/10.1016/j.jenvman.2018.04.016.
295. Thind, S. S.; Ryane, B. A.; Hayden, J. B.; Chagunda, I.; Paul, M.; McIndoe, J. S. Bias Enhanced Electro-Photocatalysis on TiO_2 Nanoporous Materials for Decomposition of Forever Chemicals in Saltwater. Environ. Sci.: Adv. 2025, 4, 1024–1034. https://doi.org/10.1039/D4VA00423J.
296. Tucci, A. P.; Murgolo, S.; De Ceglie, C.; Mascolo, G.; Carmagnani, M.; Ronco, P.; Bestetti, M.; Franz, S. Photoelectrocatalytic Advanced Oxidation of Perfluoroalkyl Substances in Groundwaters of the Veneto Region, Italy. Catal. Today 2025, 450, 115205. https://doi.org/10.1016/j.cattod.2025.115205.

View Article Online
DOI: 10.1039/D5MA01247C

297. Fernandes, A.; Makoś, P.; Wang, Z.; Boczkaj, G. Synergistic Effect of TiO_2 Photocatalytic Advanced Oxidation Processes in the Treatment of Refinery Effluents. *Chem. Eng. J.* 2020, *391*, 123488. https://doi.org/10.1016/j.cej.2019.123488
298. Tanos, F.; Razzouk, A.; Lesage, G.; Cretin, M.; Bechelany, M. A Comprehensive Review on Modification of Titanium Dioxide-Based Catalysts in Advanced Oxidation Processes for Water Treatment. *ChemSusChem* 2024, *17*, e202301139. https://doi.org/10.1002/cssc.202301139
299. Navidpour, A. H.; Abbasi, S.; Li, D.; Mojiri, A.; Zhou, J. L. Investigation of Advanced Oxidation Process in the Presence of TiO_2 Semiconductor as Photocatalyst: Property, Principle, Kinetic Analysis, and Photocatalytic Activity. *Catalysts* 2023, *13*, 232. https://doi.org/10.3390/catal13020232
300. Fazli, A.; Athanassiou, A.; Fragouli, D. Current Approaches and Challenges in Advanced Oxidation Processes for Nanoplastic Degradation. *Adv. Sci.* 2025, *12*, e04352. https://doi.org/10.1002/advs.202504352
301. Šuligoj, A.; Kete, M.; Černigoj, U.; Fresno, F.; Lavrenčič Štangar, U. Synergism in TiO2 Photocatalytic Ozonation for the Removal of Dichloroacetic Acid and Thiacloprid. Environ. Res. 2021, 197, 110982. https://doi.org/10.1016/j.envres.2021.110982.
302. Zazouli, M. A.; Yousefi, M.; Ghanbari, F.; Babanezhad, E. Performance of Photocatalytic Ozonation Process for Pentachlorophenol (PCP) Removal in Aqueous Solution Using Graphene-TiO2 Nanocomposite (UV/G-TiO2/O3). J. Environ. Health Sci. Eng. 2020, 18 (2), 1083–1097. https://doi.org/10.1007/s40201-020-00529-1.
303. Huang, J.; Wang, X.; Pan, Z.; Li, X.; Ling, Y.; Li, L. Efficient Degradation of Perfluorooctanoic Acid (PFOA) by Photocatalytic Ozonation. Chem. Eng. J. 2016, 296, 329–334. https://doi.org/10.1016/j.cej.2016.03.116.
304. Xu, B.; Ahmed, M. B.; Zhou, J. L.; Altaee, A. Visible and UV Photocatalysis of Aqueous Perfluorooctanoic Acid by TiO2 and Peroxymonosulfate: Process Kinetics and Mechanistic Insights. Chemosphere 2020, 243, 125366. https://doi.org/10.1016/j.chemosphere.2019.125366.
305. Venkatesan, A. K.; Lee, C.-S.; Gobler, C. J. Hydroxyl-Radical Based Advanced Oxidation Processes Can Increase Perfluoroalkyl Substances beyond Drinking Water Standards: Results from a Pilot Study. Sci. Total Environ. 2022, 847, 157577. https://doi.org/10.1016/j.scitotenv.2022.157577.
306. Lashuk, B.; Pineda, M.; AbuBakr, S.; Boffito, D.; Yargeau, V. Application of Photocatalytic Ozonation with a WO_3/TiO_2 Catalyst for PFAS Removal under UVA/Visible Light. *Sci. Total Environ.* 2022, *843*, 157006. https://doi.org/10.1016/j.scitotenv.2022.157006
307. Satyam, S.; Patra, S. Innovations and Challenges in Adsorption-Based Wastewater Remediation: A Comprehensive Review. Heliyon 2024, 10 (9), e29573. https://doi.org/10.1016/j.heliyon.2024.e29573.
308. Fouda-Mbanga, B. G.; Onotu, O. P.; Tywabi-Ngeva, Z. Advantages of the Reuse of Spent Adsorbents and Potential Applications in Environmental Remediation: A Review. Green Anal. Chem. 2024, 11, 100156. https://doi.org/10.1016/j.greeac.2024.100156.
309. Sanzana, S.; Fenti, A.; Iovino, P.; Panico, A. A Review of PFAS Remediation: Separation and Degradation Technologies for Water and Wastewater Treatment. J. Water Process Eng. 2025, 74, 107793. https://doi.org/10.1016/j.jwpe.2025.107793.

View Article Online
DOI: 10.1039/D5MA01247C

310. Wang, J.; Zhu, M.; Sun, A.; Yuan, R.; Chen, H.; Zhou, B. The Influence Mechanism of Dissolved Organic Matter on the Photocatalytic Oxidation of Pharmaceuticals and Personal Care Products. Molecules 2025, 30, 2266. https://doi.org/10.3390/molecules30112266.
311. Fattahi, A.; Jaciw-Zurakowsky, I.; Srikanthan, N.; Bragg, L.; Liang, R.; Zhou, N.; Servos, M.; Arlos, M. Effect of Background Water Matrices on Pharmaceutical and Personal Care Product Removal by UV-LED/TiO2. Catalysts 2021, 11, 576. https://doi.org/10.3390/catal11050576.
312. Anjorin, E. O.; Alfred, M. O.; Sotunde, B.; Nnamani, E. A.; Bayode, A. A.; Unuabonah, E. I.; Helmreich, B.; Omorogie, M. O. Overview of the Mechanism of Degradation of Pharmaceuticals by Persulfate/Peroxysulfate Catalysts. ChemBioEng Rev. 2024, 11, e202300079. https://doi.org/10.1002/cben.202300079.
313. Samah, N. A.; Sánchez-Martín, M.-J.; Sebastián, R. M.; Valiente, M.; López-Mesas, M. Molecularly Imprinted Polymer for the Removal of Diclofenac from Water: Synthesis and Characterization. Sci. Total Environ. 2018, 631–632, 1534–1543. https://doi.org/10.1016/j.scitotenv.2018.03.087.
314. Cantarella, M.; Carroccio, S. C.; Dattilo, S.; Avolio, R.; Castaldo, R.; Puglisi, C.; Privitera, V. Molecularly Imprinted Polymer for Selective Adsorption of Diclofenac from Contaminated Water. Chem. Eng. J. 2019, 367, 180–188. https://doi.org/10.1016/j.cej.2019.02.146.
315. Wu, Y.; Li, Y.; Tian, A.; Mao, K.; Liu, J. Selective Removal of Perfluorooctanoic Acid Using Molecularly Imprinted Polymer-Modified TiO2 Nanotube Arrays. Int. J. Photoenergy 2016, 7368795, 10 pages. https://doi.org/10.1155/2016/7368795.
316. Hu, L.; Li, Y.; Zhang, W. Characterization and Application of Surface-Molecular-Imprinted-Polymer Modified TiO2 Nanotubes for Removal of Perfluorinated Chemicals. Water Sci. Technol. 2016, 74 (6), 1417–1425. https://doi.org/10.2166/wst.2016.321.
317. McQueen, A. D.; Tedrow, O.; Ballentine, M. L.; et al. Demonstration of Photocatalytic Degradation of Per- and Polyfluoroalkyl Substances (PFAS) in Landfill Leachate Using 3D Printed TiO2 Composite Tiles. Water Air Soil Pollut. 2022, 233, 444. https://doi.org/10.1007/s11270-022-05911-3.
318. Khalid, Z.; Hadi, F.; Xie, J.; Chandrabose, V.; Oh, J.-M. The Future of MXenes: Exploring Oxidative Degradation Pathways and Coping with Surface/Edge Passivation Approach. Small 2025, 21, 2407856. https://doi.org/10.1002/smll.202407856
319. Brame, J.; Long, M.; Li, Q.; Alvarez, P. Inhibitory Effect of Natural Organic Matter or Other Background Constituents on Photocatalytic Advanced Oxidation Processes: Mechanistic Model Development and Validation. *Water Res.* 2015, *84*, 362–371. https://doi.org/10.1016/j.watres.2015.07.044.
320. Qudsieh, I. Y.; Ali, M. A.; Maafa, I. M. Effect of Water Matrix on Photocatalytic Degradation of Organic Pollutants in Water: A Literature Review. *Rev. Chem. Eng.* 2025, *41* (6), 539–573. https://doi.org/10.1515/revce-2024-0093.
321. Younis, S. A.; Kim, K.-H. Heterogeneous Photocatalysis Scalability for Environmental Remediation: Opportunities and Challenges. *Catalysts* 2020, *10* (10), 1109. https://doi.org/10.3390/catal10101109.
322. Khader, E. H.; Muslim, S. A.; Saady, N. M. C.; Ali, N. S.; Salih, I. K.; Mohammed, T. J.; Albayati, T. M.; Zendehboudi, S. Recent Advances in Photocatalytic Advanced Oxidation Processes

View Article Online
DOI: 10.1039/D5MA01247C

for Organic Compound Degradation: A Review. *Desalin. Water Treat.* 2024, *318*, 100384. https://doi.org/10.1016/j.dwt.2024.100384.

323. Gaur, N.; Dutta, D.; Singh, A.; Dubey, R.; Kamboj, D. V. Recent Advances in the Elimination of Persistent Organic Pollutants by Photocatalysis. *Front. Environ. Sci.* 2022, *10*, 872514. https://doi.org/10.3389/fenvs.2022.872514.
324. Kumari, P.; Kumar, A. Advanced Oxidation Process: A Remediation Technique for Organic and Non-Biodegradable Pollutants. *Results Surf. Interfaces* 2023, *11*, 100122. https://doi.org/10.1016/j.rsurfi.2023.100122.
325. Wang, W.-L.; Wu, Q.-Y.; Huang, N.; Xu, Z.-B.; Lee, M.-Y.; Hu, H.-Y. Potential Risks from UV/H_2O_2 Oxidation and UV Photocatalysis: A Review of Toxic, Assimilable, and Sensory-Unpleasant Transformation Products. *Water Res.* 2018, *141*, 109–125. https://doi.org/10.1016/j.watres.2018.05.005.
326. Dong, T.; Cheung, H. Y. M.; Man, J. H. K.; et al. Recent Advances in Oxidant-Involved Photoelectrochemical Systems for Sustainable Wastewater Treatment: Mechanisms, Applications, and Perspectives. *npj Mater. Sustain.* 2025, *3*, 41. https://doi.org/10.1038/s44296-025-00084-6.
327. Wetchakun, K.; Wetchakun, N.; Sakulsermsuk, S. An Overview of Solar/Visible Light-Driven Heterogeneous Photocatalysis for Water Purification: TiO_2- and ZnO-Based Photocatalysts Used in Suspension Photoreactors. *J. Ind. Eng. Chem.* 2019, *71*, 19–49.
328. Binjhade, R.; Mondal, R.; Mondal, S. Continuous Photocatalytic Reactor: Critical Review on the Design and Performance. *J. Environ. Chem. Eng.* 2022, *10* (3), 107746. https://doi.org/10.1016/j.jece.2022.107746.
329. Chang, S.; Yang, X.; Sang, Y.; Liu, H. Highly Efficient Photocatalysts and Continuous-Flow Photocatalytic Reactors for Degradation of Organic Pollutants in Wastewater. *Chem. Asian J.* 2016, *11*, 2352–2363.
330. Basha, S.; Vijeev, A.; Pranavi, K. S.; Chattopadhyay, A.; Pai, A. R.; Mahato, K. K. Ultraviolet Light-Emitting Diode Technologies in Water Disinfection. *Water Res. X* 2025, *29*, 100454. https://doi.org/10.1016/j.wroa.2025.100454.
331. Zango, Z. U.; Ibnaouf, K. H.; Haruna, A.; Lawal, M. A.; Wadi, I. A.; Ibrahem, M. A.; Shittu, F. B.; Adamu, H. Toward Sustainable PFAS Elimination: Engineering TiO_2 Photocatalysts for Complete Mineralization and Defluorination. *J. Sci.: Adv. Mater. Devices* 2025, *10* (4), 101041. https://doi.org/10.1016/j.jsamd.2025.101041.

View Article Online
DOI: 10.1039/D5MA01247C

Data Availability Statement

Multifaceted Advances in TiO_2-Based Photocatalysts for PFAS Degradation: A Critical Review of Mechanisms, Modifications, and Challenges

No new data were created or analyzed in this study.